NAEC-ASL 1094

U. S. NAVAL AIR ENGINEERING CENTER

PHILADELPHIA, PENNSYLVANIA

AERONAUTICAL STRUCTURES LABORATORY
Report No. NAEC-ASL-1094 Volume IV

Date: 31 August 1966

APPLICATION OF APPLIED LOAD RATIO STATIC TEST SIMULATION TECHNIQUES TO FULL-SCALE STRUCTURES; VOLUME IV, SUMMARY OF RESULTS, CONCLUSIONS AND RECOMMENDATIONS

by
R. W. Gehring and C. H. Maines
North American Aviation, Inc., Columbus Div.
Columbus, Ohio

Contract No. N156-45330

Distribution of this document is unlimited

DISCLAIMER NOTICE

THIS DOCUMENT IS BEST QUALITY PRACTICABLE. THE COPY FURNISHED TO DTIC CONTAINED A SIGNIFICANT NUMBER OF PAGES WHICH DO NOT REPRODUCE LEGIBLY.

NOTICE

Reproduction of this document in any form by other than naval activities is not authorized except by special approval of the Secretary of the Navy or the Chief of Naval Operations as appropriate.

The following Espionage notice can be disregarded unless this document is plainly marked CONFIDENTIAL or SECRET.

This document contains information affecting the national defense of the United States within the meaning of the Espionage Laws, Title 18, U.S.C., Sections 793 and 794. The transmission or the revelation of its contents in any manner to an unauthorized person is prohibited by law.

FOREWORD

This study was performed under Naval Air Engineering Center Contract N156-45330 and is primarily an analytical study and experimental data correlation. The analysis and data correlation portion of the program was performed by the Structural Development Group, Vehicle Technology Engineering, North American Aviation, Inc., Columbus Division. The experimental data was obtained from static tests performed on aircraft horizontal stabilizer assemblies at room and elevated temperature by the Aeronautical Structures Laboratory, Naval Air Engineering Center, Philadelphia, Pennsylvania, with Mrs. Elise Alter as Project Engineer. This volume represents that portion of the final report describing the application of the methods of Volume I, the material properties data of Volume II, and the analytical-experimental data correlation using the data obtained from the experimental program described in Volume III. Conclusions, recommendations, and problem areas related to the realistic use of applied load ratio simulation are also included in this volume. This program was begun in July 1964 and the final draft of Volume IV was completed in January 1966.

SUMMARY

The objectives of Volume IV are to correlate analytical predictions with experimental results, and to present a general summary of results, also related studies, special analysis and experimental problems encountered, and detailed conclusions and recommendations; therefore this Volume IV is a summary report that includes significant data from Volumes I through III. The main objective of this study was to demonstrate the applicability of applied load ratio simulation and the degree of accuracy to be expected when simulating the elevated temperature static test in a room temperature environment.

The results of Part 1 of Volume IV support the use of applied load ratios for room temperature simulation of elevated temperature static tests within the limitations of the analytical methods. The accuracy to be expected for bending tests is shown to be within ±10% based upon the failing load comparison, but depends, to a large extent, on the accuracy of the basic material properties.

Part 2 of this study investigates the feasibility and applicability of applied load ratios to the strength verification of a multi-plate, multi-fastener splice joint at elevated temperatures by room temperature testing. The analytical methods used apply to axially-loaded splices, and were successfully applied to the study of the horizontal stabilizer root end splice joint which was heated both symmetrically and unsymmetrically and loaded primarily by shear loads normal to the stabilizer surface and a bending moment in the splice joint area. The accuracy demonstrated for splice joint static test simulation is shown to be within ±16% based upon the failing load comparison and depends upon the accuracy of fastener-plate load-deformation data.

VOLUME IV

TABLE OF CONTENTS

TABLES AND ILLUSTRATIONS

SYMBOLS

A_f = flange element area, $in.^2$

A_n = element area, $in.^2$

A_s = skin element area, $in.^2$

C_f, C_r = thermal moment distribution factors for front and rear beam areas, respectively

c = maximum value of y_n, inches

d = depth of beam or cross-section, inches

d_{max} = maximum beam depth, inches

E.A. = elastic axis

E_f = flange element modulus of elasticity, psi

E_n = element modulus of elasticity, psi

E_s = skin element modulus of elasticity, psi

e_c = incremental applied constant axial strain, in./in.

e_{cr} = critical buckling strain, in./in.

e_f = elastic strain in flange element, in./in.

e_s = elastic strain in skin element, in./in.

F_{cy} = compressive yield stress, psi

F_{ty} = tensile yield stress, psi

F_{tu} = tensile ultimate stress, psi

h_e = equivalent beam height, inches

I = cross-section moment of inertia, $in.^4$

K = joint spring constant representing the elastic slope of fastener load-deformation curve, lbs./in.

K_{ap_x} = applied moment rotational strain about x axis

K_T = thermal moment rotational strain

K_{T_X} = thermal moment rotational strain about x axis

K_{p_X} = inelastic moment rotational strain about x axis

L' = bending moment at elastic axis station, in.-lbs.

M = bending moment, in.-lbs.

M_{cr} = critical ultimate bending moment, in.-lbs.

M_o = reference ultimate bending moment at elastic axis station 75.625, in.-lbs.

M_T = elastic thermal moment, in.-lbs.

P = axial load, lbs.

P_c = couple load, lbs.

P_y = yield load, lbs.

R_{ap} = applied load ratio

R.T. = room temperature

S_{cr} = critical ultimate shear load in fastener, lbs.

T_f = flange temperature change from datum, ^oF.

$T_{f\ell}$ = lower flange temperature, ^oF.

T_{fu} = upper flange temperature, ^oF.

T_ℓ = lower surface temperature, ^oF.

T_s = skin temperature change from datum, ^oF.

T_u = upper surface temperature, ^oF.

T_w = web temperature, ^oF.

V_{cr} = critical ultimate applied shear load, lbs.

$V_{E.T.}$ = ultimate shear load at elevated temperature at outboard loading former, lbs.

$(V_{R.T.})_{Ref.}$ = reference ultimate shear load at room temperature at outboard loading former, lbs.

Y'_H = elastic axis station, inches

y_n = distance from neutral axis to centroid of element "n", inches

Subscripts

ap = applied

c = constant; couple

cr = critical

E.T. = elevated temperature

e = effective; equivalent

f = flange; front

ℓ = lower

n = element no.

o = static applied

p = inelastic

R.T. = room temperature

r = rear

s = skin

T = thermal

u = upper

w = web

y = yield

Greek Symbols

α_f = coefficient of thermal expansion for skin element, in./in./°F.

α_s = coefficient of thermal expansion for flange element, in./in./°F.

Δ = incremental

δ = deflection, inches

REFERENCES

(a) Gehring, R.W. and Maines, C.H., U.S. Naval Air Engineering Center Report No. NAEC-ASL-1094, "Application of Applied Load Ratio Static Test Simulation Techniques to Full-Scale Structures; Volume I, Methods of Analysis and Digital Computer Programs", of 31 December 1965.

(b) Gehring, R.W. and Lumm, J.A., U.S. Naval Air Engineering Center Report No. NAEC-ASL-1094, "Application of Applied Load Ratio Static Test Simulation Techniques to Full-Scale Structures; Volume II, Material Properties Studies and Evaluation", of January 1966.

(c) Alter, Elise, U.S. Naval Air Engineering Center Report No. NAEC-ASL-1094, "Application of Applied Load Ratio Static Test Simulation Techniques to Full-Scale Structures; Volume III, Experimental Program", of January 1966.

(d) Gehring, R.W. and Engle, R.L., North American Aviation, Inc., Report No. NA62H-973, "A Feasibility Study of Applied Load Ratios to Simulate Elevated Temperature Static Tests at Room Temperature", of May 1963. Prepared under Department of the Navy, Bureau of Naval Weapons Contract NOw61-0963-d.

(e) MIL-HDBK-5, Strength of Metal Aircraft Elements, dated August 1962, through Change Notice No. 5, 15 June 1965.

(f) Allen, H.F., WADC Technical Report 56-227, "An Experimental Study Relating to the Prediction of Elevated-Temperature Structural Behavior From the Results of Tests at Room Temperature", of June 1956.

(g) Gatewood, B.E., Thermal Stresses, McGraw-Hill Book Company, Inc., 1957.

1.0 INTRODUCTION

A previous analytical-experimental program performed under Department of the Navy, Bureau of Naval Weapons Contract NOw61-0963-d used simple box beam structures loaded in bending or compression to verify the feasibility of simulating elevated temperature static tests at room temperature. Test and analysis data for room temperature, and for symmetrically and unsymmetrically heated box beam structure under static loads indicated that the effects of material properties degradation and thermal stresses could be accounted for analytically by using strain analysis procedures which allowed the construction of load-deformation curves for the critical cross-section. The comparison of the curves for room temperature with those of any other temperature environment provided the applied load ratios for yield load ultimate load and for any other desired value of permanent set at the critical cross-section. Analytical-experimental comparisons, using critical element strain gage data versus calculated strains, indicated that this approach was feasible.

A verification program was then instituted to perform similar studies on full-scale aircraft components. The basic method was to perform the static strength simulation test at room temperature on an airframe component designed to operate in an elevated temperature environment. Then, using reliable analytical solutions for strength and deformation analyses based on discrete element strains and temperature dependent material properties, it is possible to define applied limit, yield, and ultimate load ratios to relate the room temperature test results to any desired temperature environment. The analytical procedures must be the same for room temperature load-deformation definition as for elevated temperature with the inclusion of the additional temperature terms in the elevated temperature analysis. It is equally essential that the analytical procedures allow for inelastic stress-strain relationships as well as buckling, temperature-time dependent material properties, and thermal stresses.

Previous reports have defined the basic methods and procedures used for the analytical studies (Volume I), the definition of material properties and Ramberg-Osgood parameters necessary for stress-strain curve description (Volume II), and the room-temperature elevated-temperature experimental program performed on the horizontal stabilizer assemblies (Volume III). This volume contains specific information on the use of the analytical studies for experimental-analytical comparisons and includes summaries for plane-strain cross-section and splice joint test simulation, conclusions and recommendations.

2.0 DISCUSSION OF ANALYTICAL PROGRAM

The analytical portion of this study was performed using specific strain-oriented analysis procedures applicable to elastic and inelastic structures, and room and elevated temperatures. Load-deformation defines a common basis whereby the room temperature and elevated temperature results can be compared, with the only analytical differences being the inclusion of temperature terms in the equations and the temperature-dependent material properties data input. In order to define the strength, and, therefore the applied load ratios, the analytical studies were performed using the methods described in Volume I which allow for

(a) Inelastic stress-strain relationships
(b) Buckling of individual elements
(c) Thermal stresses which may be elastic or inelastic
(d) Combined thermal and applied stresses on a realistic strain basis
(e) Temperature-time dependent material properties and recovery of properties after exposure to elevated temperature.

The methods of Volume I were utilized to define the horizontal stabilizer strength at room temperature and in four different elevated temperature environments in order to establish applied load ratios for room temperature simulation. Parts 1 and 2 depend upon two different method of analysis: Part 1 is concerned with characteristics of the outboard cross sections using the plane-strain method of analysis; Part 2 is concerned with the axially-loaded mechanically-fastened splice joints, using the virtual work method of analysis.

2.1 Strength and Deformation Analysis Procedures

The general methods used for the analytical investigation are described in Volume I, Section 3.2 for the cross-section analysis of Part 1, and Section 3.3 for the inboard splice joint analysis of Part 2. The following sections (2.1.1 and 2.1.2) illustrate with typical data the input data of major importance to the digital computer programs outlined in block diagram form in Sections 4.1 (cross-section analysis) and 4.2 (splice joint analysis) of Volume I. The data presented in Sections 2.1.1 and 2.1.2 are primarily the temperature-time dependent material properties, typical calculations and descriptions of the various mechanical properties, and, in Section 2.1.2, a description of the applied axial load input to the axially loaded splice joint based on an external applied bending moment.

2.1.1 Cross-Section Analysis, Part 1

Using the procedures described in Volume I, the load-deformation curves and the ultimate loads are calculated for each instrumented cross-section for each of the temperature environments of the test program. The load-deformation curves are plotted for the critical element in the cross-section which is defined as that having the maximum permanent set, e_{ps_m}, where the maximum value is calculated by

$$e_{ps_m} = \sum_j e_{p_j} + \left(\sum_j K_{px_j}\right) \frac{y_m}{c} + \left(\sum_j K_{py_j}\right) \frac{x_m}{b_x}$$

The resulting load-deformation curves and ultimate loads are described in Sections 4.1 and 5.1 respectively.

The predicted failure station is defined by plotting the ultimate bending moment versus span (elastic axis station) curve using the calculated ultimate values at the four instrumented cross-sections, and by plotting on the same set of coordinates an applied bending moment line which is tangent to the ultimate strength curve. The point of tangency of the two curves defines the critical station for ultimate strength. Yield, limit load, or any specified strength can be established for the "strength curve". This procedure is applied to this program and is described in detail in Section 4.2.

The cross-section analysis procedures as defined in Volume I for ultimate strength and load-deformation prediction rely heavily on the accurate representation and definition of the basic material properties in any temperature environment and any exposure time or soaking period. Therefore, the material properties must be defined at temperature to compute the strength at temperature and at room temperature after exposure to temperature to compute the strength and any permanent set remaining at room temperature after exposure to the elevated temperature environment. The individual element temperatures are defined by curves as described in Section 3.0 which utilize span-wise plots of the external thermocouples at the time of failure of the particular horizontal stabilizer and generalized plots of temperature gradient data obtained from the temperature survey stabilizer (Horizontal Stabilizer Test No. 2). The equivalent soaking times at temperature and the element temperatures are shown in Table 2.1 along with the yield and ultimate Larson-Miller Parameters for use with the parametric curves of Volume II for material properties definition (F_{ty} and F_{tu}) at temperature and at room temperature after exposure to the elevated temperature environment.. The remaining Ramberg-Osgood parameters, modulus of elasticity (E), and stress-strain curve shape factor (m)

are obtained from the temperature dependent data and curves in Volume II for the specific materials. These properties, and tables identical to that shown in Table 2.1, were calculated and defined for each instrumented cross-section (Elastic Axis Stations 91, 102, 113, and 124) for each test horizontal stabilizer (Horizontal Stabilizer Tests 1, 3, 4, 5, and 6). Table 2.1 is shown as a typical illustrative example of material properties input data for Elastic Axis Station 102, Horizontal Stabilizer Test 6, 425°F. Unsymmetrical temperature environment. For Test 4, 425°F. Symmetrical, where a lamps-off, lamps-on study was performed, it was necessary to define two separate sets of material property data for the two different sets of temperature data.

The cross-section analysis procedures also provide the necessary data in the form of applied, thermal, and inelastic moment rotational strain values (Kap_X, K_{TX}, and Kp_X respectively) as basic input to the deflection analysis procedures of Section 2.2.

Table 2.1. Typical Material Properties Summary,
Part 1, Test No. 6 (425°F. Unsymm.), E.A. Sta. 102

Element No.	Description	Material	Element Temperature, °F.	Soaking Time*, t, hours	Yield Larson-Miller Parameter	Ultimate Larson-Miller Parameter	Yield Stress at Temp., F_y, psi.	Ultimate Stress at Temp., F_u, psi.	Modulus of Elasticity at Temp., E,psi. x 10^{-6}	Ramberg-Osgood Shape Factor n	R.T. Recovery Yield Stress F_y,psi.	R.T. Recovery Ultimate Stress F_u, psi.
1	Leading Edge	Stainless Steel	206	------	------	------	56000	136800	27.2	10	58000	150000
2	Fwd. Box Skin	AZ31B-H24	413	------	------	------	14700	14700	2.6	13	31000	35000
3	Main Box Skin	7079-T6	438	0.588	12632	13350	31200	31200 †	7.88	38	44500	57500
4	Main Box Skin		457	0.588	12534	13268	30100	29950 †	7.77		47000	59000
5	Main Box Skin		450	0.588	12439	13167	32300	31700 †	7.77		49300	60500
6	Fwd. Beam Flange		380	0.822	11605	12277	43750	45000	8.25		64500	71600
7	Fwd.Interbeam Flange		380	0.822	11605	12277	43750	45000	8.25		64500	71600
8	Aft Interbeam Flange		399	0.822	11867	12554	40500	42600	8.12		60800	68700
9	Rear Beam Flange	7079-T6	385	0.822	11674	12350	43400	44500	8.25	38	63800	70900
10	Aft Box Skin	AZ31B-H24	415	------	------	------	14700	14700	2.6	13	31000	35000
11	T.E.Honeycomb Facing	7075-T6	103	0.791	7768	8219	66200	72300	9.67	35	66200	72300
12	T.E.Honeycomb Facing	7075-T6	100	0.791	7727	8175	66200	72300	9.67	35	66200	72300
13	Aft Box Skin	AZ31B-H24	212	------	------	------	29400	34900	4.55	18	39700	49500
14	Main Box Skin	7079-T6	280	0.791	10210	10802	62300	65500	8.72	37	71900	79000
15	Main Box Skin		270	0.791	10072	10656	63500	66400	8.78		72000	79200
16	Main Box Skin		273	0.791	10114	10700	63500	66400	8.78		72000	79200
17	Rear Beam Flange		302	0.791	10514	11124	59600	62800	8.63		71300	78500
18	Aft Interbeam Flange		289	0.791	10335	10934	61400	64500	8.70		71700	78800
19	Fwd.Interbeam Flange		250	0.791	9796	10364	65000	68000	8.87		72200	79200
20	Front Beam Flange	7079-T6	292	0.791	10376	10978	61000	64200	8.70	37	71600	78600
21	Fwd. Box Skin	AZ31B-H24	198	------	------	------	30700	36400	4.70	18	39700	40500
22	Front Beam Web	7079-T6	330	0.811	10909	11541	55100	57100	8.50	38	69800	77200
23	Fwd.Interbeam Web		306	0.811	10578	11190	59400	62400	8.60		71000	78500
24	Aft Interbeam Web		335	0.811	10978	11614	54400	55900	8.50		69500	76800
25	Rear Beam Web		336	0.811	10992	11629	54400	55900	8.50		69500	76800
26	Rear Beam Web		336	0.811	10992	11629	54400	55900	8.50		69500	76800
27	Aft Interbeam Web		335	0.811	10978	11614	54400	55900	8.50		69500	76800
28	Fwd.Interbeam Web		306	0.811	10578	11190	59400	62400	8.60		71000	78500
29	Front Beam Web	7079-T6	330	0.811	10909	11541	55100	57100	8.50	38	69800	77200
30	Leading Edge	Stainless Steel	206	------	------	------	103000	136800	27.2	10	110000	150000

* Equivalent time at element temperature.

† Tensile ultimate ≈ Tensile yield at high temperature for high strength aluminum alloys. Values from exposure curves in Volume II.

2.1.2 Inboard Splice Joint Analysis, Part 2

In order to perform the analysis for splice joint strength as described in Volume I and provide input data for the computer program certain data must be obtained, and/or defined, pertaining to the applied loads and the necessary mechanical properties for both fasteners and plate elements. This section describes the numerical definition of the applied axial loads for the splice analysis as derived from the applied shear loads and bending moments applied to the outboard end of the splice joint. Loads in the statically determinate structure are shown which apply to all temperature environments except as noted for the restrained-in-bending thermal moment cases of Test No's. 11 and 12 which had unsymmetrical temperature distributions. A typical set of calculations is shown (room temperature environment) for fastener-plate Ramberg-Osgood parameters to describe the load-deflection characteristics of individual fasteners in the analysis. In addition, typical sets of fastener properties and plate element properties are tabulated for one particular temperature environment to illustrate the magnitude and units of typical values and the exact data required for a complete stress analysis of the splice joint. Briefly, the four sections are described below.

(a) Load Distribution Assumptions in Inboard Splice Joint

This section includes the assumptions made to obtain the equivalent axial loading of the splice joint for analysis by the methods described in Section 3.3 of Volume I. The calculations to define the axial loads are shown and these are assumed to apply in general to all temperature environments. Tables 2.2 and 2.3 are presented to show the load distribution in the static load path of the redundant fastener-plate structure. The cross-section geometry is shown in Figures 4.20 and 4.21.

(b) Ramberg-Osgood Parameters for Fastener-Plate Intersections at Room Temperature

Typical calculations are shown for the room temperature case where the Ramberg-Osgood parameters are defined for each fastener-plate intersection according to fastener diameter, plate thickness, and plate material. The calculated values shown are those used in the analysis of Test No. 7 and are obtained by using the curves and material property data for fastener-plate combinations in Volume II.

(c) Summary Tables for Fastener Properties

Tables 2.4 through 2.7 provide the necessary mechanical

properties to describe fastener deformation, local bearing deformation, and ultimate strength cut-off values for a typical elevated temperature test (425°F. Symmetrical; Test No. 10). Four separate tables are shown, each for a particular component of the splice joint; i.e., main box skin, splice plate, interbeams, and main beam fitting.

(d) Summary Tables for Plate Element Properties

Tables 2.8 through 2.11 provide the necessary temperature-dependent material properties for all plate elements in the splice joint using Test No. 10 (425°F. Symmetrical) as a typical example. These properties describe the Ramberg-Osgood parameters for plate element stress-strain curve representation in a similar manner to that for the axially-loaded cross-section elements of Part 1. The temperatures shown are the plate element temperatures on the tension side of the splice at the time of failure and were obtained from thermocouple readings and the procedure and curves of Section 3.2. In these tables the Larson-Miller values represent the effects of 1/2 hour exposure time for the temperatures shown since the test temperature exposure times did not vary sufficiently from 1/2 hour to warrant more detailed approximations of elevated temperature properties.

The calculations for items (a) and (b) immediately follow this section on pages 8 through 15. The fastener property tables of item (c) are on pages 16 and 17, and the plate element property tables of item (d) are on pages 18 and 19.

(a) Load Distribution Assumptions In Inboard Splice Joint

The bending moment is applied to the splice joint area by concentrated loads of equal magnitude at Elastic Axis Stations 80 and 95.

From the original static test at room temperature the critical ultimate bending moment at Elastic Axis Station 49.56 is

$$M_{cr} \approx 1.13 \times 10^6 \text{ in.-lbs.}$$

Two loading formers were used for more accurate matching of design ultimate moment curve slope at root and to preclude a cross-section failure just outboard of the splice area.

The critical applied shear load at each loading former, V_{cr}, is defined by

$$V_{cr}\ (95\text{-}49.56) + V_{cr}\ (80\text{-}49.56) = 1{,}130{,}000$$

$$45.44\ V_{cr} + 30.44\ V_{cr} = 1{,}130{,}000$$

$$75.88\ V_{cr} = 1{,}130{,}000$$

$$V_{cr} = 14{,}900\#\text{ ultimate}$$

The bending moment at the outboard line of fasteners (Elastic Axis Station 75.625) for V_{cr} = 14,900# is

$$\begin{aligned} M &= 14900\ (95\text{-}75.625) + 14900\ (80\text{-}75.625) \\ &= 14900\ (19.375) + 14900\ (4.375) \\ &= 288{,}700 + 65{,}150 \\ &= 353{,}850 \text{ in.-lbs. at Station } 75.625 \end{aligned}$$

The reference ultimate loads for room temperature at Station 75.625 are defined as M_o and V_o where

$$M_o = 353{,}850 \text{ in.-lbs. and } V_o = 29{,}800 \text{ lbs.}$$

Load Distribution Assumptions

(1) Cross-section analysis (elastic $\frac{My}{I}$) at Elastic Axis Station 75.625 is represented by fastener line (1) - (24) - (47) to obtain axial load distribution between skin and interbeam flanges.

For a unit moment M_o = 100,000 in.-lbs. (Refer to Volume I) the axial load distribution is

Main Box Skin Load = 39,150#, Interbeam Flange Load = 1914#

For M_o = 353,850 in.-lbs. the load distribution is,

Main Box Skin Load = 138,600#, Interbeam Flange Load = 6780#

(2) Applied axial loads of 138,600# and 6780# are constant between Stations 75.625 and 65.76 in the statically determinate plate elements.

(3) The shear load of 29,800# is assumed to be transferred inboard as a couple load in the main box skins only, producing variable loads in skin elements between (1) and (10) . The shear load is then transferred to the static fastener segments represented by (10) , (33) and (56) at Elastic Axis Station 65.76.

This simplifying assumption is made because of the relatively small areas of the interbeam flanges and the splice plate plus the fact that the majority of the 29,800# shear load is in the front and rear beams. Also it may be seen from the axial load distribution at Station 75.625 that the maximum error in this assumption could be only about 4% at most.

Table 2.2 on page 10 gives the average incremental loads in the main box skin plate elements between (1) and (10).

For the thermal moment restraint conditions considered to be present in Test No's. 11 and 12 the couple loads shown on page 79 must be added, where applicable, to the values in Tables 2.2 and 2.3 for applied load distribution in the statically determinate structure.

Table 2.2. Moment in Static Main Box Skin Elements Between (1) and (10)

Elastic Axis Sta.	Moment Arm, inches	Shear Load, lbs.	Bending Moment, M in-lbs.	$d_{max.}$, inches	$h_e = 0.86\ d_{max.}$ inches	Couple Load $P_c = M/h_e$ lbs.	Plate Element No.	Avg. Element Load, lbs.
75.625	0	29800	0	2.85	2.45	0		
74.625	1		29800	2.875	2.473	12040	1	6020
73.625	2		59600	2.90	2.493	23920	2	17980
72.625	3		89400	2.924	2.515	35550	3	29735
71.625	4		119300	2.949	2.535	47000	4	41275
71.125	4.5		134200	2.962	2.55	52600	5	49800
69.656	5.969		178000	3.00	2.58	69000	6	60800
67.975	7.65		228000	3.039	2.613	87250	7	78125
66.855	8.770		261300	3.067	2.64	98900	8	93075
65.735	9.890	29800	294800	3.095	2.665	110700	9	104800

Table 2.3. Moment in Static Main Beam Fitting Elements Between (56) and (69)

Elastic Axis Station	Moment Arm, inches	Bending Moment in.-lbs.	Effective Couple Height, h_e inches	Couple Load, $P_c = M/h_e$ lbs.	Element No.	Avg. Element Load, lbs.
65.735	0					
64.195	1.54	45850	2.38	19270	56	9635
63.175	2.56	76250	2.44	31250	57	25260
62.155	3.58	106700	2.45	43500	58	37375
61.135	4.60	137200	2.47	55500	59	49500
60.115	5.62	167400	2.48	67500	60	61500
59.095	6.64	198000	2.49	79500	61	73500
58.075	7.66	228200	2.50	91300	62	85400
56.84	8.91	265500	2.52	105300	63	98300
55.34	10.41	310000	2.56	121000	64	113150
54.18	11.566	344500	2.60	132500	65	126750
52.56	13.191	392700	2.63	149500	66	141000
51.278	14.472	431000	2.67	161500	67	169350
49.56	16.190	482000	2.72	177200	68	169350

Shear Load of 29,800# applied at Station 65.735 for loads in above table. Approximate Design ultimate load.

(b) Ramberg-Osgood Parameters For Fastener-Plate Intersections at Room Temperature

The following set of calculations is provided to illustrate the approximate procedure used to obtain fastener-plate Ramberg-Osgood parameters for the individual fastener-plate intersections within the splice joint. P_y, n, and K represent the yield load per fastener, the shape factor for the Ramberg-Osgood representation of the fastener load-deflection curve, and the initial elastic slope of the curve, respectively.

Allowable bearing yield stress reference value is 50,000 psi. for critical stainless steel sleeve as shown in Volume II. Use Figure 5.3 of Volume II for bearing yield factor.

(1) For $\frac{1}{4}$" Hi-Shear Blind Bolts in .290" alum. alloy; applies to fastener-plate intersections (1), (2), (3), (4), (5), (6), and (7).

Bearing Area = .25(.29) = .0725 in.^{2}

P_y = 1.02(50,000)(.0725) = 3695 lbs./fastener, n = 2.762

K = 1.02(451,750) = 460,000, S_{cr} = 9750# (Two fasteners)

(2) For 3/8" Hi-Shear Blind Bolts in .290" alum. alloy; applies to fastener-plate intersections (11), (12), (13), (14), (15), (16), (17).

Bearing Area = .375(.29) = .10875 in.^{2}

P_y = 1.175(50000)(.10875) = 6380 lbs./fastener, n = 2.762

K = 1.175(451,750) = 530,000, S_{cr} = 21,300# (Two fasteners)

(3) For 7/16" Hi-Shear Blind Bolts in .290" alum. alloy; applies to fastener-plate intersections (8), (9), (10), (18), (19), (20), (21), (22), (23).

Bearing Area = .4375(.29) = .127 in.^{2}

P_y = 1.255(50000)(.127) = 7960 lbs./fastener, n = 4.55

K = 1.255(451,750) = 566,500, S_{cr} = 35,150#(Two fasteners)

(4) For $\frac{1}{4}$" Hi-Shear Blind Bolts in .090" steel splice plate; applies to fastener-plate intersections (24) , (25) , (26) (27) , (28) , (29) , (30) .

Bearing Area = .25(.09) = .0225 in.^{2}

P_y = 0.8(50,000)(.0225) = 900 lbs./fastener, n = 2.762

K = 0.8(451,750) = 361,000, S_{cr} = 9750#(Two fasteners)

(5) For 7/16" Hi-Shear Blind Bolts in .090" steel splice plate; applies to fastener-plate intersections (31) , (32) , (33) .

Bearing Area = .4375(.09) = .0394 in.^{2}

P_y = 0.87(50,000)(.0394) = 1714 lbs./fastener, n = 4.55

K = 0.87(451,750) = 392,500, S_{cr} = 35,150# (Two fasteners)

(6) For $\frac{1}{4}$" Hi-Shear Blind Bolts in 0.152", alum, inter-beam; applies to fastener-plate intersections (47) , (48) , (49) , (51) .

Bearing Area = .25(.152) = .038 in.^{2}

P_y = 0.865(50,000)(.038) ; 1643 lbs./fastener, n = 2.762

K = 0.865(451,750) = 390,500, S_{cr} = 9750# (Two fasteners)

(7) For 7/16" Hi-Shear Blind Bolts in 0.125" steel main beam flange; applies to fastener-plate intersections (54) , (55) , (56) .

Bearing Area = .4375(.125) .0547 in.^{2}

P_y = 0.935(50,000)(.0547) = 2555 lbs./fastener, n = 4.55

K = 0.935(451,750) = 422,000, S_{cr} = 35,150" (Two Fasteners)

(8) For 3/8" Hi-Shear Blind Bolts in 0.187" steel main beam flange; applies to fastener-plate intersection (57) only.

Bearing Area = 0.375(.187) = .0701 in.^{2}

P_y = 1.01(50,000)(.0701) = 3540 lbs./fastener, n = 2.762

K = 1.01(451,750) = 455,500, S_{cr} = 21,300# (Two fasteners)

(9) For 3/8" Hi-Shear Blind Bolts in 0.143" steel main beam flange; applies to fastener-plate intersection (58) only.

Bearing Area = 0.375(.143) = .0536 in.^{2}

P_y = 0.93(50,000)(.0536) = 2493 lbs./fastener, n = 2.762

K = 0.93(451,750) = 420,000, S_{cr} = 21,300# (Two fasteners)

(10) For 3/8" Hi-Shear Blind Bolts in 0.155" steel main beam flange; applies to fastener-plate intersection (59) only.

Bearing Area = 0.375(.155) = .0581 in.^{2}

P_y = 0.95(50,000)(.0581) = 2760 lbs./fastener, n = 2.762

K = 0.95(451,750) = 429,000, S_{cr} = 21,300# (Two fasteners)

(11) For 3/8" Hi-Shear Blind Bolts in 0.168", steel main beam flange; applies to fastener-plate intersection (60) only.

Bearing Area = 0.375(.168) = .063 in.^{2}

P_y = 0.975(50,000)(.062) = 3070 lbs./fastener, n = 2.762

K = 0.975(451,750) = 440,500, S_{cr} = 21,300# (Two fasteners)

(12) For 3/8" Hi-Shear Blind Bolts in 0.182" steel main beam flange; applies to fastener-plate intersection (61) only.

Bearing Area = 0.375(.182) = .06825 in.^{2}

P_y = 1.0(50,000)(.06825) = 3415 lbs./fastener, n = 2.762

K = 1.0(451,750) = 451,750, S_{cr} = 21,300# (Two fasteners)

(13) For 3/8" Hi-Shear Blind Bolts in 0.195" steel main beam flange; applies to fastener-plate intersection (62) only.

Bearing Area = 0.375(0.195) = .0731 in.^{2}

P_y = 1.02(50,000)(.0731) = 3725 lbs./fastener, n = 2.762

K = 1.02(451,750) = 460,000, S_{cr} = 21,300# (Two fasteners)

(14) For 3/8" Hi-Shear Blind Bolts in 0.207" steel main beam flange; applies to fastener-plate intersection (63) only.

Bearing Area = 0.375(.207) = .0777 in.^{2}

P_y = 1.04(50,000)(.0777) = 4035 lbs./fastener, n = 2.762

K = 1.04(451,750) = 470,000, S_{cr} = 21,300# (Two fasteners)

(15) For 7/16" Hi-Shear Blind Bolts in 0.224" steel main beam flange; applies to fastener-plate intersection (64) only.

Bearing Area = 0.4375(.224) = .0979 in.^{2}

P_y = 1.127(50,000)(.0979) = 5520 lbs./fastener, n = 4.55

K = 1.127(451,750) = 509,000, S_{cr} = 35,150# (Two fasteners)

(16) For 7/16" Hi-Shear Blind Bolts in 0.230" steel main beam flange; applies to fastener-plate intersections (65), (66), (67), (68), and (69).

Bearing Area = .23(.4375) = .1007 in.^{2}

P_y = 1.14(50,000)(.1007) = 5740 lbs./fastener, n = 4.55

K = 1.14(451,750) = 515,000, S_{cr} = 35,150# (Two fasteners)

Table 2.4. Typical Fastener Allowables, Main Box Skin, 425°F. Symm. (Test No. 10)

Fastener-Plate Intersection	Temperature, °F.	Ramberg-Osgood Exponent, n_f	Yield Load Per Fastener at Temp., lbs.	k Per Fastener at Temp., lbs./in.	Ultimate Shear For Two Fasteners at Temp., lbs.	Allowable Bearing Deformation Cut-Off at Temp., inches
1	408	3.82	2673	315000	6335	0.0612
2	↓	↓	↓	↓	↓	↓
3						
4						
5						
6						
7		3.82	2673	315000	6335	0.0612
8		5.6	5760	388000	20150	0.1072
9	408	5.6	5760	388000	20150	0.1072
10	420	5.63	5520	388000	19070	0.1028
11	430	3.9	4250	363000	12620	0.0844
12	434	↓	4150	↓	12300	0.0825
13	435		4150		12300	0.0825
14	434		4150		12300	0.0825
15	430	3.9	4250		12620	0.0844
16	425	3.88	4345		12900	0.0863
17	418	3.85	4430	363000	13280	0.0882
18	408	5.6	5760	388000	20150	0.1072
19	392	5.53	6070	389000	21330	0.1138
20	378	5.5	6325	390000	22300	0.1182
21	355	5.42	6700	391000	23780	0.1258
22	336	5.37	6980	393000	24900	0.1312
23	309	5.28	7300	396000	26200	0.1378

Table 2.5. Typical Fastener Allowables
Steel Splice Plate, 425°F, Symm. (Test No. 10)

Fastener-Plate Intersection	Temperature, °F.	Ramberg-Osgood Exponent, n_f	Yield Load Per Fastener at Temp., lbs.	K Per Fastener at Temp., lbs./in.	Ultimate Shear For Two Fasteners at Temp., lbs.	Allowable Bearing Deformation Cut-Off at Temp., inches
24	406	3.8	860	345000	6385	0.0617
25	↓	↓	↓	↓	6385	0.0617
26					6385	0.0617
27					----	-----
28					6385	0.0617
29					----	-----
30		3.8	860	345000	----	-----
31		5.58	1638	375000	20300	0.1082
32	406	5.58	1638	375000	20300	0.1082
33	417	5.58	1638	375000	19380	0.1082

Table 2.6. Typical Fastener Allowables, Interbeams, 425°F, Symm. (Test No. 10)

Fastener-Plate Intersection	Temperature, °F.	Ramberg-Osgood Exponent, n_f	Yield Load Per Fastener at Temp., lbs.	K Per Fastener at Temp., lbs./in.	Ultimate Shear For Two Fasteners at Temp., lbs.	Allowable Bearing Deformation Cut-Off at Temp., inches
47	387	3.75	1272	268000		0.0642
48	387	3.75	1272	268000	See	0.0662
49	387	3.75	1272	268000	Table 2.5	0.0662
51	387	3.75	1272	268000		0.0642

Table 2.7. Typical Fastener Allowables, Main Beam Fitting, 425°F, Symm. (Test No. 10)

Fastener-Plate Intersection	Temperature, °F.	Ramberg-Osgood Exponent, n_f	Yield Load Per Fastener at Temp., lbs.	K Per Fastener at Temp., lbs./in.	Ultimate Shear For Two Fasteners at Temp., lbs.	Allowable Bearing Deformation Cut-Off at Temp., inches
54	407	5.59	2440	402500	↓	0.1072
55	407	5.59	2440	402500		0.1072
56	418	5.62	2435	402000	See	0.1028
57	428	3.9	3360	433000	Tables	0.0843
58	432	↓	2370	399000		↓
59	433		2620	407500	2.4	
60	432		2920	419000		
61	428	3.9	3245	429000		0.0843
62	423	3.87	3550	440000	&	0.0862
63	417	3.85	3850	448000	2.5	0.0888
64	407	5.59	5270	486000		0.1072
65	390	5.53	5510	494000		0.1138
66	376	5.5	5510	494000		0.1194
67	353	5.42	5540	497000		0.1260
68	332	5.35	5570	500000		0.1313
69	317	5.28	5590	501000	↓	0.1378

Table 2.8. Plate Element Properties,
Main Box Skin, 425°F, Symm. (Test No. 10)

Fastener Line Interval	Material	Element Temp., °F.	Yield Larson-Miller Parameter	Ultimate Larson-Miller Parameter	Per Cent R.T. F_{ty}	Per Cent R.T. F_{tu}	Allowable Yield Stress F_{ty}, psi	Allowable Ultimate Stress F_{tu}, psi	Modulus of Elasticity E_{t_0}, psi x 10^6
1	7079-To	408	11800	12500	.535	.523	39350	41700	8.08
2	Aluminum	↓	↓	↓	↓	↓	↓	↓	↓
3	Alloy								
4	↓								
5									
6									
7									
8		↓	↓	↓	↓	↓	↓	↓	↓
9		408	11800	12500	.535	.523	39350	41700	8.08
10		420	11960	12670	.509	.496	37450	39000	8.0
11		430	12100	12820	.475	.456	34950	36300	7.92
12		434	12150	12870	.460	.449	33850	35750	7.9
13		435	12170	12890	.459	.446	33750	35500	7.9
14		434	12150	12870	.460	.449	33850	35750	7.9
15		430	12100	12820	.475	.456	34950	36300	7.92
16		425	12030	12740	.487	.475	35800	37800	7.97
17		418	11930	12650	.511	.500	37600	39800	8.02
18		408	11800	12500	.535	.523	39350	41700	8.08
19		392	11560	12270	.585	.565	43000	45000	8.2
20		378	11400	12070	.620	.589	45600	46900	8.27
21	7079-To	355	11080	11730	.694	.659	51000	52400	8.38
22	Aluminum	336	10820	11460	.749	.717	55000	57100	8.5
23	Alloy	309	10440	11070	.[illegible]	.777	58800	61800	8.6

Table 2.9. Plate Element Properties
Steel Splice Plate, 425°F, Symm. (Test No. 10)

Fastener-Plate Interpretation	Material	Element Temp., °F.	Yield Larson-Miller Parameter	Ultimate Larson-Miller Parameter	Per Cent R.T. F_{ty}	Per Cent R.T. F_{tu}	Allowable Yield Stress F_{ty}, psi	Allowable Ultimate Stress F_{tu}, psi	Modulus of Elasticity E, psi x 10^{-6}
24	4340 Steel, H.T. 180,000 psi.	406	Not Applicable Use Ref. (e).	Not Applicable Use Ref. (e).	.905	.94	147700	169200	27.5
25									
26									
27									
28									
29									
30									
31		406			.905	.94	147700	169200	27.5
32		417			.900	.938	146800	169000	27.4

Table 2.10. Plate Element Properties,
Interbeams, 425°F, Symm. (Test No. 10)

Fastener-Plate Interpretation	Material	Element Temp., °F.	Yield Larson-Miller Parameter	Ultimate Larson-Miller Parameter	Per Cent R.T. F_{ty}	Per Cent R.T. F_{tu}	Allowable Yield Stress F_{ty}, psi	Allowable Ultimate Stress F_{tu}, psi	Modulus of Elasticity E, psi x 10^{-6}
47	7079-T6 Aluminum Alloy	387	11500	12190	.595	.583	43750	46400	8.2
48		387	11500	12190	.595	.583	43750	46400	8.2
49		387	11500	12190	.595	.583	43750	46400	8.2
50		387	11500	12190	.595	.583	43750	46400	8.2

Table 2.11. Plate Element Properties,
Main Beam Fitting, 425°F, Symm. (Test No. 10)

Fastener-Plate	Material	Element Temp., °F.	Yield Larson-Miller Parameter	Ultimate Larson-Miller Parameter	Per Cent R.T. F_{ty}	Per Cent R.T. F_{tu}	Allowable Yield Stress F_{ty}, psi	Allowable Ultimate Stress, F_{tu}, psi	Modulus of Elasticity E, psi x 10^{-6}
54	4340 Steel, H.T. 260,000 psi	407	Not Applicable Use Ref. (e)	Not Applicable Use Ref. (e)	.905	.94	196500	244500	27.4
55		407			.905	.94	196500	244500	27.4
56		418			.900	.938	195500	244800	27.4
57		428			.895	.935	194300	243000	27.3
58		432							
59		433							
60		432							
61		428			.895	.935	194300	243000	27.3
62		423			.90	.938	195500	244000	27.4
63		417			.90	.938	195500	244000	27.4
64		407			.905	.94	196500	244500	27.4
65		390			.91	.943	197500	245000	27.5
66		376			.917	.947	199000	246000	27.5
67		353			.925	.953	201000	248000	27.7
68		334			.933	.958	202500	249000	27.8
69		307			.938	.96	203500	249500	27.8

3.0 TEMPERATURE SURVEY PROGRAM

3.1 Part 1 - Cross-Section Temperature Survey

One horizontal stabilizer Test 2 was used for temperature and temperature distribution studies only to provide a means of approximating the temperatures on internal structural elements of the test stabilizers. Volume III shows the location of thermocouples on the temperature survey stabilizer and also on the test stabilizers. Note that internal thermocouples are provided on the temperature survey stabilizer, but not on those stabilizers which are tested to failure by externally applied loads. The construction of the stabilizers does not provide ready access to the spars and spar flanges; therefore it was necessary to cut access holes in the main box skin for internal thermocouple installation. Flush patches were tolerable from a temperature distribution standpoint but structural repairs in the main box areas would be intolerable for comparative failure analysis of the test stabilizers.

It should also be noted that the external thermocouples on the temperature survey stabilizer and the test stabilizers are located in identical locations to allow relationships to be established between external and internal temperatures. These relationships could best be established using the temperature survey stabilizer with both internal and external thermocouples and performing temperature studies under similar temperature environments to the steady-state operating conditions during the static load tests. The four operating conditions were nominally as follows:

(a) 250°F. control temperature on upper and lower skins; symmetrically heated (upper and lower surfaces).

(b) 250°F. control temperature on upper skin; heated upper surface and air cooled lower surface.

(c) 425°F. control temperature on upper and lower skins; symmetrically heated (upper and lower surfaces).

(d) 425°F. control temperature on upper skin; heated upper surface and air cooled lower surface.

Considering that joint conductivity may be a significant item in the overall heat conductance problem the experimental temperature data from the temperature survey specimen are considered to be more reliable than those obtained by analytical means.

A method was devised for using thermocouple data from the temperature studies performed by NAEC-ASL (Volume III) for realistic internal temperature predictions for all test stabilizers by relating the upper flange, spar web, and lower flange temperatures to the maximum temperature (main box skin) over the spar flange and to the temperature

gradient through the depth of the spar. This gradient is measured by external thermocouples in the upper and lower skins over the spar flanges at the stations indicated in Figure 3.1. The curves in Figures 3.3, 3.4, and 3.5 were derived on this basis and apply to the four main spars and any elastic axis station by interpolating between the two curves shown. Note that the inboard and outboard stations (Elastic Axis Station 90 and Elastic Axis Station 125) tend to produce separate groups of data ($T_u/T_\ell \approx 1.0$) and slightly different curves for the range of T_u/T_ℓ . These curves are considered to be sufficiently accurate for determining internal structural element temperatures and the corresponding element material properties. The significance of these curves is that they require only a knowledge of external temperatures, as obtained from the static test stabilizers to define the internal structural element temperatures.

Figures 3.1 and 3.2 show a typical example (425°F. Unsymmetrical, Test No. 6) of spanwise temperature variations which are used in conjunction with Figures 3.3, 3.4, and 3.5 to define internal element temperatures.

The main box skin and spar temperatures and temperature distributions in Figures 3.1, 3.2, 3.3, 3.4, and 3.5 are designated by the following symbols.

T_u = upper surface (external) temperature in °F. measured by thermocouples

T_ℓ = lower surface (external) temperature in °F. measured by thermocouples

T_{fu} = upper spar flange temperature in °F. and applies to front spar, rear spar, and interbeams

$T_{f\ell}$ = lower spar flange temperature in °F. and applies to front spar, rear spar, and interbeams

T_w = average spar web temperature in °F. and applies to front spar, rear spar, and interbeams

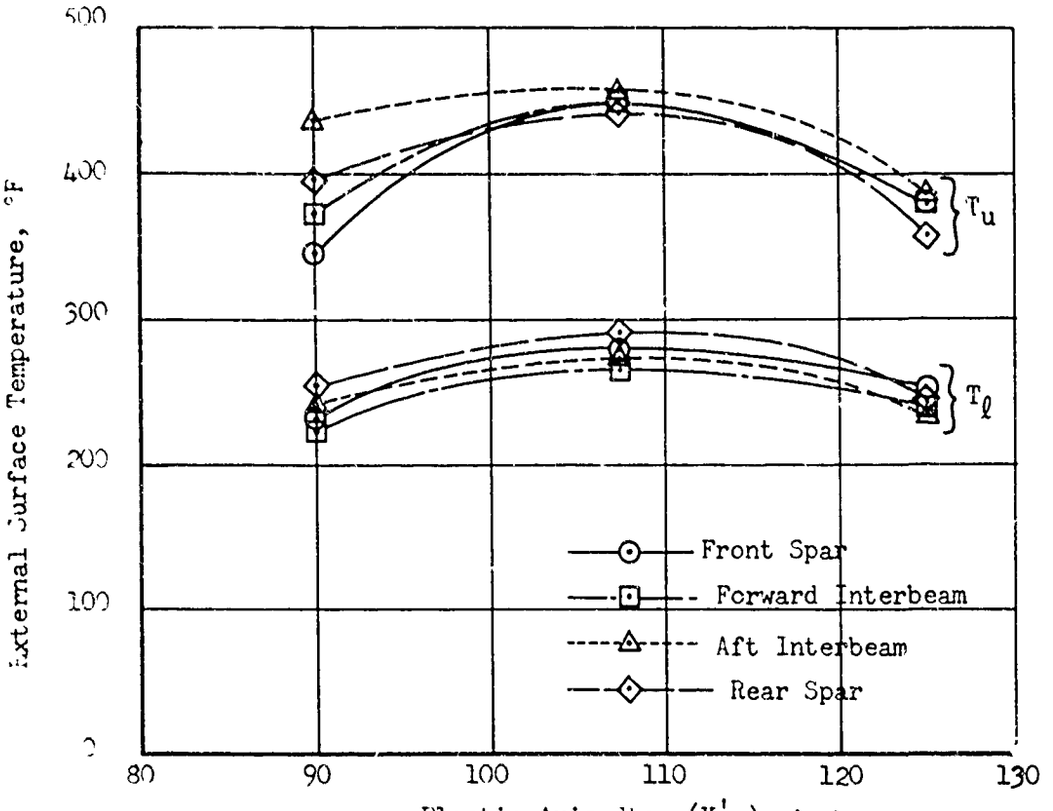

Figure 3.1 Main Box Spar External Surface Temperatures, Part 1, Cross-Section Analysis, (Test No. 6)

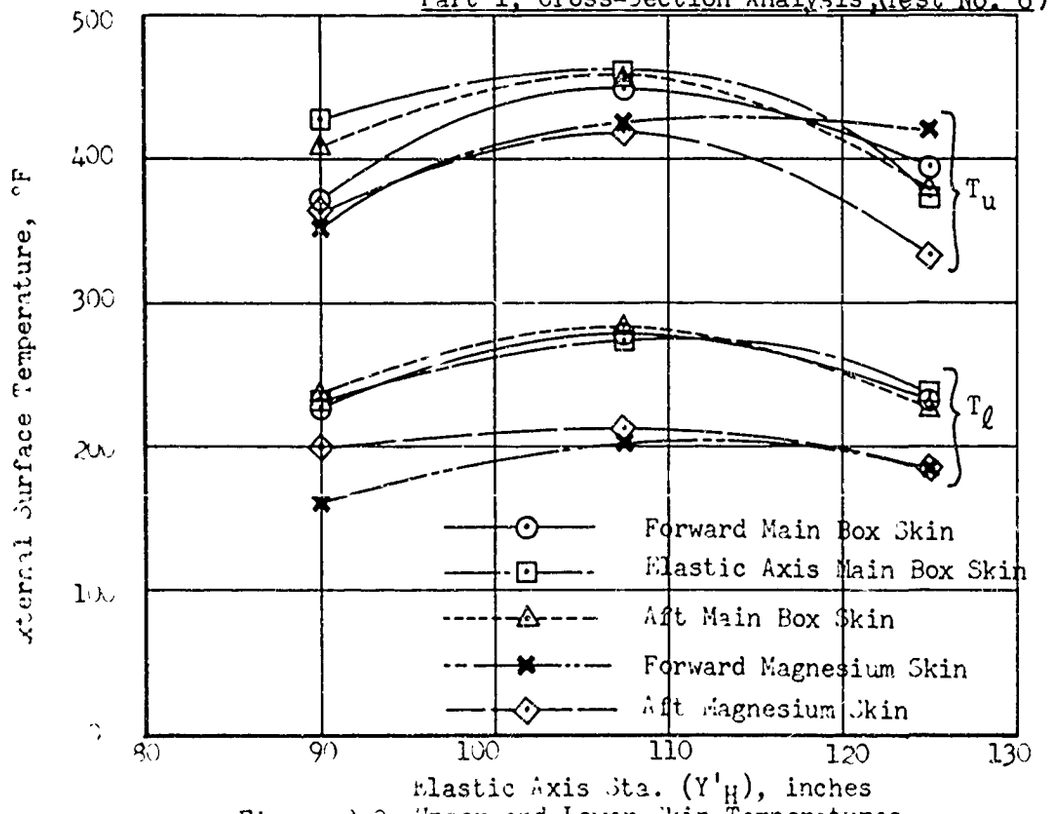

Figure 3.2 Upper and Lower Skin Temperatures, Part 1, Cross-Section Analysis, (Test No. 6)

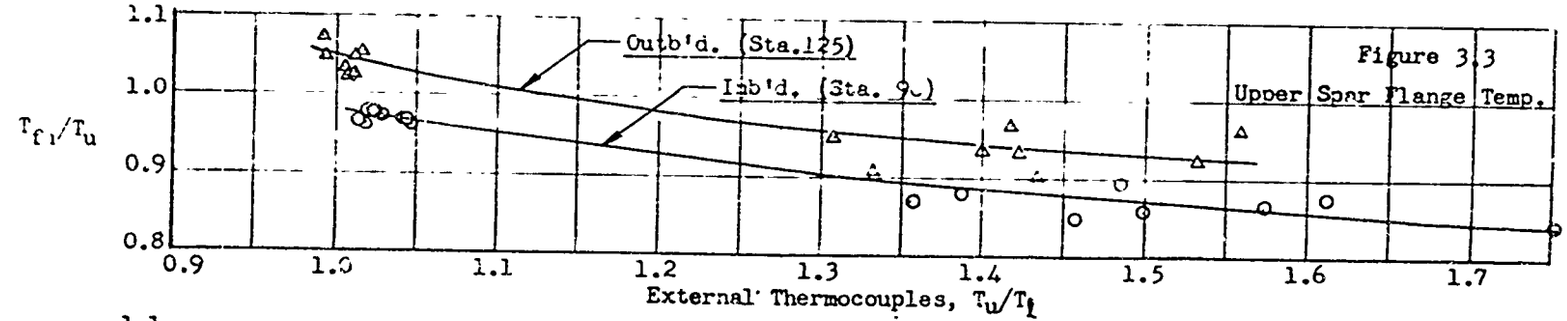

Figure 3.3
Upper Spar Flange Temp.

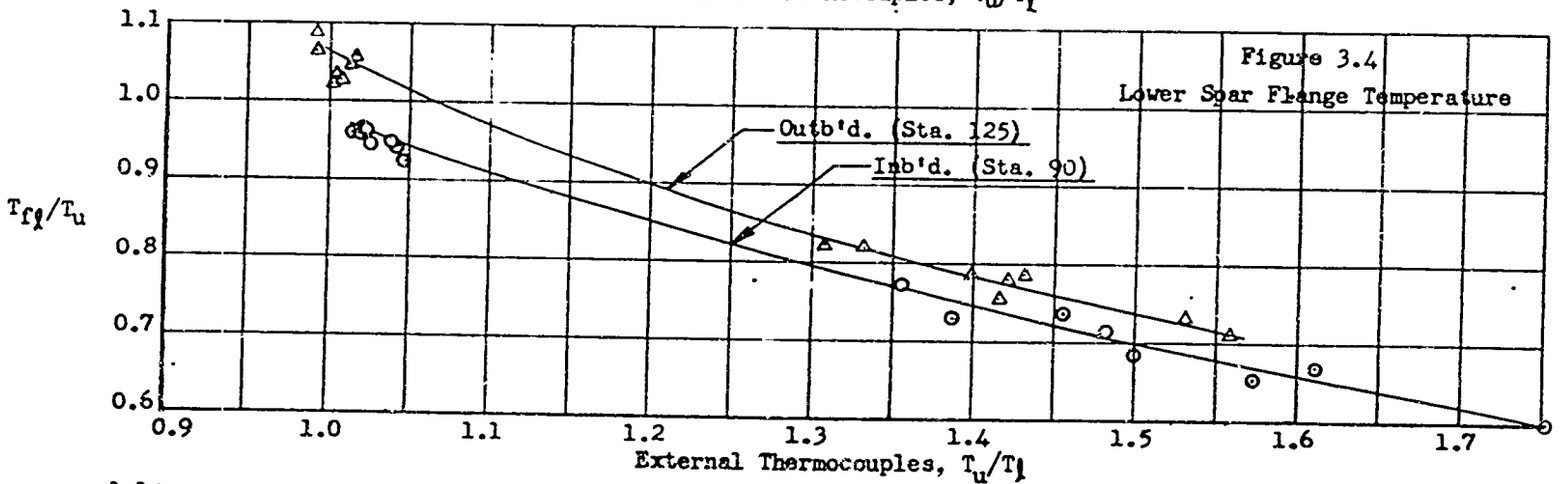

Figure 3.4
Lower Spar Flange Temperature

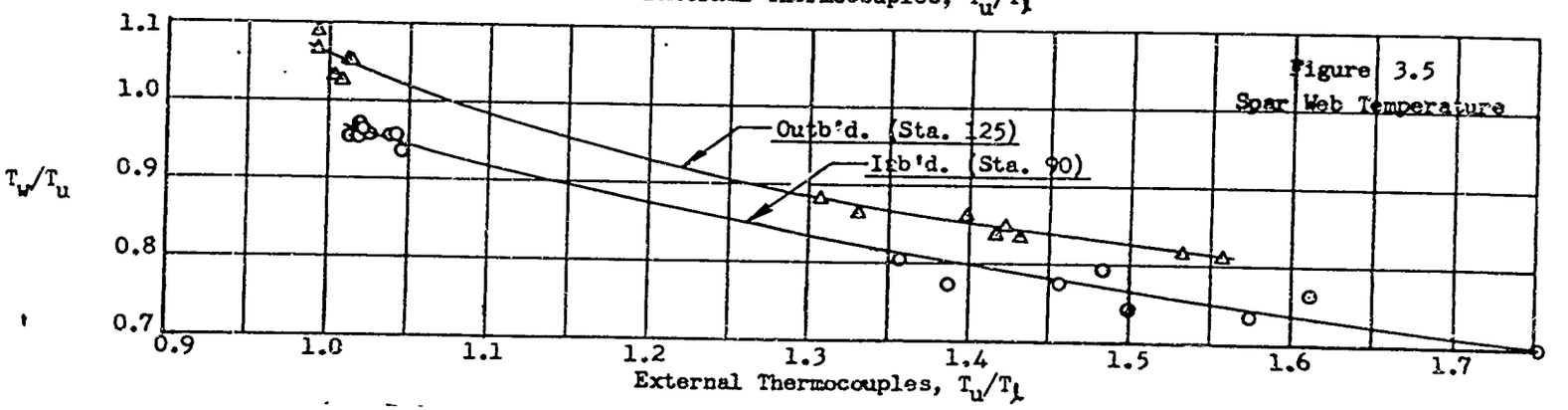

Figure 3.5
Spar Web Temperature

3.2 Inboard Splice Joint Temperature Survey

Internal and external thermocouples in the splice joint area in Test 8 provided data for each of the four elevated temperature environments whereby the internal temperature distributions in the main-box-skin, main-beam-fitting splice joint area could be approximated for the static test components. As noted in Section 3.1 for the cross-section survey, the external thermocouples on the temperature survey stabilizer and the static test stabilizers are located identically to allow reliable temperature relationships to be established. The relationships between external temperatures and internal temperatures were established by the temperature surveys of test 8 in which temperature studies were made with the required temperature environments of the anticipated steady-state elevated temperature test conditions. The four elevated temperature conditions were basically those described in Items (a), (b), (c), and (d) of Section 3.1 with a fundamental difference being that the heated area was generally restricted to the area bounded by the ribs at the inboard and outboard ends of the main beam fitting, and between the front and rear beams. The difference in material between the main beam fitting (steel) and the main box skins (aluminum alloy) together with the mechanically-fastened joint makes a theoretical temperature distribution highly questionable and data from a heated stabilizer is considered more reliable.

Four temperature survey tests were performed for the anticipated static test temperature environments by NAEC-ASL as reported in Volume III. As in the cross-section temperature survey tests (Section 3.1), the internal temperature predictions for all test stabilizers were made by relating the upper and lower main beam fitting flanges and the main beam web temperatures to the temperature gradient between the upper and lower main box skins. The gradient is defined by the thermocouples in the upper and lower skins directly over the main beam fitting flange at the stations shown in Figure 3.6. The non-dimensional procedure results in the general sets of curves for internal element temperature prediction shown in Figure 3.7 for the upper and lower main beam fitting flanges and splice plate and in Figure 3.8 for the forward and aft interbeams. Figures 3.7 and 3.8 were defined by thermocouple data from the four temperature survey tests and are used in conjunction with the spanwise temperature distribution curves for each test as shown in the typical example in Figure 3.6. For the specified temperature condition in Figure 3.6 the proper value of T_u/T_ℓ is selected at any desired station and the values of flange and web temperatures are determined by reading on the appropriate curve of Figure 3.7 or 3.8 for the particular value of T_u/T_ℓ .

These curves are sufficiently accurate for temperature definition, both for temperature data input to the analysis as well as the definition of temperature-time exposure histories for defining material properties.

The definition of the terms T_u, T_ℓ, T_{fu}, $T_{f\ell}$, and T_w in Figures 3.6, 3.7, and 3.8 is identical to that shown in Section 3.1.

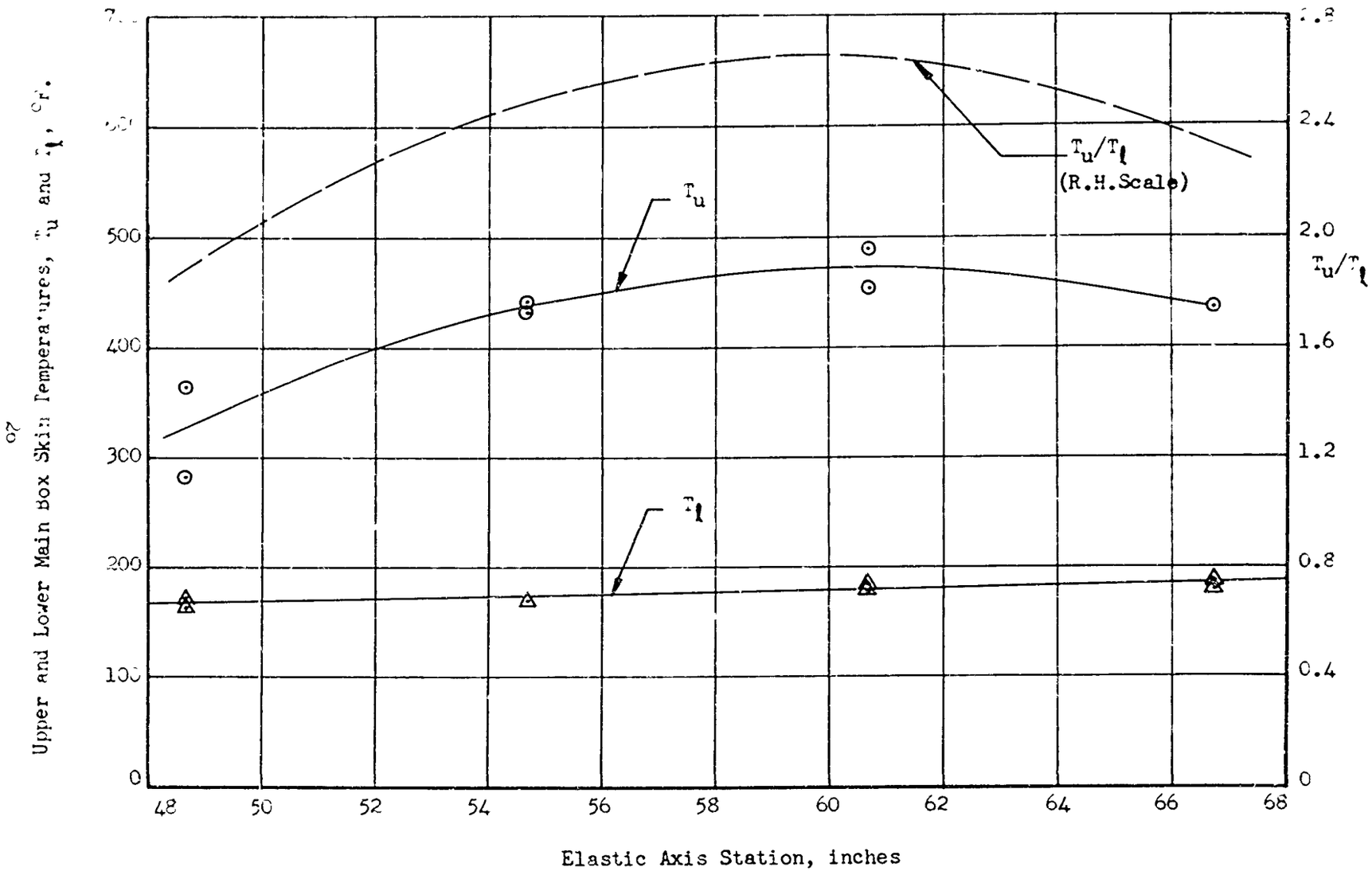

Figure 3.6 Typical Spanwise Temperature Distribution Curve, Part 2, Inboard Splice Joint Study, 425°F, Unsymmetrical Condition

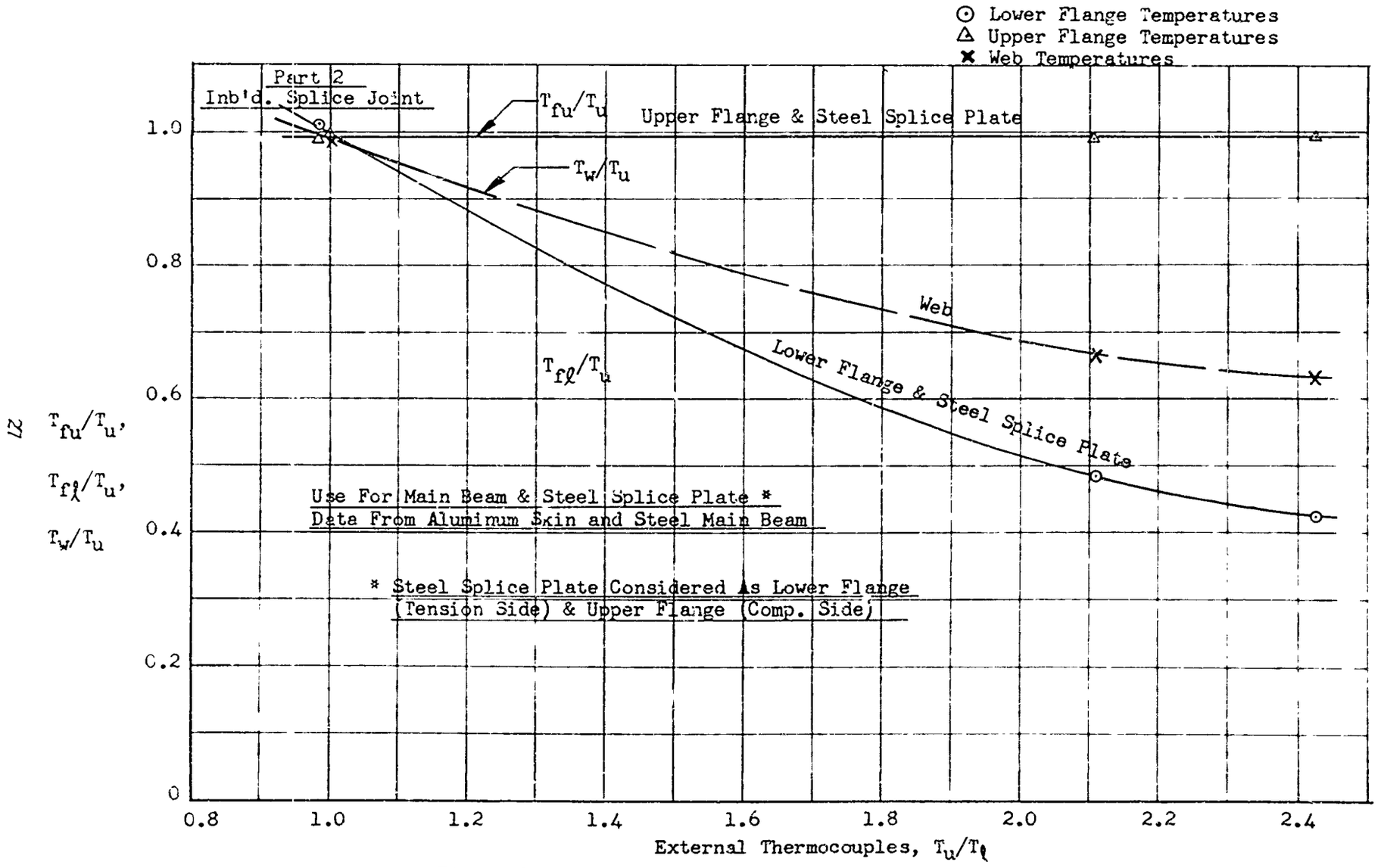

Figure 3.7. Main Beam Fitting Flange and Splice Plate Temperatures

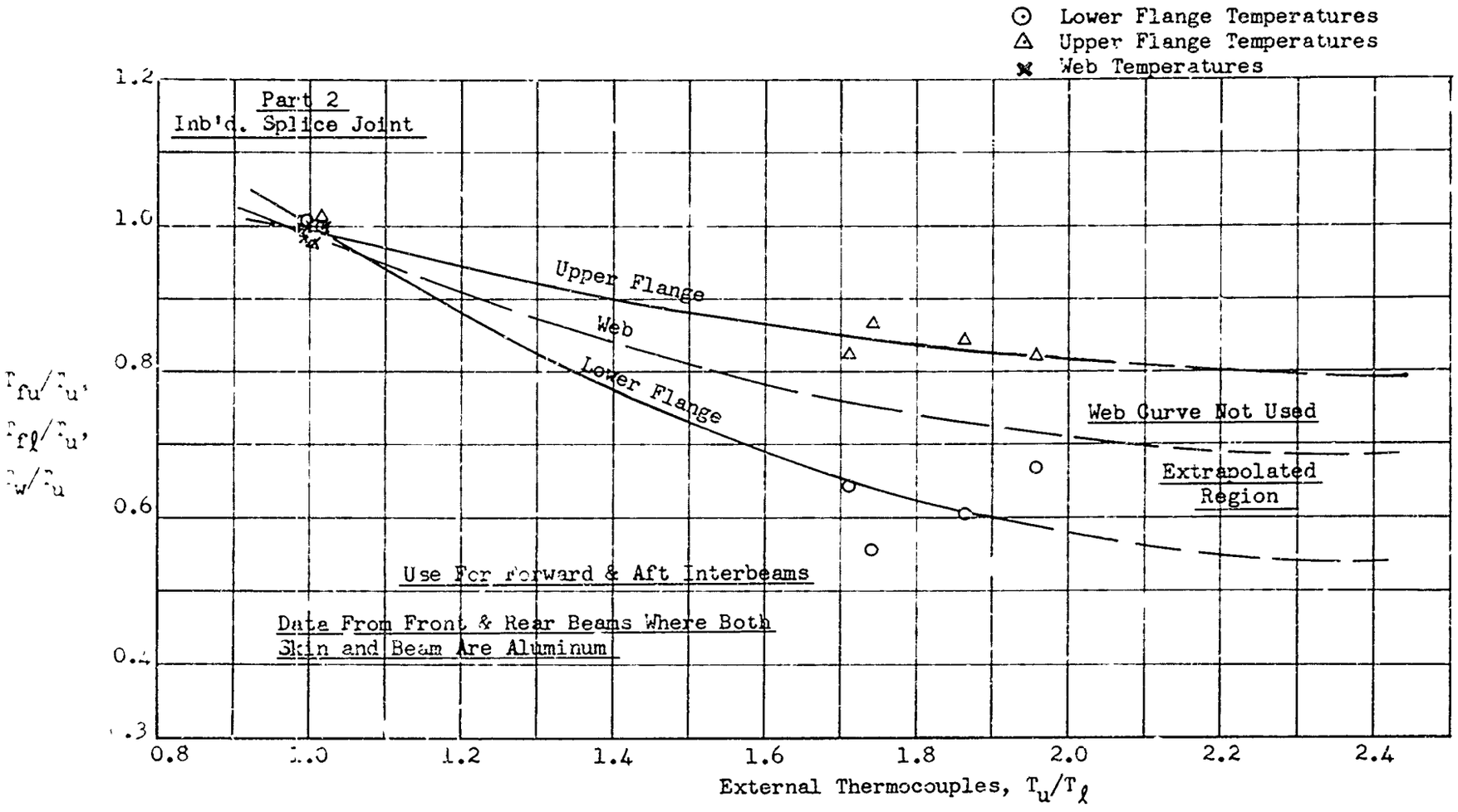

Figure 3.8. Forward and Aft Interbeam Temperatures

3.3 Equivalent Input Temperatures for Unsymmetrically Heated Inboard Splice Joints

For the two unsymmetrically heated inboard splice joints (Test No's. 11 and 12, 250°F. unsymmetrical and 425°F. unsymmetrical, respectively) the temperature distributions and restraint conditions are such that the thermal strains computed by cross-section bending procedures and those computed by axial procedures only, using the actual plate element temperatures, are not the same. Therefore, for axial load equivalence to provide the same thermal strains as the unrestrained-in-bending condition, it is necessary to compute equivalent main beam flange or main box skin temperatures to use in the analysis to replace the actual temperature when calculating the thermal strains. In this case the skin temperature was taken from the elevated temperature surveys and a fictitious flange temperature for equivalent thermal strains was calculated.

Expressions for the axial strains e_s and e_f, which are known from calculations by the cross-section thermal strain analysis, are

$$\left.\begin{aligned} e_s &= -\alpha_s T_s + e_T \\ e_f &= -\alpha_f T_f + e_T \end{aligned}\right\} \text{ axial thermal strain equations} \qquad (3.3.1)$$

where

$$e_T = \frac{E_s A_s \alpha_s T_s + E_f A_f \alpha_f T_f}{E_s A_s + E_f A_f} \qquad (3.3.2)$$

Equating e_T values and solving for flange temperature, T_f ,

$$T_f = \frac{1}{\alpha_f} (\alpha_s T_s + e_s - e_f) \qquad (3.3.3)$$

where T_f and T_s represent a temperature change from datum for the flange and skin elements, respectively, and e_s and e_f are the thermal strains obtained from the cross-section analysis for a ΔT step. The temperature change, T_s, in Equation (3.3.3) is the actual temperature change for the main box skin element. Geometric and material property data for Equation (3.3.2) is shown below.

Flange and Skin Data (Inboard Splice Joint)

$A_f = 0.772$ in.^{2}	$A_s = 3.58$ in^2
$E_f = 28.7 \times 10^6$ (Test No. 11)	$E_s = 9.2 \times 10^6$ (Test No. 11)
$= 28.5 \times 10^6$ (Test No. 12)	$= 9.1 \times 10^6$ (Test No. 12)
$\alpha_f = 7 \times 10^{-6}$	$\alpha_s = 13 \times 10^{-6}$
Actual $T_f = 59°F$ (Test No. 11)	Actual $T_s = 51°F$ (Test No. 11)
$= 111°F$ (Test No. 12)	$= 98°F$ (Test No. 12)

The calculated axial equivalent flange temperature for the two unsymmetrically heated splice joints (Test No's. 11 and 12) are as follows:

$$T_f = \frac{(13 \times 10^{-6})(51) - .000197 - .000175}{7 \times 10^{-6}} = 41.6°F. \text{ (Test No.11)}$$

$$T_f = \frac{(13 \times 10^{-6})(98) - .000422 - .000366}{7 \times 10^{-6}} = 69.4°F. \text{ (Test No.12)}$$

where $e_s = -.000197$ in./in.
$e_f = .000175$ in./in
} Test No. 11, 250°F Unsymm.

and
$e_s = -.000422$ in/in.
$e_f = .000366$ in./in.
} Test No. 12, 425°F. Unsymm.

are the thermal strain values calculated by the cross-section procedures. The actual temperature changes and the fictitious flange temperature changes are shown above only for the tension (critical) side of the beam which is also the cooler side.

For complete compatibility and equilibrium a constant strain on the skin and flange is necessary for equivalence to the axial load case. This constant strain is obtained by substituting the equivalent skin and flange temperatures in Equation (3.3.1) and solving for values of e_s and e_f. The difference between this strain and the e_s and e_f values for the cross-section thermal strain analysis is small and represents an additional applied compression strain on the skin and

flange elements in this case. This incremental strain is designated as e_c and the values are as follows.

e_c = -.000047 in./in (Test No. 11)

e_c = -.000103 in./in (Test No. 12)

This small strain represents an additional small compression load in the flange and skin on the tension side as calculated below.

$P = e_c(E_sA_s + E_fA_f)$ = -.000047 (55×10^6) = -2585 lbs (Test No. 11)

= -.000103 (54.6×10^6) = -5620 lbs (Test No. 12)

These loads are relatively small and of no major consequence in the strength evaluation of the splice joint; therefore, they were not added to the applied load input for the axial splice joint analysis.

The element input flange temperatures of 41.6°F. for Test No. 11 and 69.4°F. for Test No. 12 are specifically associated with the skin temperatures 51°F. and 98°F., respectively. Since the actual skin temperatures varied somewhat along the span of the splice joint area the analysis input values of the fictitious flange temperatures were also assumed to vary and were corrected for each element along the span by the gradient established by the above temperatures.

4.0 ANALYTICAL-EXPERIMENTAL COMPARISON STUDIES

4.1 Load Deformation Curves, Part 1

The load-deformation curves, Figures 4.2 through 4.6, use the bending moment at the particular elastic axis station as ordinate and the critical element strain as abscissa, where element (4) is the critical element at all cross-sections in all temperature environments. Element (4) is the center main box skin area between the forward and aft interbeams and was defined as the critical element (by the definition shown in Section 3.5.1 of Volume I where the element with the maximum permanent set after removal of all load and temperature is designated as the critical element.) Output data from the analysis showed element (4) to have the highest calculated permanent set strain. This was also indicated by the test results where the highest strain gage readings were just forward and aft of element (4). The mode of failure also indicated that skin element (4) was generally critical because of the compression instability failure of the stabilizers. The single exception was Horizontal Stabilizer Pilot Study a which failed in tension of the lower main box skin. The tension failure may be explained by the nearly equally critical nature of the tension and compression covers, high buckling (crippling) allowables of the compression covers, and possibly some slight variations in the cover plate manufacture and/or material properties. Figure 4.1 shows the cross-section and discrete element representation.

Each figure includes four separate groups of curves; one for each of the instrumented cross-sections at Elastic Axis Stations 91, 102, 113, and 124. In general, each group contains three curves; two associated with the analysis and one with the test data. A solid line represents the analytical load-deformation curve calculated for the temperature-load sequence +T, +P (apply temperature, then apply load) and is based on elevated temperature material properties. The dashed line represents the permanent set curve where the inelastic effects are associated with the temperature-load sequence +T, +P, -P, -T (apply temperature, apply load, remove load, then remove temperature) and room temperature recovery material properties after exposure to the test temperature environment. The experimental data is represented by specific data points and a solid curve drawn through these points to indicate that the test-analysis comparison is between the data points and the solid analytical curve. The early separation of the analytical load-deformation and permanent set curves indicates the onset of initial buckling in the forward and aft box magnesium skins which have extremely low critical buckling strains (e_{cr}). The data points shown represent the strain gage results at each elastic axis station using the "temperature on" strain readings as the reference zero. Therefore, the strain gage curves shown represent an experimental applied load-deformation

curve which is comparable to the solid analytical curve. The better overall reliability of the room temperature test may be noted in this group of curves. It should also be noted that agreement between test strain data and plane-strain analysis results is better at the three inboard stations which are farthest away from the local effects of the outboard loading former. The lower strain gage readings at a given bending moment at Elastic Axis Station 124 appear to reflect the effects of shear lag typical of a shallow beam loaded by a single concentrated load. The extension of the experimental strain data into the inelastic region at Elastic Axis Stations 102 and 113 indicates this spanwise segment to be critical with failure expected between the two stations, probably closer to Elastic Axis Station 102 due to the larger inelastic strains shown at this station.

Two groups of load-deformation curves are shown for Horizontal Stabilizer No. 4 (425°F. symmetrical temperature environment) since the heat lamps were shut off just prior to the end of the load application portion of the test. The decreases in structural temperature associated with the time between lamp shut-off and failure of the stabilizer apparently warranted material property recovery considerations in the analysis. However, when the lower temperature and higher properties were considered, the analysis tended to over-predict the failure by a wider margin than expected when compared with the results of the other tests. In order to investigate the material properties effect the analysis was also performed using material properties associated with the higher temperatures prior to lamp shut off. The question then arises as to whether the material property changes from the higher to the lower temperature actually had time to take place and stabilize before failure occurred. Subsequent tensile coupon data from Horizontal Stabilizer No. 4 shows that the actual yield stress values were approximately 4% less than the values used for the "lamps off" analysis using recovered material properties at the temperature at time of failure. Refer to Section 4.5 for the tensile coupon data evaluation. This may indicate the presence of a lag in material properties vs. soaking time which may vary considerably in highly transient temperature environments. In this case the prediction of overall strength at any particular time within the transient temperature environment may be quite difficult since material properties data may not be sufficient or defined well enough in their present form. Further study in this area appears to be warranted where structural components subjected to severe transient heating could be loaded to failure fairly rapidly after exposure to temperature environments where loss and recovery would occur rapidly. The material properties for the highly transient temperature environment must be defined specifically at the time of failure by using tensile coupons from the test components and reference coupons from similar plate material. This procedure for material properties verification was investigated and the results are shown in Table 3.15 of Volume II and in Section 4.5 of this volume.

Good agreement is shown by the comparison of strain gage data points with the analytical curve, particularly in the region of failure between Elastic Axis Stations 102 and 113 for all temperature environments. In most cases the elastic slope shown by the experimental data indicates slightly greater stiffness than the analytical data. Although no specific reason for this difference is known, there are several items which contribute to this trend. The geometry (skin thickness, spar flange and web thickness, tolerances, effects of local pads) and material properties (primarily the modulus of elasticity) may vary. The strain gages are not located exactly on the centroid of analysis element (4) . The element idealization for the analysis procedures may tend to slightly underestimate the moment of inertia of the cross-section. Finally, the loading former and load line setup (canted inboard for normal surface loads at yield load) produces slightly smaller bending moments at each elastic axis station than those used for plotting the experimental data. This effect was produced by the large deflections and relatively small radius of curvature of the stabilizer at yield load where the components of the normal surface load gave somewhat reduced bending moments at each cross-section.

The strain data plotted in Figure 4.6 for the 425°F. unsymmetrical temperature environment (Horizontal Stabilizer Test 6) are particularly noteworthy since strain data was obtained at relatively high strains (.010 in./in.) very close to ultimate load.

Element Description

(1) & (30) Stainless steel leading edge

(2), (10), (13), & (21) Magnesium alloy forward and aft box skins

(3), (4), (5), (14), (15), & (16) 7079-T6 aluminum alloy main box skins

(6), (7), (8), (9), (17), (18), (19), & (20) 7079-T6 aluminum alloy beam flanges

(11) & (12) 7075-T6 aluminum alloy trailing edge honeycomb facings

(22), (23), (24), (25), (26), (27), (28), & (29) 7079-T6 aluminum alloy beam webs

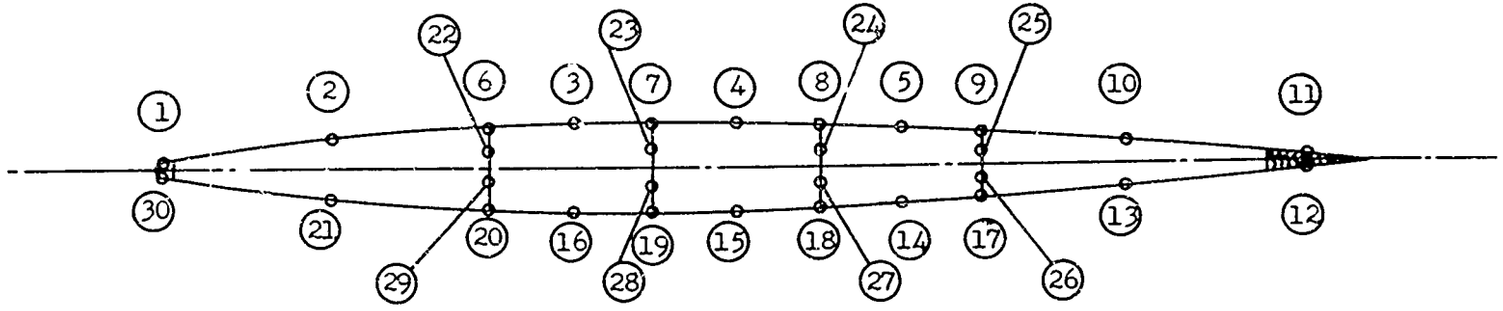

Figure 4.1
Cross-Section Geometry, Part 1
Elastic Axis Station Structural Element Locations

Element (4) is the critical element at all elastic axis stations. Refer to Figure 4.1.

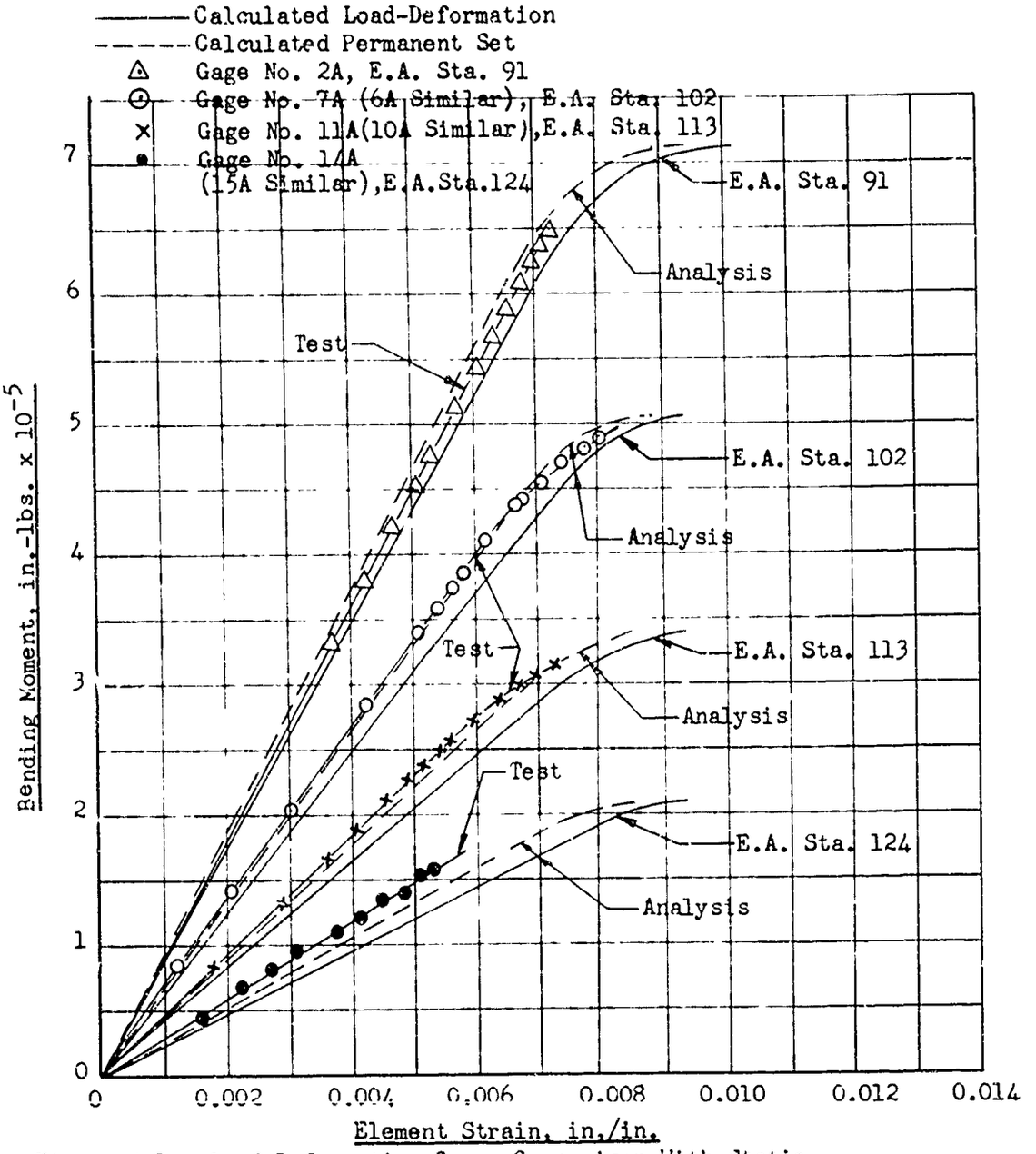

Figure 4.2. Load-Deformation Curve Comparison With Static Test Results, Room Temperature

Element (4) is the critical element at all elastic axis stations. Refer to Figure 4.1.

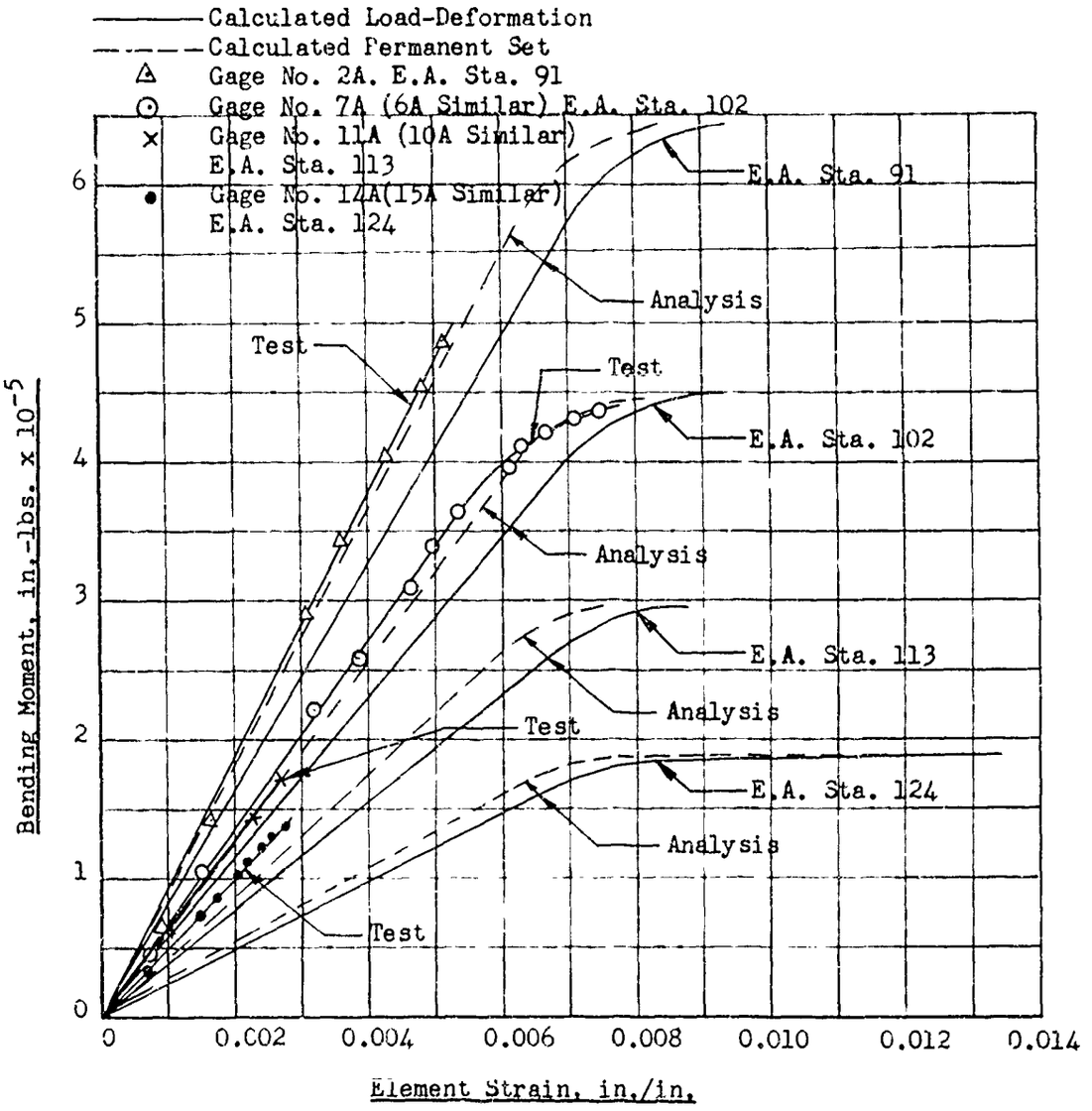

Figure 4.3 Load-Deformation Curve Comparison With Static Test Results, 250°F, Symmetrical

Element (4) is the critical element at all elastic axis stations. Refer to Figure 4.1.

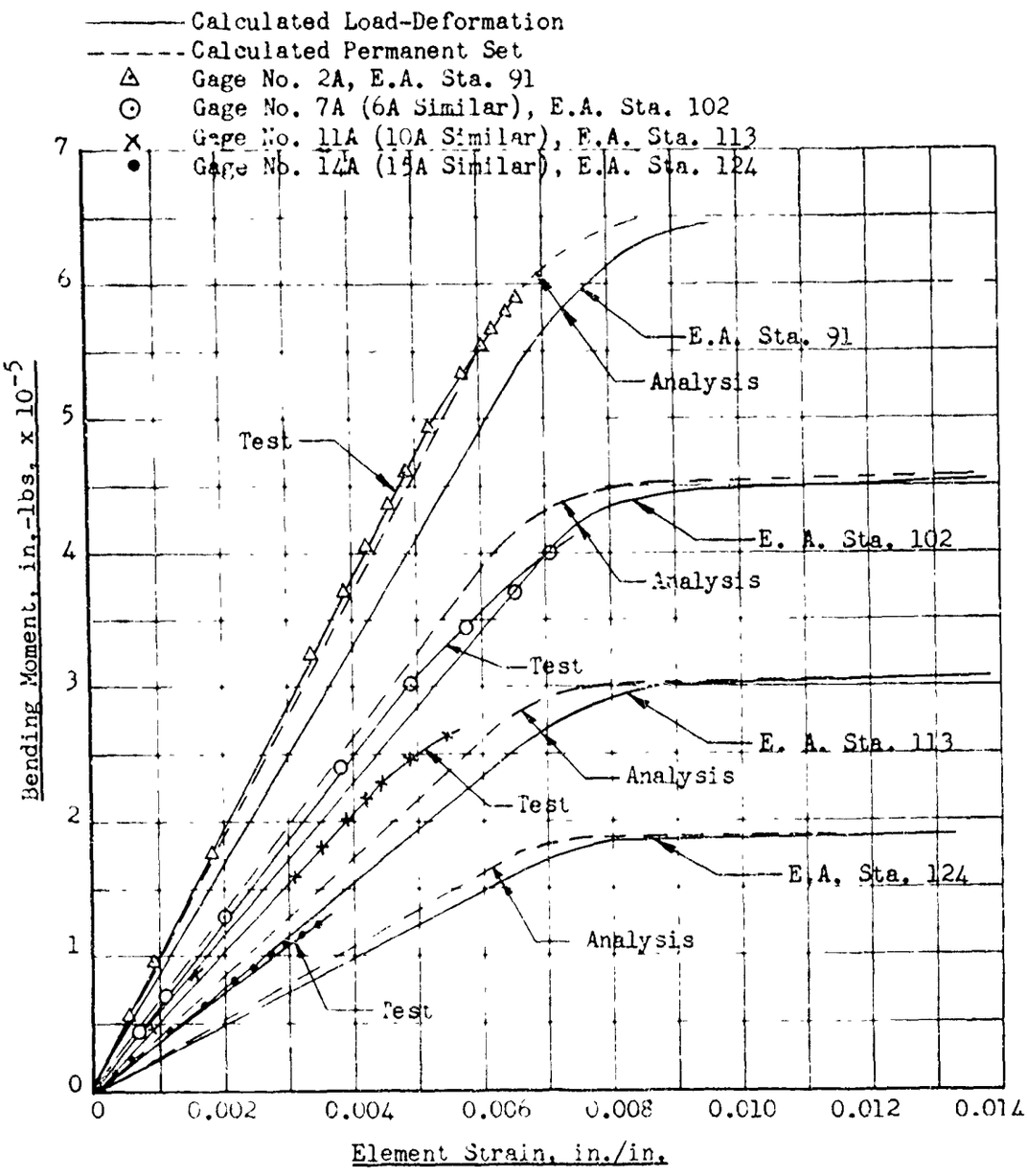

Figure 4.4 Load-Deformation Curve Comparison With Static Test Results, 250°F. Unsymmetrical

Element (4) is the critical element at all elastic axis stations. Refer to Figure 4.1.

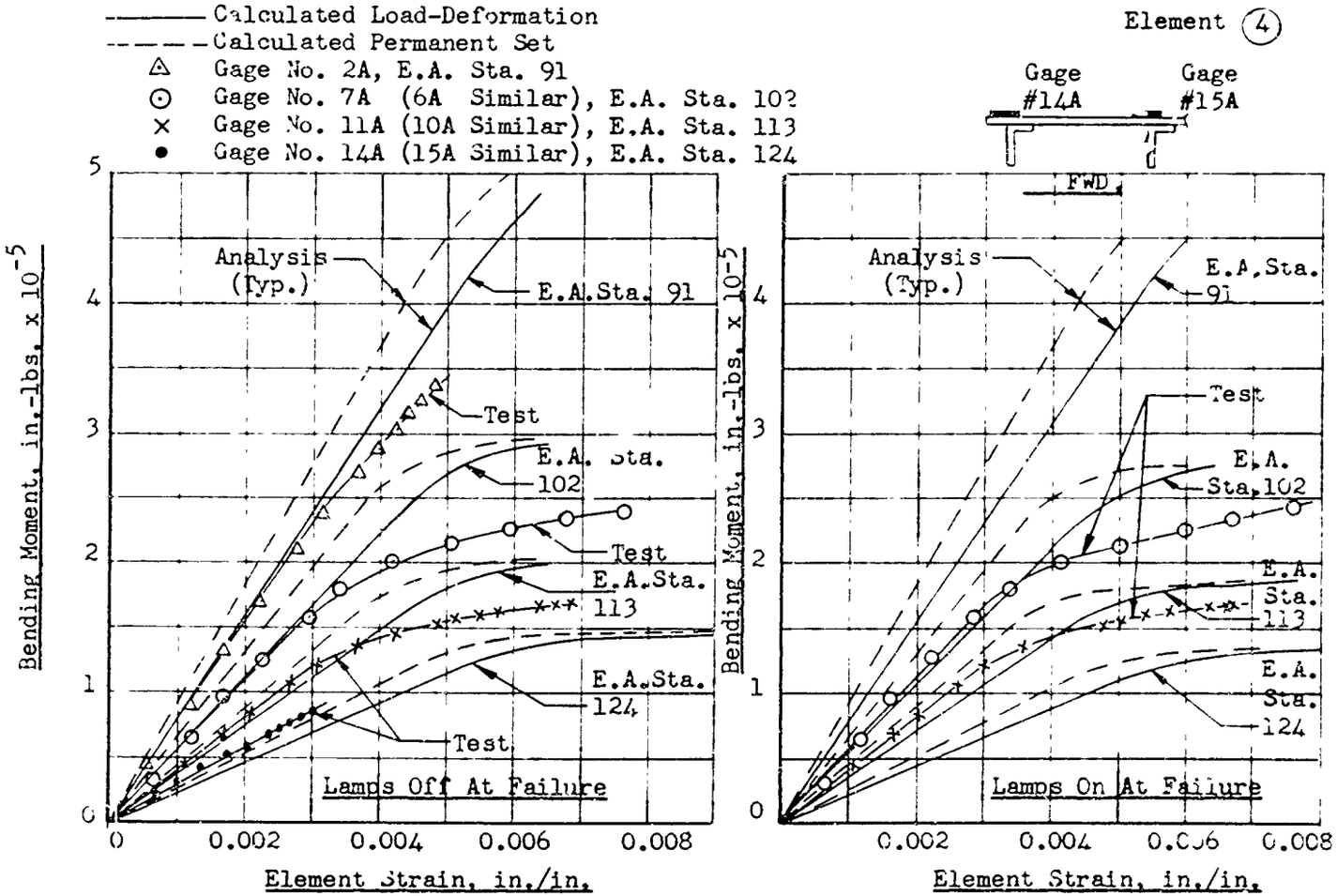

Figure 4.5 Load-Deformation Curve Comparison With Static Test Results, 425°F, Symmetrical

Element (4) is the critical element at all elastic axis stations. Refer to Figure 4.1.

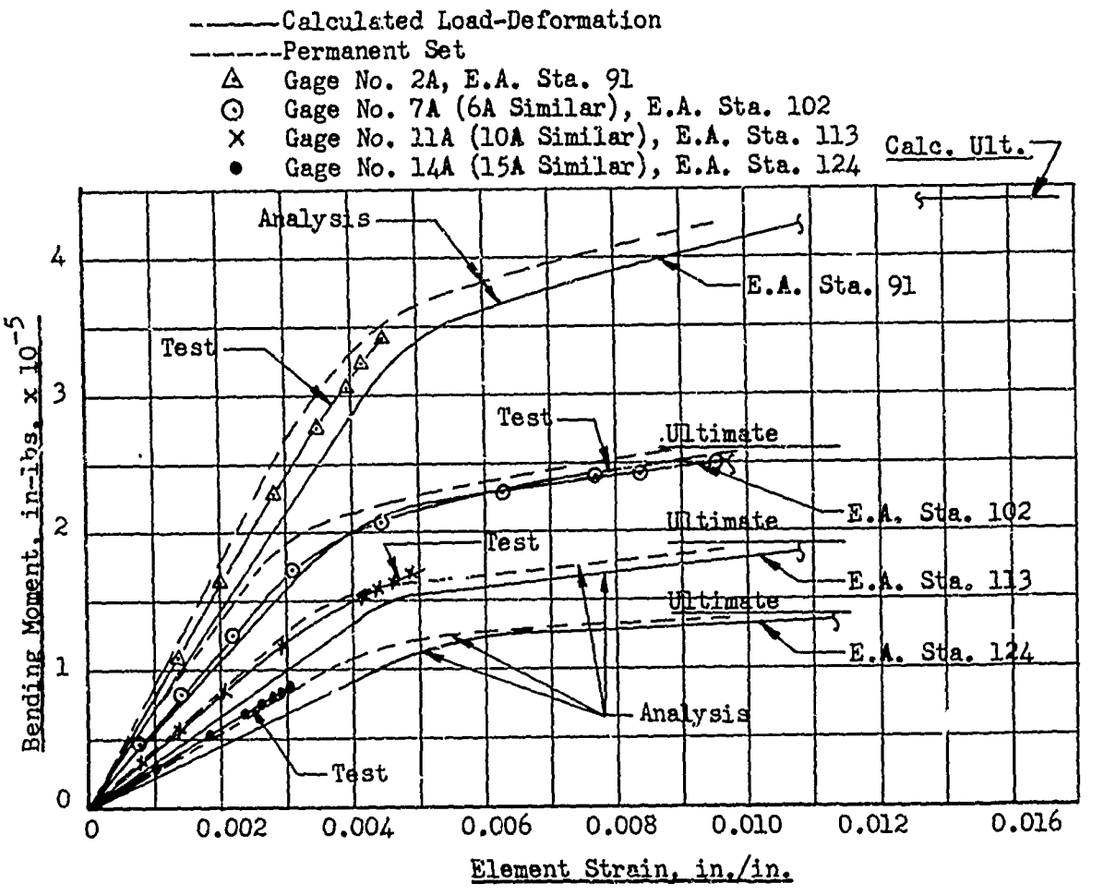

Figure 4.6. Load-Deformation Curve Comparison With Static Test Results, 425°F, Unsymmetrical

4.2 Available Ultimate Strength and Critical Station Selection, Part 1

Since the actual calculations are performed for the four specific instrumented cross-sections, the critical cross-section at which failure could be expected cannot be determined directly. However, since the structure is continuous and no sudden or major changes in cross-section occur within the test region, it is possible to plot a curve of available ultimate strength versus elastic axis station for each temperature environment. The expected failure station defined by analysis is determined by the intersection or point of tangency of the applied moment curve with the available strength curve. This intersection or tangent point also indicates the value of the critical bending moment at which the failure can be expected. The applied bending moment distribution is represented by a straight line with L' = 0 at Elastic Axis Station 135. This line drawn tangent to the available strength curve represents the ultimate applied bending moment distribution for a single concentrated load at Elastic Axis Station 135 (outboard loading former location). These curves are shown in Figures 4.7 through 4.11 for each of the five test temperature environments. The test ultimate loads and failure station are also indicated on these curves by individual data points for each horizontal stabilizer. Figures 4.7 through 4.11 are presented as another means of demonstrating the feasibility of the applied load ratio method and comparing analytical and test data. If a heated test structure had severe spanwise transient temperature distributions then thermal stress and material property degradation effects would vary considerably along the span. In this case it is entirely possible that the critical station for the simulated room temperature test may be quite different from that for the elevated temperature test. For the simulated static test this may mean a redistribution of external applied shear loads and a modified shape for the test applied shear and bending moment curves. The additional complexity and work involved to investigate critical station variation between elevated temperature and room temperature is relatively small since the required data would be available from the cross-section calculations. Essentially all that is required are additional curves similar to Figures 4.7 through 4.11 with allowable yield and ultimate bending moment, and yield and ultimate applied bending moments plotted versus span.

Although the curves in Figures 4.7 through 4.11 show only the ultimate load comparison the same procedure can be followed for yield load, limit load, or any selected level of the applied load which represents a design criterion. Yield curves would be of particular interest when the materials and/or structural geometry are such that there is a distinct difference between the yield and ultimate

load. However, in many realistic cases the airframe component will fail by compression instability where yield and ultimate are very nearly the same value. The horizontal stabilizer failures were of this type where yield data based on 0.002 in./in. offset strain of the load-deformation curves of Section 4.1 would not produce significantly lower curves than those shown for ultimate in Figures 4.7 through 4.11. Past experience on crippling failures and the study of various semi-empirical approaches to crippling analysis as well as the previous box beam studies of Reference (d) tends to confirm the yield load criteria for compression-loaded structures. For this reason, no yield curves are shown and the yield-critical and ultimate-critical stations are assumed to be the same.

The variation in the location of the contact point of the tangent line and the calculated available ultimate strength curve shows a generally critical span to exist between Elastic Axis Stations 102 and 113 for this particular applied moment distribution.

The analytically predicted ultimate loads (bending moments) and failure stations shown in Tables 5.1, 5.2, and 5.3 were obtained from the curves of Figures 4.7 through 4.11 where the predicted failure station is defined by the point of tangency of the applied moment curve with the ultimate allowable moment curve.

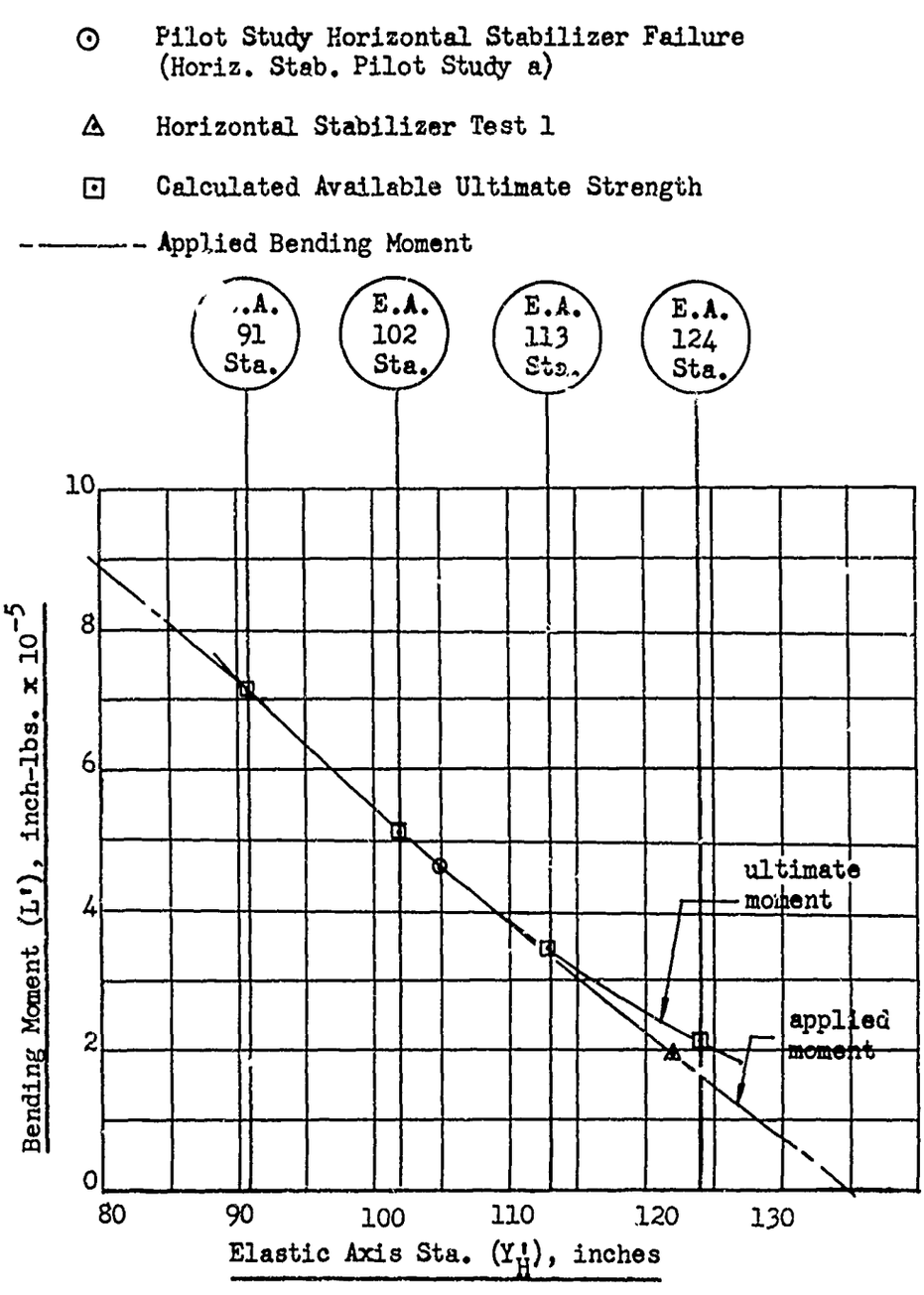

Figure 4.7
Ultimate Bending Moment vs. Span, Room Temperature

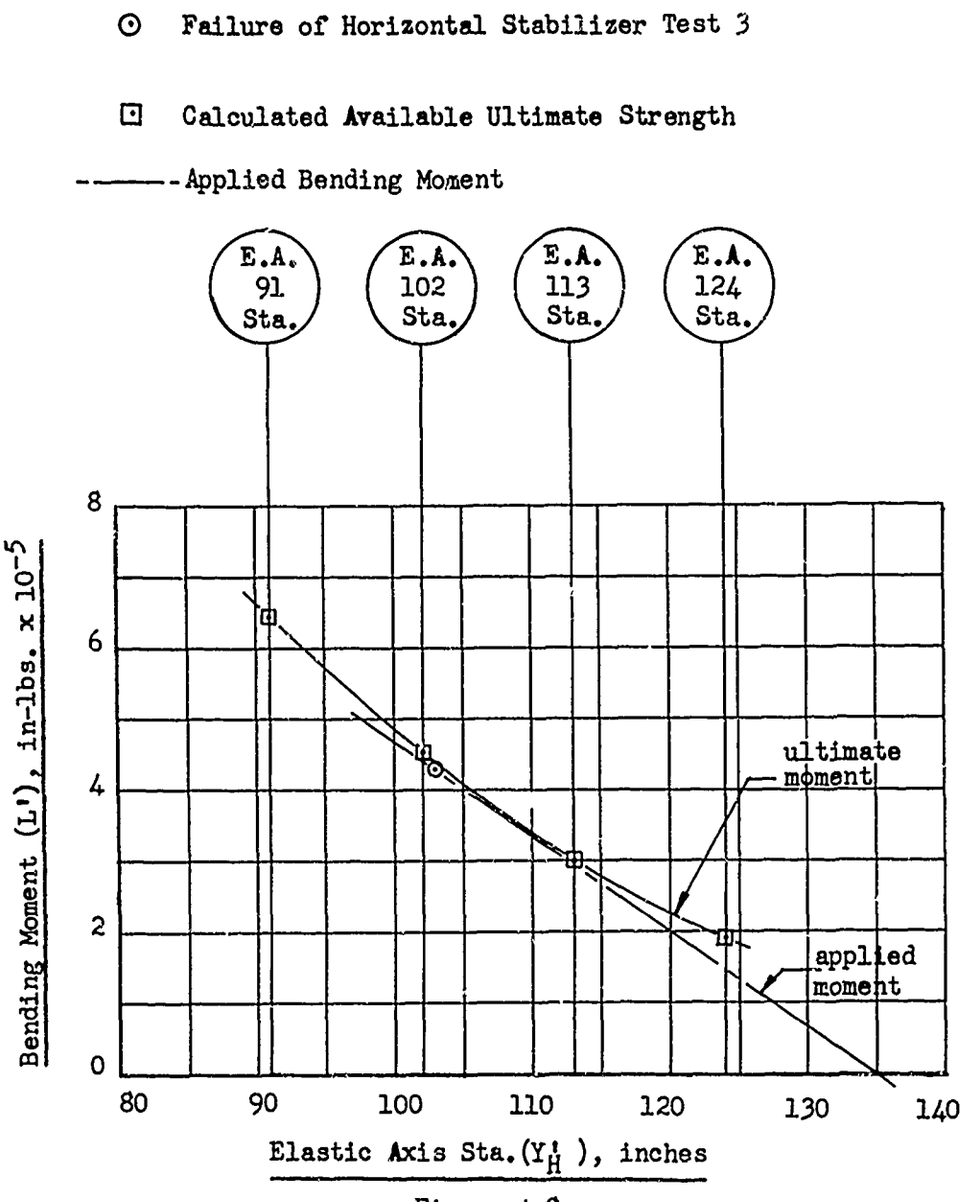

Figure 4.8
Ultimate Bending Moment vs. Span, 250°F. Symmetrical

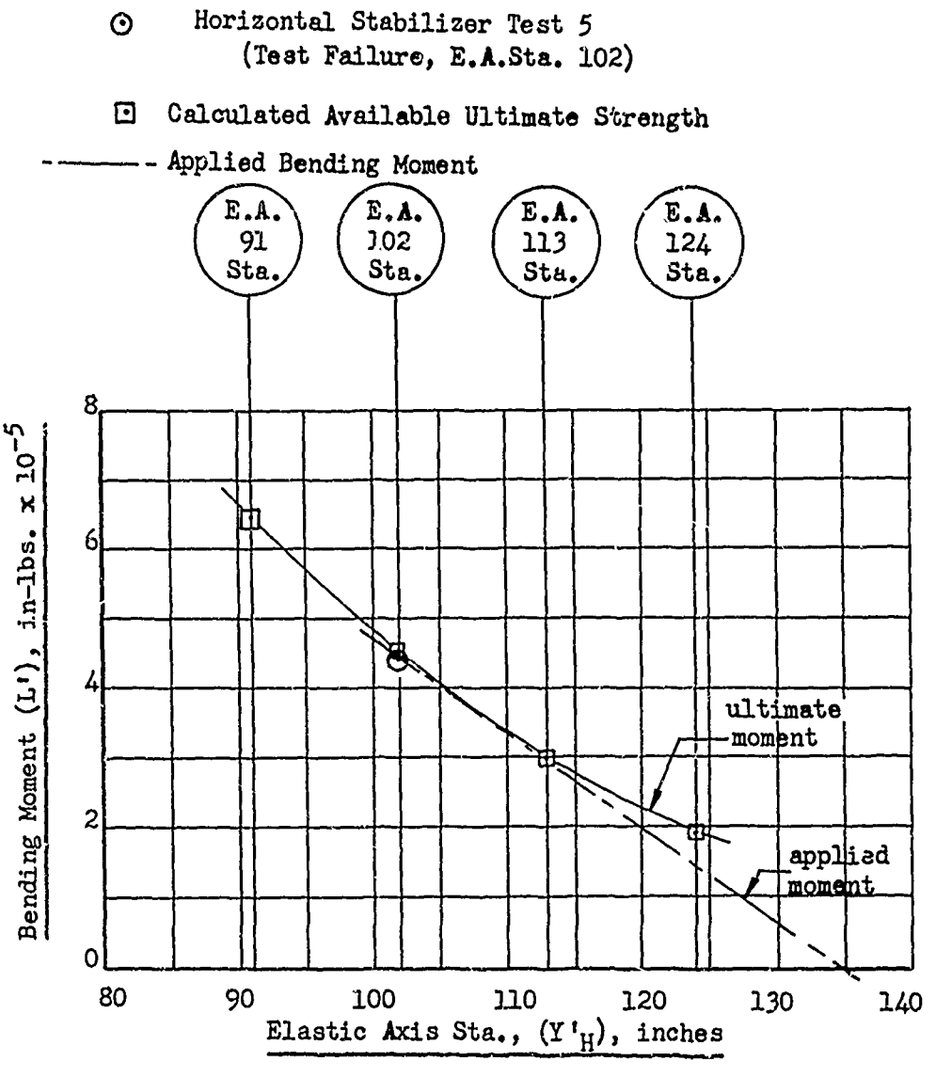

Figure 4.9
Ultimate Bending Moment vs. Span, 250°F, Unsymmetrical

⊙ Failure of Horizontal Stabilizer Test 4

✖ Calculated points using material properties for temperature distribution assuming heat lamps were on at time of failure. No temperature reduction and no recovery of properties.

⊡ Calculated Available Ultimate Strength (Recovery of material properties for lower temperatures as heat lamps were off prior to failure)

——— lamps-on
- ——— - lamps-off } Bending Moments

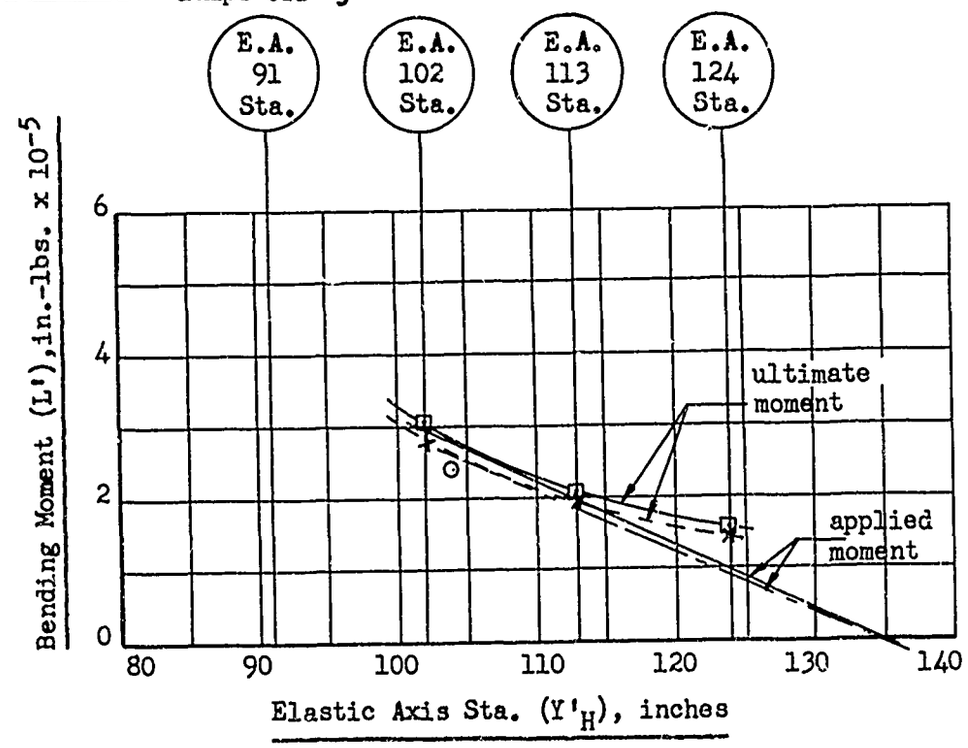

Figure 4.10
Ultimate Bending Moment vs. Span, 425°F, Symmetrical

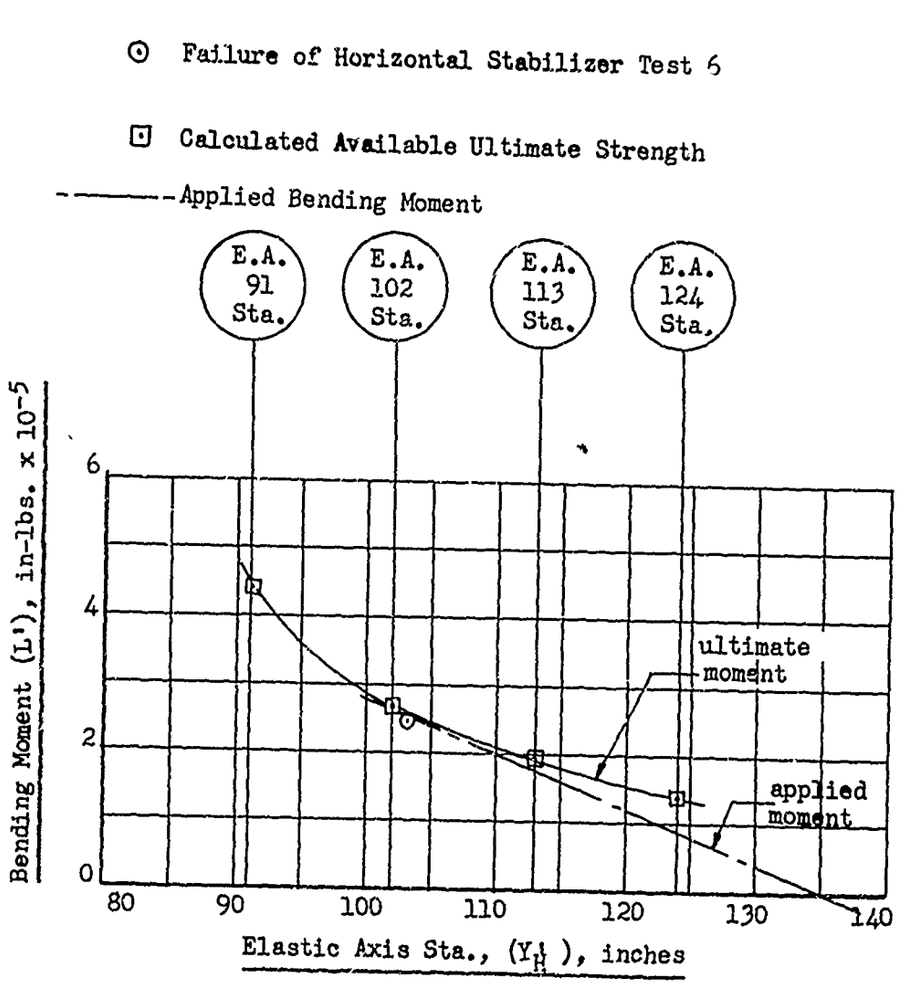

Figure 4.11
Ultimate Bending Moment v.s. Span, 425°F, Unsymmetrical

4.3 Analytical-Experimental Deflection Comparisons, Part 1

Deflection studies were performed in order to show comparison between analytical and experimental deflection results. Using the procedures shown in Section 3.4 of Volume I, the deflected shape of the horizontal stabilizer at failure, under the various thermal environments, was obtained. The analytical spanwise deflection plots were then compared to the corrected experimental spanwise deflection. The corrections to the experimental deflection data were obtained by plotting load-deflection curves for each gage and then correcting each plot to assure a zero intersection. Once each gage had been corrected to zero, the magnitude of the correction was added to the value of the deflection of that gage for all values of the applied load.

A deflection rate study was performed using both the corrected experimental data and the analytical deflection data. In the case of the analytical data, the actual test failure loads were used, rather than the predicted analytical failure loads, to denote the maximum applied loads. This was done in order to show a direct comparison between the analytical and the experimental results. Using various percentages of the test failure load to establish ΔP values, the values of $\Delta\delta$, the change in deflection corresponding to the load increment chosen, were computed. The deflection rate plots were then used to show a prediction of the failure station. A table has been included in Section 4.4 showing the predicted failure station due to the analytical deflection rate data, the predicted failure station due to the experimental deflection rate data, and the actual test failure station.

The plots presented in this section show a similarity between the experimental and analytical deflection data for the Part 1, or cross-section, portion of the study. No meaningful deflection data was obtained experimentally for the Part 2, or joint test, portion of the study. Since the Part 2 portion of the study was concentrated on the stabilizer root end joint, no spanwise test data was obtained outside the local area of the joint. Deflection gages used in the Part 2 study were located at the leading and trailing edges of the stabilizer. Thus, the gage readings were a function of the twist or warping of the cross-section. If the gages had been placed on the stabilizer main spars, then an indication of the rigid body rotation of the stabilizer would have been obtained. However, some chordwise, or anticlastic deflections were present which could not be accounted for within the limitations of the analytical procedures.

Figures 4.12 and 4.13 show spanwise plots of calculated deflection data and corrected experimental deflection data for the five tests. Load-deflection curves for each gage were plotted to obtain the necessary zero corrections for the experimentally obtained deflection data.

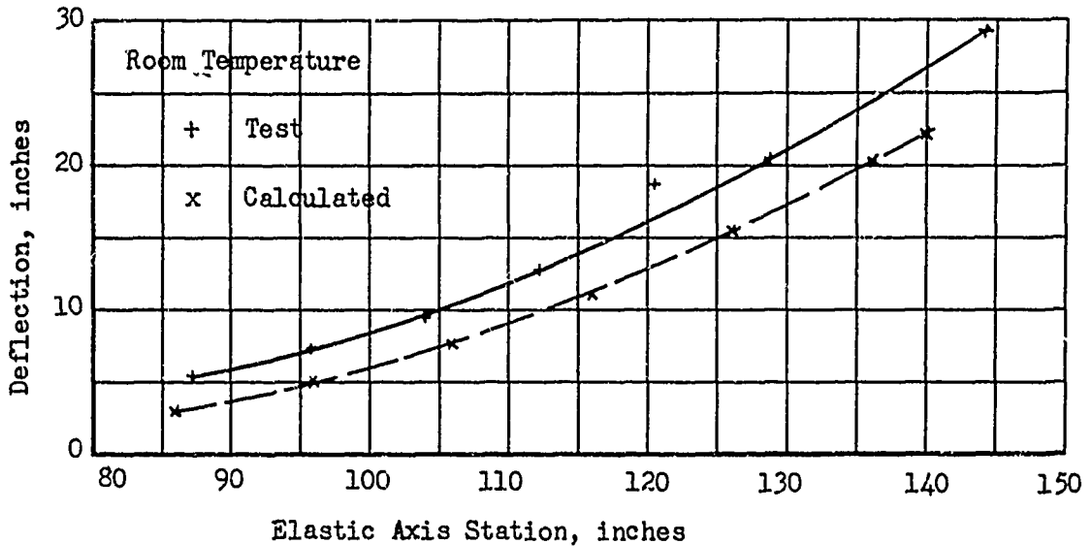

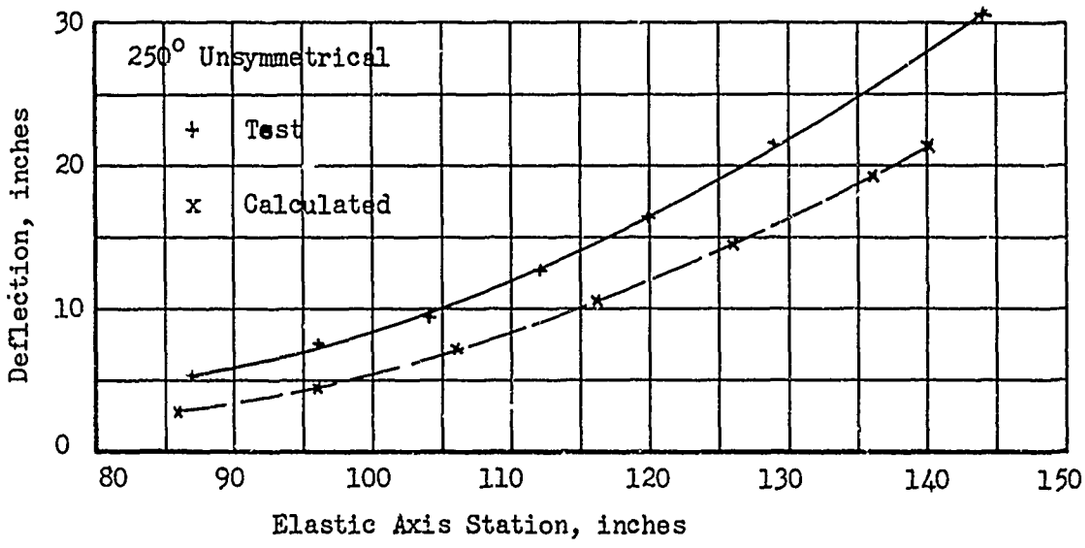

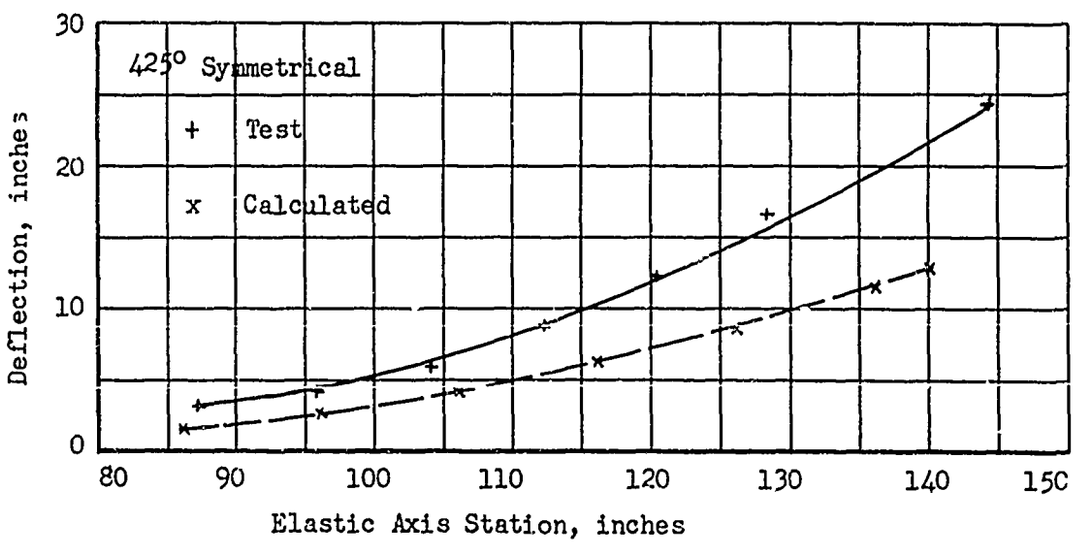

Figure 4.12. Comparison of Test and Calculated Deflections, Part 1

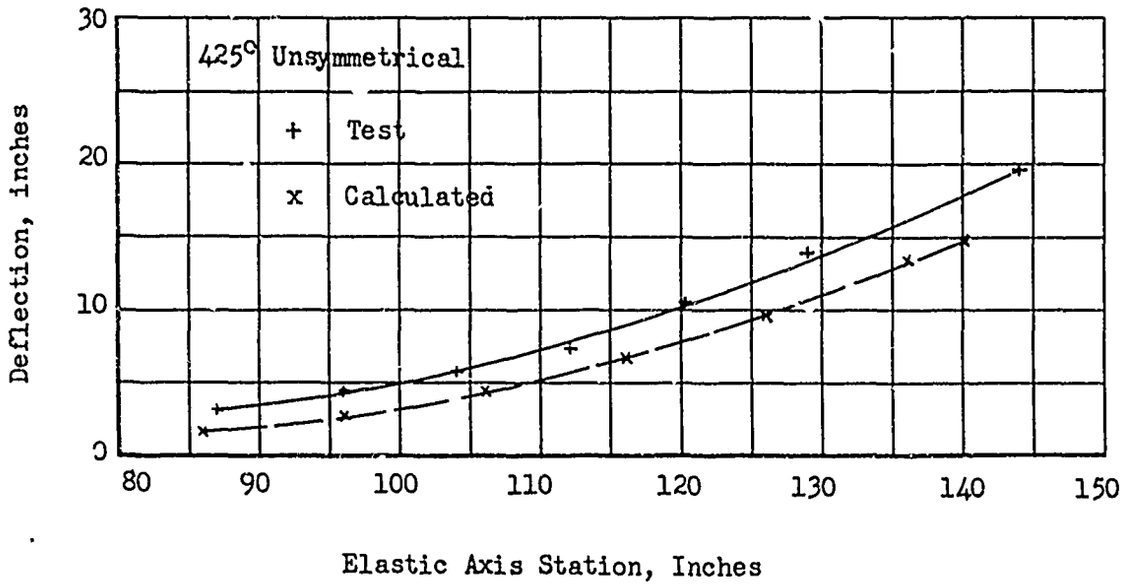

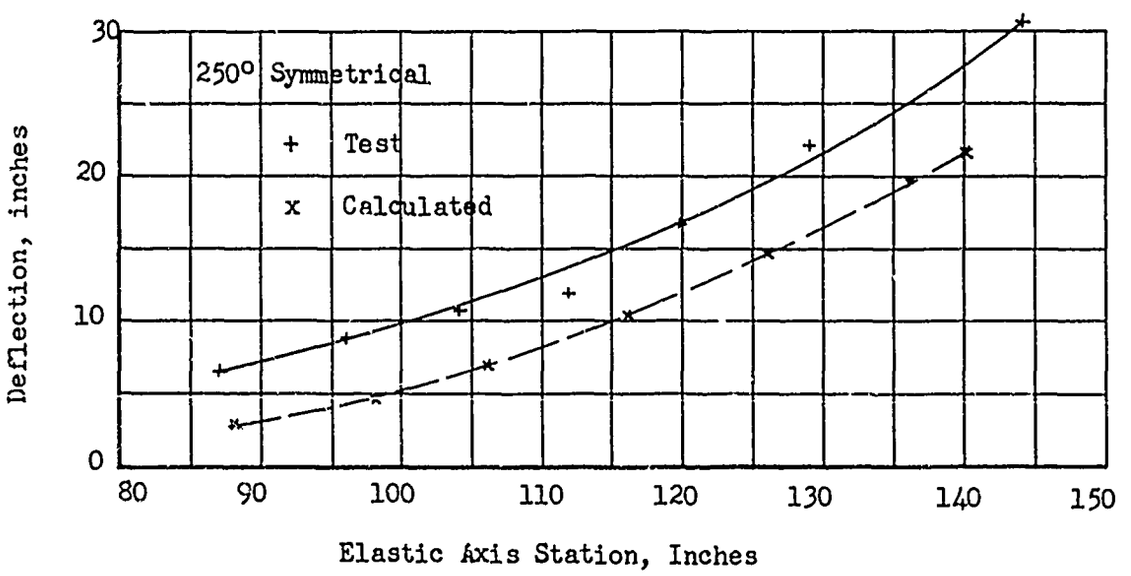

Figure 4.13. Comparison of Test and Calculated Deflections, Part 1

A study of the experimental and analytical deflection data reveals that the shape of the analytical curves agrees very well with the shape of the experimental deflection curves. In all cases the measured deflection was greater than the calculated deflection. In general, it can be seen that the analytical deflection curves vary from the experimental deflection curves as a function of some angle of rotation. If the root end of the stabilizer is rotated slightly the two curves will match almost exactly. The necessary angles of rotation vary from 1.7° to 3.7°. These small angles would be difficult to detect during the progress of a test unless dial gage information were available for root end fitting deflection. The inboard end of the stabilizer, with its attach fitting and horn, is incapable of transferring high reaction loads from the stabilizer without deformation. In the analytical procedure, of course, a fixed end condition is faithfully reproduced; and the root end slope is zero.

An investigation was undertaken to attempt to compare the results of the deflection studies with those of Allen, Reference (f). In conclusion 2 of his box beam study, Allen states that the deflection at ultimate load in a built-up aluminum alloy aircraft structure which fails by buckling is substantially independent of temperature up to at least 400° and decreases somewhat above this point. He then presents a formula by which the deflection of a structure at any temperature may be determined if the room temperature deflection is known. From Reference (f) the relationship is

$$\left[\frac{\delta_T}{\delta_{RT}}\right]_{ult} = K \frac{\left[\frac{P_T}{P_{RT}}\right]_{ult}}{\frac{(E)_T}{(E)_{RT}}} \qquad (4.3.1)$$

where K = 1 below 400°F. and K = 0.9 above 500°F.

Since this formula applies to elastic conditions, it produces good results in the elastic range. The assumption here has obviously been that buckling occurs at stresses below the yield stress. The use of 2024-T4 material in the Reference (f) study makes the above formula less general. In the present study, the 7079-T6 stabilizer skins failed in buckling, but the deflection at failure was somewhat more at 425°F. than Allen's formula predicted. At 250°F. the deflection at failure, as stated by Allen, was substantially the same as the deflection at

failure in the room temperature test. If we examine the variation in yield stress with temperature for 2024-T4 and 7079-T6 the reason for the inconsistency becomes apparent. A comparative plot of this variation is given in Figure 4.14.

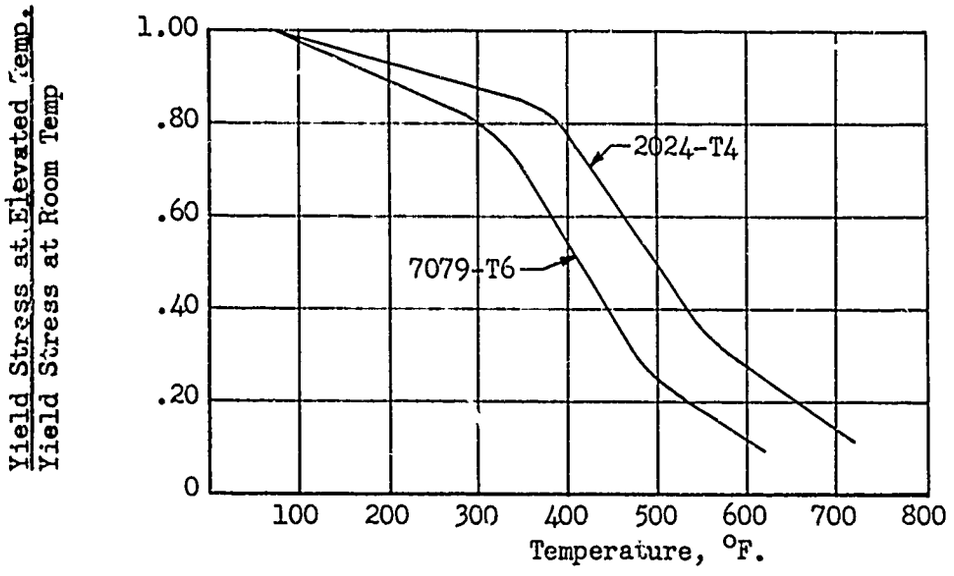

Figure 4.14 Variation of Yield Stress With Temperature

It can be seen from Figure 4.14 that the yield strength for 7079-T6 begins to drop off considerably at 300°F. whereas the 2024-T4 retains a high percentage of the room temperature value out to 400°F. Thus, in the case of the 7079-T6 material, the constant, K in Equation (4.3.1) was set equal to 0.9 for temperatures above 400°F. This is compatible with Allen's work except that the temperatures have been lowered by 100°F.

Since the load-deformation relationship for the stabilizer cross-section indicates inelastic action at failure, it was decided to modify Allen's formula into the following form where the deflections are considered to be a function of both yield stress and modulus of elasticity.

$$\left[\frac{\delta_T}{\delta_{RT}}\right]_{ult} = K \frac{\left[\frac{P_T}{P_{RT}}\right]_{ult}}{\left[\frac{(F_y)_T/E_T}{(F_y)_{RT}/E_{RT}}\right]} \qquad (4.3.2)$$

where K = 1 below 300°F. and K = 0.9 above 400°F. This form of the equation accounts for the variation in the yield strain with temperature.

Figure 4.15 shows curves of stabilizer tip deflection versus temperature. Included for comparison are the test deflections, the deflections given by Allen's Formula, and the deflections given by the modified Allen Formula. It can be seen that a formula of this type shows great promise as a means of predicting deflections empirically. No definite conclusions can be made at this time, however, due to the limited amount of available experimental data However, the comparisons illustrate deflection procedures to be an effective means of equivalence, or simulation since the deflections are a function of the spanwise strain variation.

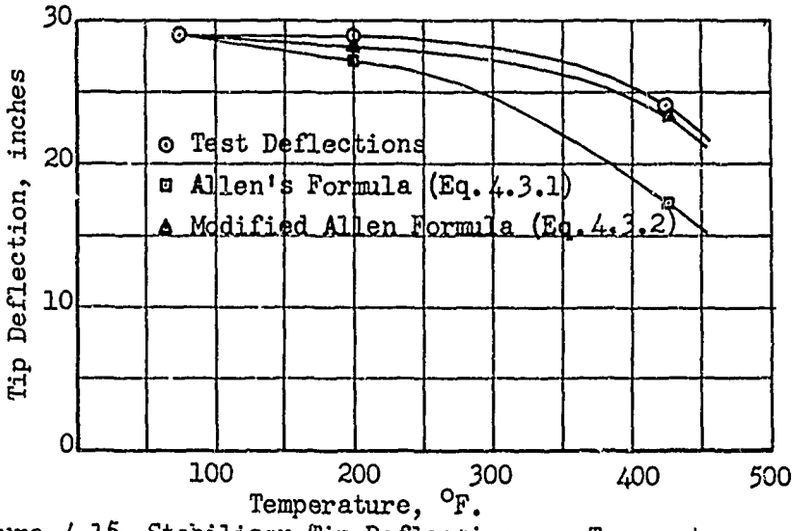

Figure 4.15 Stabilizer Tip Deflection vs. Temperature

4.4 Deflection Rate Study, Part 1

A deflection-rate study was performed using the experimental and analytical deflection data. Comparison plots are included for several cases. A table has also been included to show a comparison between the actual failure station and the failure station predicted by various techniques.

Figures 4.16 and 4.17 show the analytical and experimental deflection rate curves, respectively, for the 425°F. unsymmetrical test of Part 1. Similar curves were prepared for all of the tests. This particular test was chosen as an example to demonstrate the technique.

The analytical curves were drawn using the test failure load as the maximum load rather than the predicted analytical load. This was done to equalize the two sets of deflection rate data to the same load. The load deformation procedures, as given in Section 3.2, Volume I, for the analytical failure load prediction provided inelastic strains corresponding to the various input loads. These inelastic strains, added to the input elastic strains, give the deflections for the stabilizer under any given loading condition. From this data, the $\Delta\delta$ and ΔP values used for Figure 4.16 were obtained.

The experimental values of $\Delta\delta$ and ΔP were obtained from the data taken during the tests. The loads were used directly, while the deflection data was corrected. The data correction was performed by plotting the variation of each gage versus the load and offsetting the plotted curve to the zero origin. Study of Figures 4.16 and 4.17 shows that the plots are very similar. The failure station, as predicted by these plots, is essentially the same, and varies by two inches from the actual failure station.

Plots similar to those shown in Figures 4.16 and 4.17 were prepared for each of the five tests. The results of these plots are presented in Table 4.1. Also included in Table 4.1 are the actual test failure stations for each test and the failure stations as predicted by the analytical load-deformation procedures of Section 3.2, Volume I. In the case of the room temperature test and the 250°F. unsymmetrical test, no deflection rate solution was obtained. Due to relatively small magnitude of inelastic behavior at failure during these two tests, there was no appreciable change in deflection rate throughout the test, and thus no break point in the set of curves to indicate failure location. It is interesting to note that when the experimental deflection rate curves were unable to predict a failure station, the analytical deflection rate curves also failed to predict a failure station. Similarly, when one method did predict a failure station, the other did also.

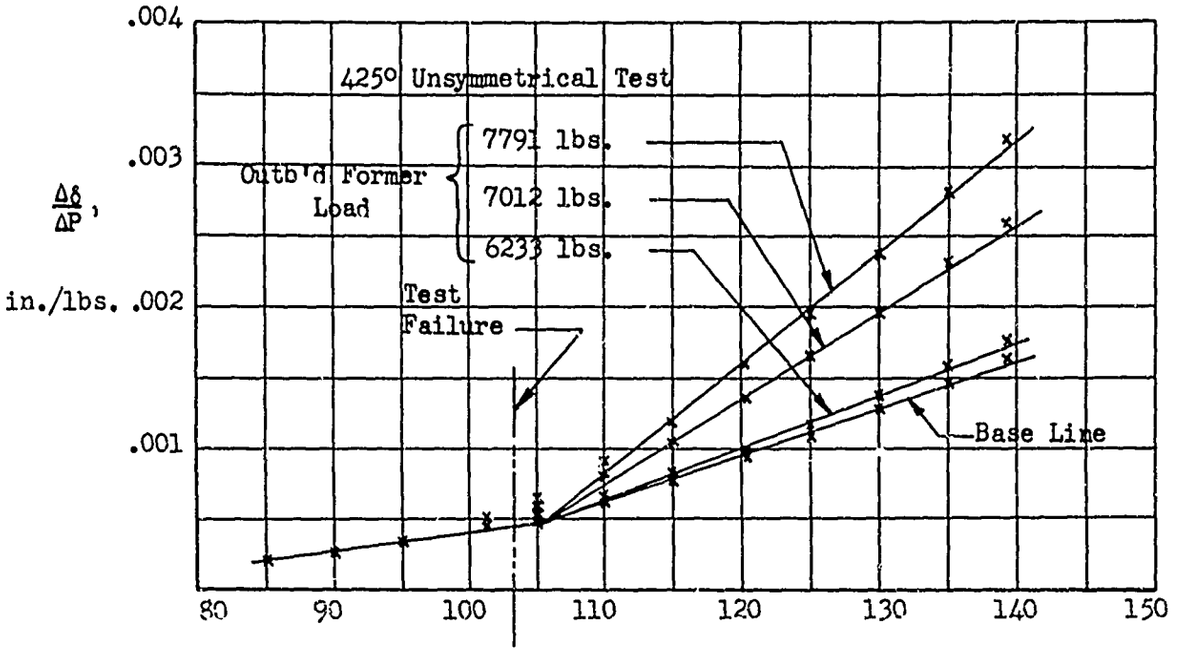

Figure 4.16. Analytical Deflection Rate Data

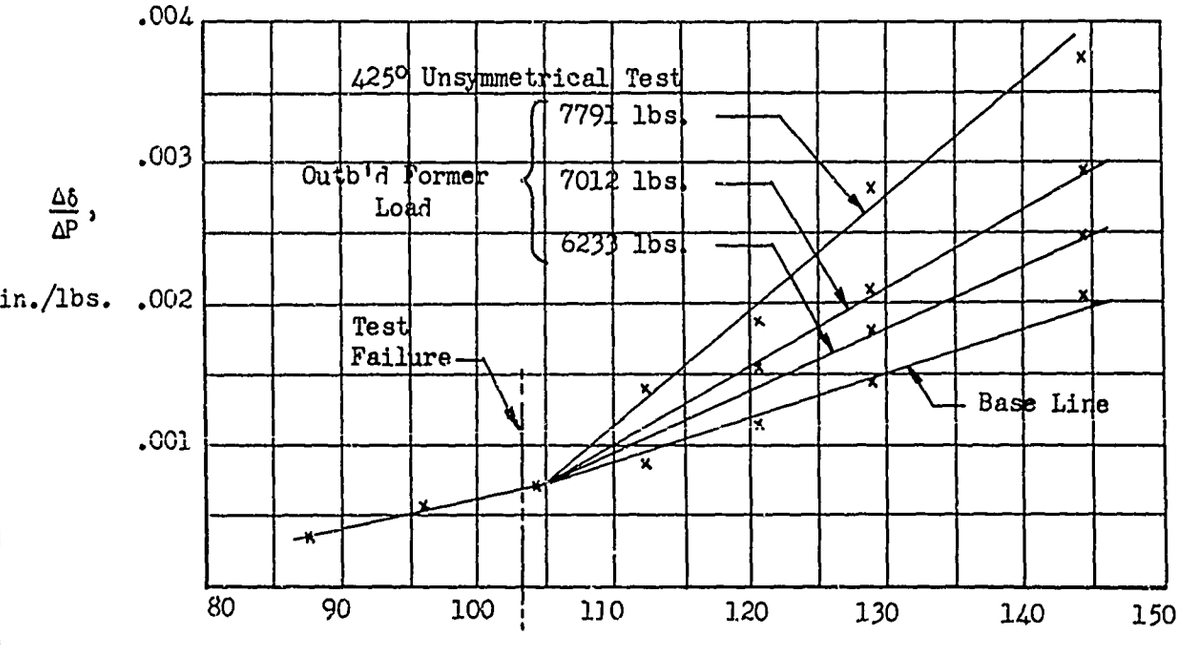

Figure 4.17. Experimental Deflection Rate Data

In the case of the 425°F. symmetrical test, an analytical deflection rate study was run for the case of lamps on at failure and for lamps off at failure. The main difference between these two analyses is that of material properties input. Early lamp shutdown during this test raised a question as to whether the material properties at failure had recovered to temperatures indicated by thermocouples. A discussion of Test 4 is given in Section 4.1 of this report.

The inelastic strains were computed for every ten percent of the test ultimate load. These inelastic strains are shown in Figures 4.18 and 4.19. It has been shown that the change in slope of the deflection rate curve is caused by an increase in the rate of incremental inelastic strain. It is noteworthy that the analysis for the lamps off at failure, which shows no incremental increase in inelastic strain with increasing load, produced no deflection rate results. The analysis for lamps on at failure, however, produced deflection rate results which agree quite well with the actual experimental results. The inelastic strain variation with increasing percentages of applied load for this case is shown in Figure 4.18. The incremental change in strain is seen to increase abruptly at full ultimate load. These deflection-rate results for this test thus support the results obtained in the analytical load deformation procedure of Section 4.1. We have, then, further evidence to support the premise that the material properties did not recover during the short time between lamp shut-off and stabilizer failure in the 425°F. symmetrical test. The significance in the curves of Figures 4.18 and 4.19 is that the greater inelastic effects and the greater incremental change from 90% to 100% shown in Figure 4.18 will increase the deflection rate more than the effects shown in Figure 4.19.

The analytical deflection-rate studies tended to divide the tests into two distinct types in regard to the incremental variation of inelastic strain with increasing load. In the case of the 425°F. symmetrical test 4, the 425°F. unsymmetrical test 6, and the 250°F. symmetrical test 3, the plots of inelastic strain versus increasing load were similar to Figure 4.18. The room temperature test 1 and the 250°F. unsymmetrical test 5, however, produced plots of inelastic strain versus increasing load which were similar to Figure 4.19.

A summary of the deflection rate results is presented in Table 4.1. The predicted and test failure stations are listed for the experimental and analytical deflection rates. For comparison purposes, the failure stations predicted by the load deformation method are also presented.

The failure stations predicted by the deflection rate method are seen to be quite similar to those predicted by the load-deformation procedures. This is to be somewhat expected, since both methods rely on

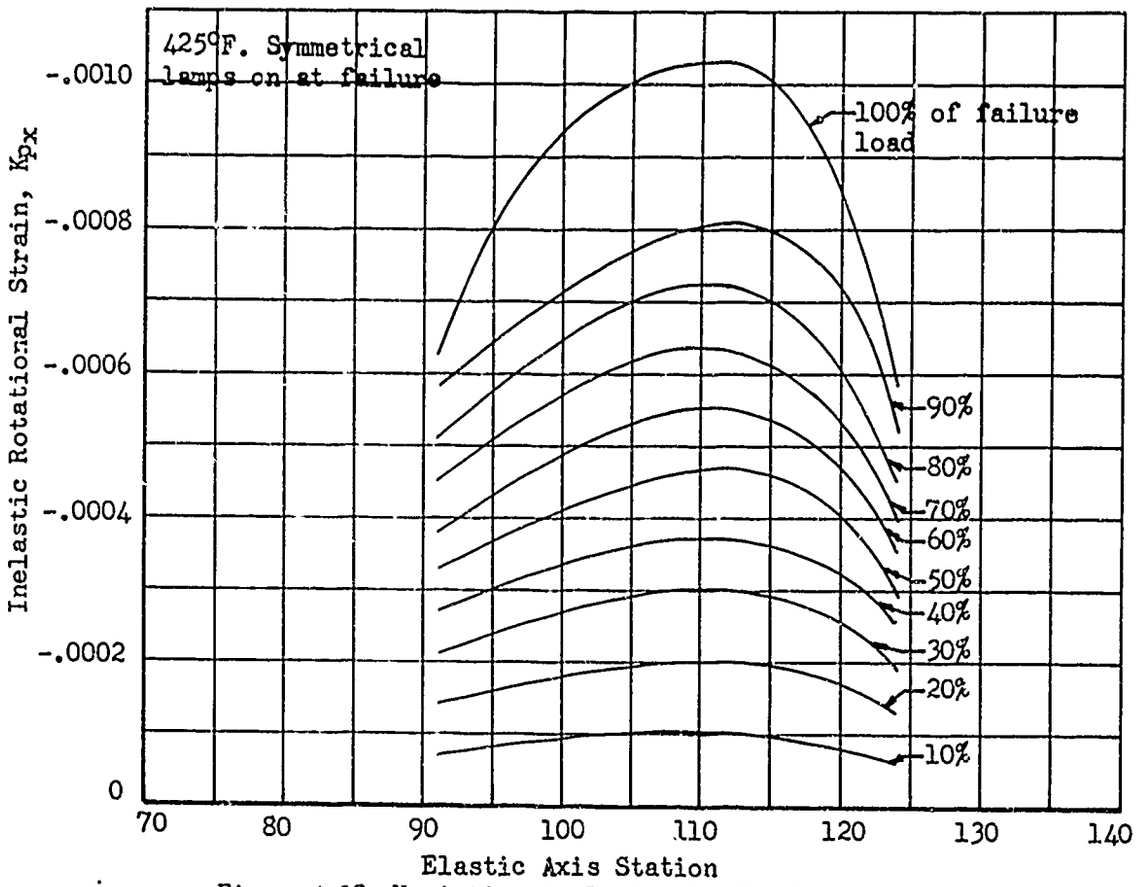

Figure 4.18, Variation in Inelastic Strain versus Elastic Axis Station For Various Percentages of Failure Load (425°F. Symmetrical Test, Lamps On at Failure)

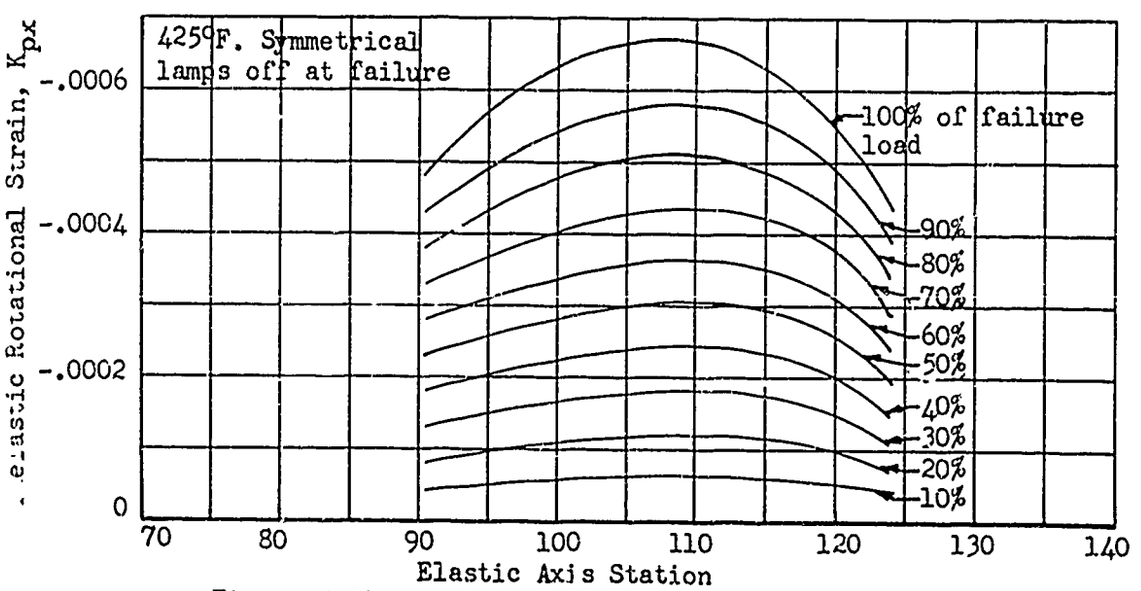

Figure 4.19, Variation in Inelastic Strain versus Elastic Axis Station For Various Percentages of Failure Load (425°F. Symmetrical Test, Lamps Off at Failure)

Table 4.1. Failure Station Summary

Test		Predicted Failure Station			Actual Test Failure Station	Remarks
Temp. Condition	No.	Experimental Deflection Rate	Analytical Deflection Rate	Analytical Load Deformation (Sec. 5.1)		
R.T.	a 1	*	*	107.5	105 122	* No prediction possible due to lack of inelastic action at failure.
250° Sym.	3	108.5	106.8	107	103	
250°Unsym.	5	*	*	106	102	* No prediction possible due to lack of inelastic action at failure.
425° Sym.	4	103	105.7 *	105.5(lamps off) 104 (lamps on)	104	* Assumed lamps on at time of failure. Same calculation for lamps off produced no results.
425°Unsym.	6	105	105.5	103	103	

the inelastic strains to find the plastic hinge location on the structure. The inelastic strains used in the deflection rate study were taken from the load-deformation output.

A comparison between the predicted failure stations and the actual test failure stations in Table 4.1 shows that a high degree of predictability exists. The maximum difference between the predicted failure station and the actual failure station is 5.5 inches, while the average difference is 3.2 inches. These distances are small enough to make the predicted failure stations lie within the failure zone of the actual test failures.

The correlation between analytical predictions and test data obtained in this study substantiates the use of analytical failure station prediction as an important tool in the area of structural testing. The load-deformation predictions are particularly useful since they are computed prior to the actual testing. In this manner, the failure region can be pre-determined and instrumented accordingly. Another advantage of the load-deformation prediction method is the fact that it accurately predicts critical areas regardless of the presence or absence of inelastic effects. The deflection rate method may be too insensitive unless large inelastic strains are present, and in general, requires accurate deflection measurement. Both methods work well at elevated temperatures on aluminum alloy when buckling and increased ductility produce larger inelastic effects.

An approach to the use of these methods might be to perform the load-deformation calculations prior to test and to plot the results. Analytical deflection rate calculations may then be made to verify the results. Then, during the actual test, the experimental deflection rate data can be plotted on the same graph as the load-deformation data. In this manner, any deviation from the predicted behavior of the structure will become immediately apparent. Indications of early failure would then appear in time to allow corrective measures to be taken.

4.5 Material Properties Investigation

The standard practice of testing tensile coupons from each test component after completion of the static test was followed in this study. Although this procedure is specified to compare the actual material properties with those used in the analysis, it is considered even more important for tests performed at elevated temperature than at room temperature. The greater variations associated with the elevated temperature environment and complex temperature-time histories make the prediction of important material properties, such as the yield stress, somewhat more difficult and questionable. In this study it was mandatory to investigate the actual versus predicted properties to evaluate the validity of the overall horizontal stabilizer results since the analytical procedures depend highly upon the yield stress parameter for accurate prediction of the load-deformation curves, permanent set, and ultimate load.

The experimental coupon investigation for defining material properties at the time of failure of each horizontal stabilizer is described in Section 3.1.3 of Volume II and the data from the individual stabilizers is summarized in Table 3.15 of Volume II. The coupons evaluated were obtained from Elastic Axis Station 127 which, according to the temperature-span plots similar to Figure 3.2, had temperature-time exposure histories as specified in Table 4.2 which summarizes actual horizontal stabilizer yield stress parameters and those predicted by the parametric curves for the tensile coupon elastic axis station and coupon test temperature.

Horiz. Stab.	Test Temp. Condition	Coupon Elastic Axis Sta., in.	Prior * Exposure Temp., °F.	Equiv. † Time at Exposure Temp., hrs.	Larson-Miller Parameter (Yield)	Tensile Coupon Test Temp., °F.	Per Cent R.T. Yield Stress	Predicted Yield Stress, F_{ty}, at Coupon Test Temp.	Tensile Coupon Yield Stress,** F_{ty}, Table 3.15, Vol. II
3	R.T.	139	R.T.	-	-	R.T.	-	73510	75023
1	250°F. Symm.	127	208	0.587	9130	250	0.885	65100	64664
4	425°F. Symm.	127	363	1.400	11570	380	0.605	44500	42768
5	250°F. Unsymm.	127	212	0.553	9160	250	0.885	65100	64493
6	425°F. Unsym...	127	33[illegible]	0.822	11680	450	0.449	33000	32323

Table 4.2. Tensile Coupon - Predicted Yield Stress Summary

* Main box skin temperature measured at Elastic Axis Sta. 125

† Main box skin element time associated with prior exposure temperature

** Each value is the average of two tests

The data summary in Table 4.2 illustrates, by comparing the last two columns, that the predicted values for a given temperature-time exposure history are verified by tensile coupon results having the same history. This indicates that the material properties used in the analytical procedures were sufficiently accurate to allow a direct comparison of overall horizontal stabilizer results such as ultimate load and load-deformation behavior.

The maximum difference between predicted and tensile coupon test properties is for Horizontal Stabilizer No. 4 (Test No. 4), 425°F. Symmetrical, and shows actual properties to be about 4% less than the predicted values. This fact coupled with the material property values used in the analysis for lamps on and lamps off tends to indicate that the overall stabilizer results for the lamps on condition might be the more reliable comparison. The analysis material properties data for Elastic Axis Station 124 (nearest to coupon area of Elastic Axis Station Station 127) indicated approximately 45000 psi used for F_{ty} for lamps on and approximately 50000 psi used for lamps off.

The differences are not too great, however, and the amount of data is too limited to allow any firm conclusions to be drawn. However, this investigation and the overall results shown in Tables 4.2, 5.1, 5.2, and 5.3 for Horizontal Stabilizer No. 4 illustrate the significant effect of the material properties evaluation (particularly yield stress) on overall test results and the applied load ratios for room temperature simulation.

In Table 4.2 the values shown in the next to the last column are typical main box skin element properties as defined by the exposure temperature and time and the yield stress parametric curve shown in Figure 3.8 of Volume II. The last column in Table 4.2 denotes the actual test values obtained from horizontal stabilizer coupons.

4.6 Analytical Results for Plate Element and Fastener Load Distributions at Ultimate Load, Part 2

The diagrams shown in Figures 4.22 through 4.26 show the distribution of plate element axial loads and fastener shear loads on the tension (critical) side of the horizontal stabilizer for each temperature environment at the calculated ultimate load. The load distributions shown include the main box skin, the steel splice plate between the interbeams and main beam fitting, the two outboard interbeams, and the steel main beam fitting flange. The figures include diagrams for the following test and analysis temperature environments and moment restraint conditions. Based on the results of the thermal moment restraint study of Section 4.7 the diagrams in Figures 4.24 and 4.26 for Test No's. 11 and 12, respectively, represent the results for the assumption of full elastic thermal bending moment restraint.

(a) Pilot Study b, Room Temperature, ultimate applied former load = 18000 lbs.

(b) Test No. 9, 250°F. Symmetrical, ultimate applied former load = 17250 lbs.

(c) Test No. 11, 250°F. Unsymmetrical, ultimate applied former load = 16770 lbs., assumed full thermal bending moment restraint.

(d) Test No. 10, 425°F. Symmetrical, ultimate applied former load = 12420 lbs.

(e) Test No. 12, 425°F. Unsymmetrical, ultimate applied former load = 13030 lbs., assumed full thermal bending moment restraint.

The calculated ultimate loads shown above were obtained using the methods of Section 3.3 of Reference (a) where the failure criteria were specified in Equation (3.3.8.1) on pages 31 and 32 of Reference (a). For each applied load investigated analytically the failure criteria of Equation (3.3.8.1) of Reference (a) were applied after convergence of the calculations for the redundant fastener shear loads. Failure of a fastener segment, plate element, or fastener-plate intersection (bearing) is noted depending upon the failure criteria tests for fastener shear, plate element strain, or fastener-plate deformation. The loads at which the splice joint failed to pass any one of the three specified tests were obtained from an IBM 7090 computer analysis programmed according to the block diagram solution of Section 4.2 of Reference (a).

The splice joints were analyzed by the inelastic method, and results were plotted on Figures 4.22 through 4.26. The inboard end fastener (or row) had higher loads than the outboard ones, and the plate areas surrounding them were deformed inelastically. Failure did not occur at this time. Instead, loads were first redistributed, and successive outboard fasteners picked up more of the redistributed load until several fasteners failed simultaneously. In Figure A1.8, several fasteners near the inboard end have failed, demonstrating that a single inboard fastener did not initiate the failure.

The splice joints were not analyzed herein by the elastic method, but Reference (g) shows that the inboard end fastener (or row) does not fail immediately after becoming critical.

For splice joint geometry and identification refer to Figures 4.20 and 4.21.

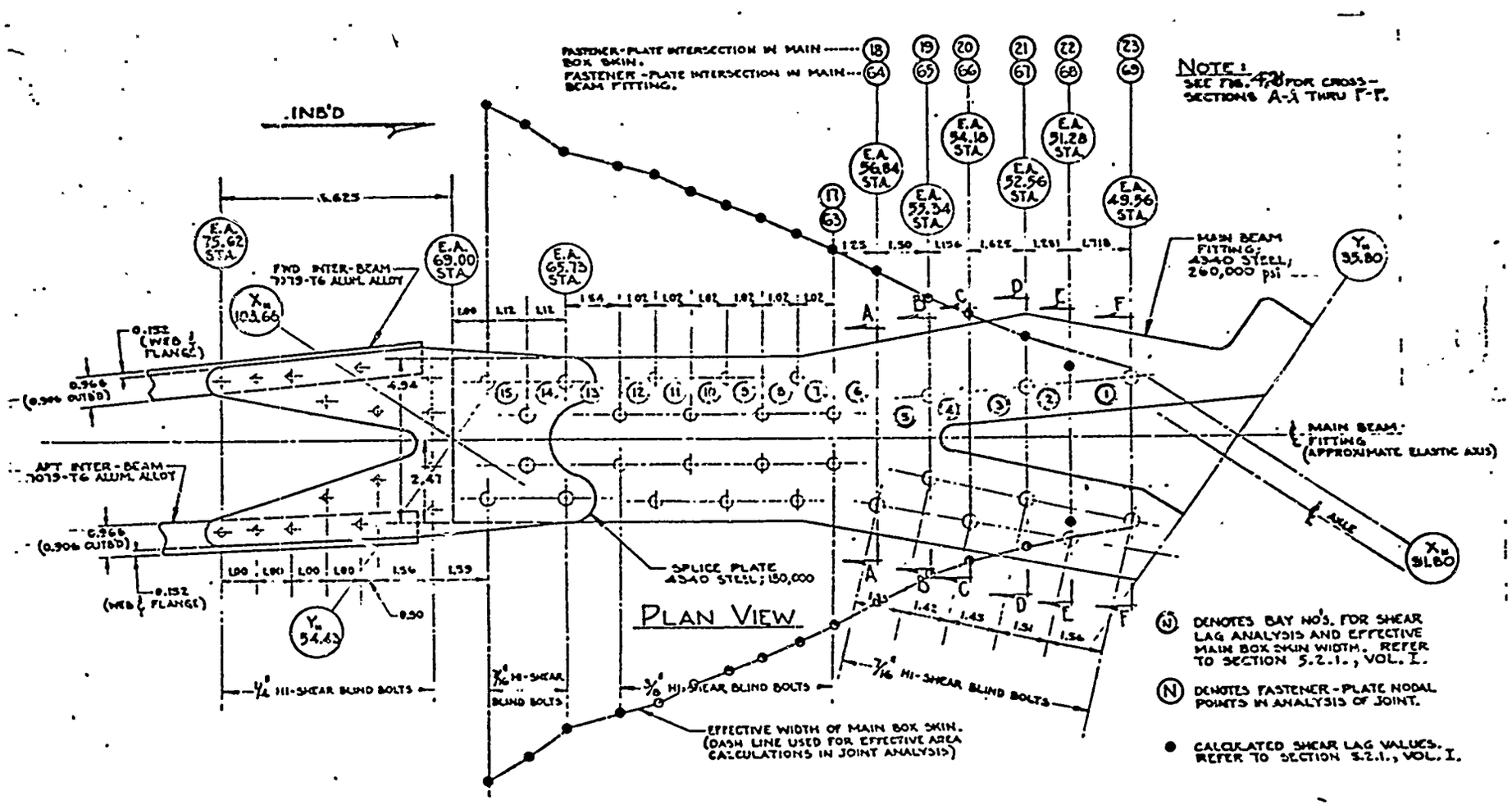

Figure 4.20. Inbourd Splice Joint Geometry

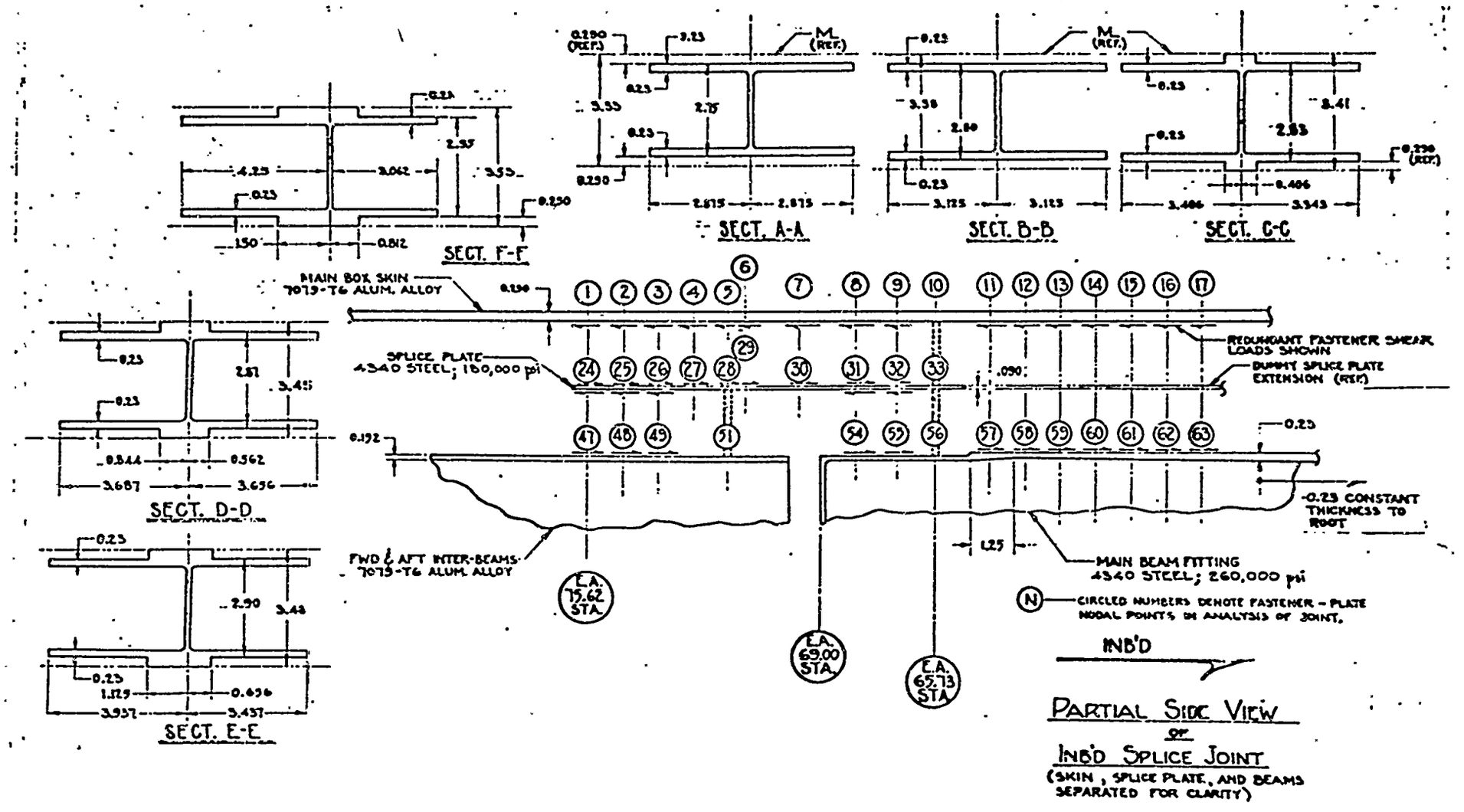

Figure 4.21. Inboard Splice Joint And Main Beam Cross-Sections

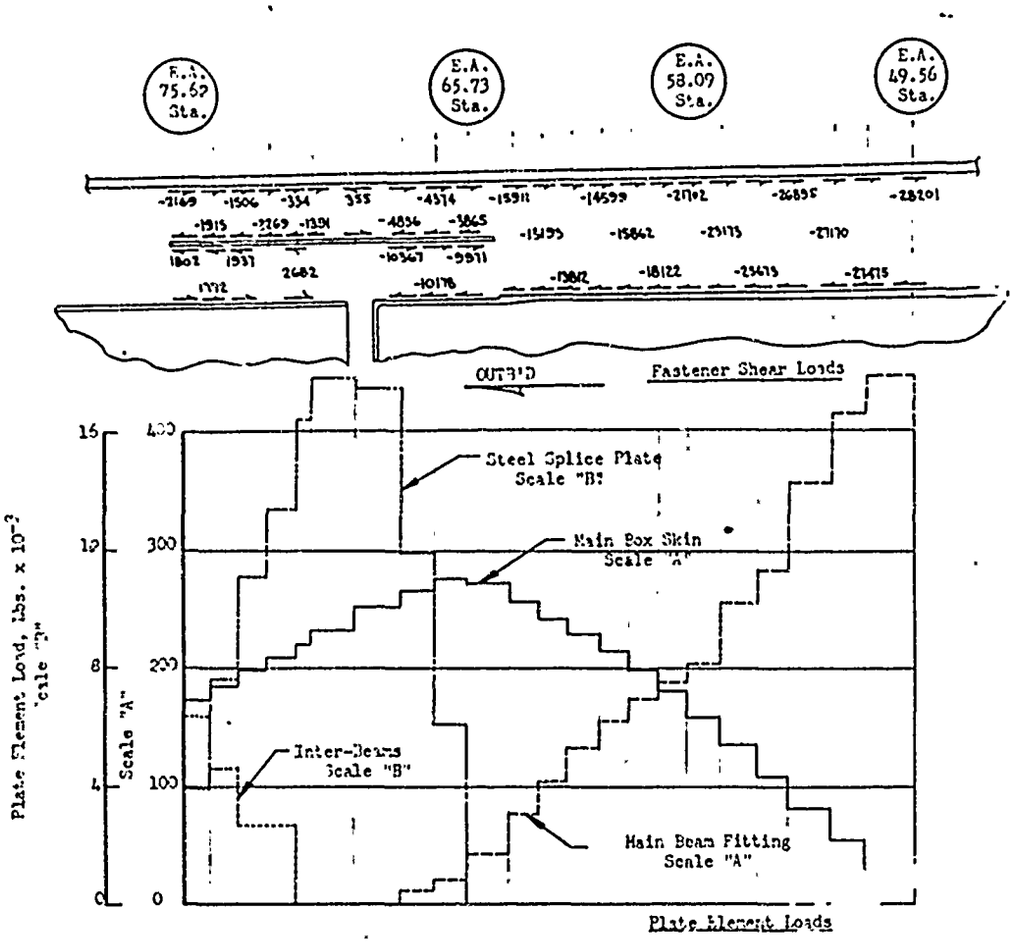

Figure 4.22 Fastener Shear Loads and Plate Element Loads at Failure, Inboard Splice Joint, Part 2, Room Temperature (Test No. 7 and Pilot Study)

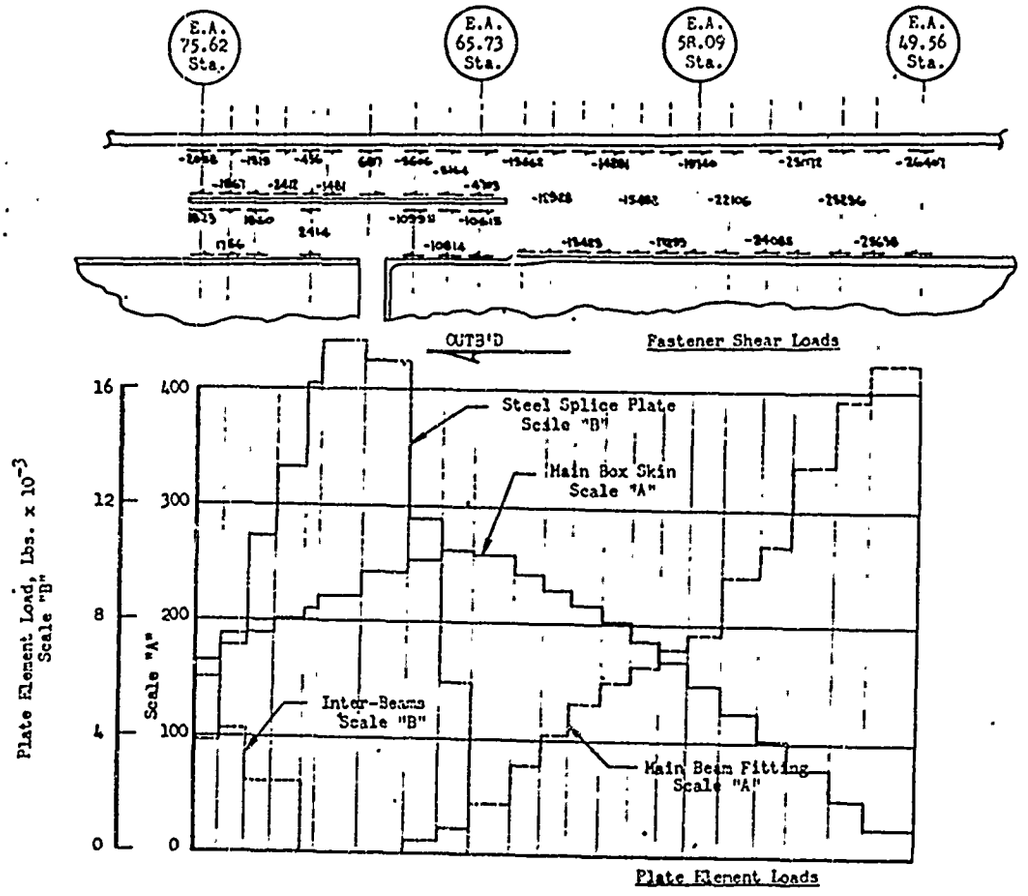

Figure 4.23 Fastener Shear Loads and Plate Element Loads at Failure, Inboard Splice Joint, Part 2, 250°F, Symm. (Test No. 9)

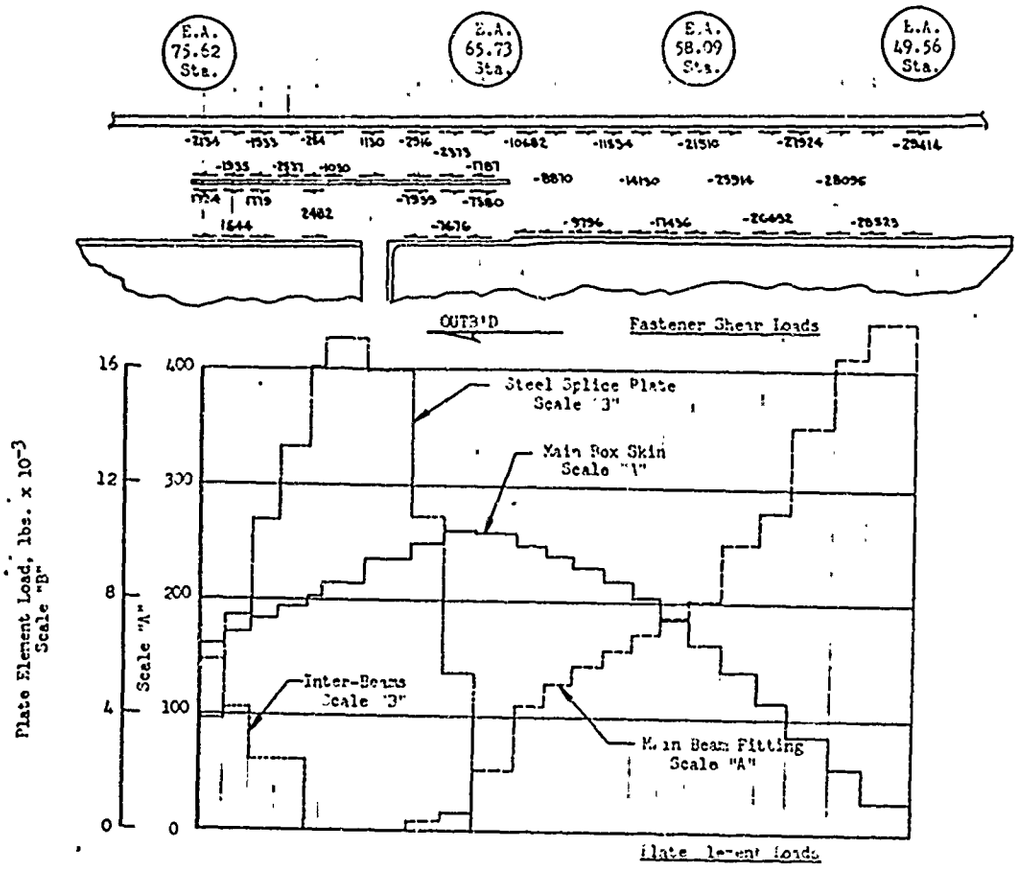

Figure 4.24 Fastener Shear Loads and Plate Element Loads at Failure, Inboard Splice Joint, Part 2, 250°F, Unsymm. (Test No. 11), Restrained-in-Bending For Thermal Moment

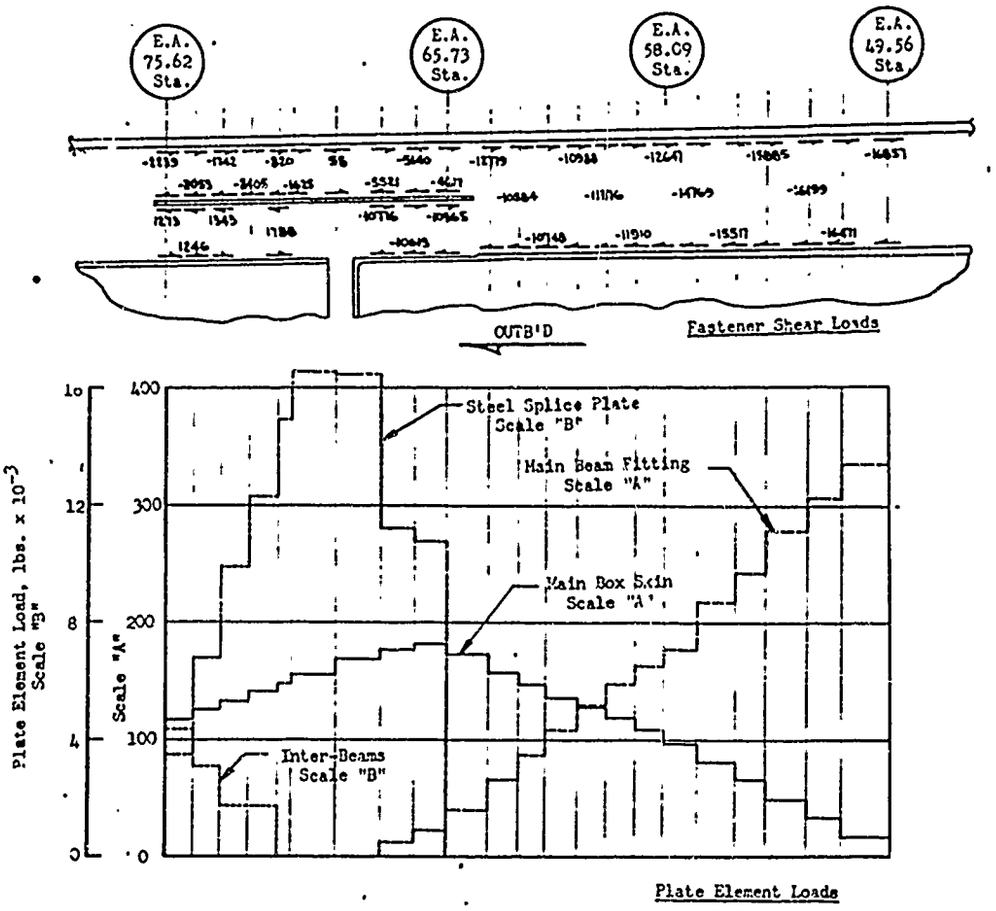

Figure 4.25 Fastener Shear Loads and Plate Element Loads at Failure, Inboard Splice Joint, Part 2, 425°F, Symm, (Test No. 10)

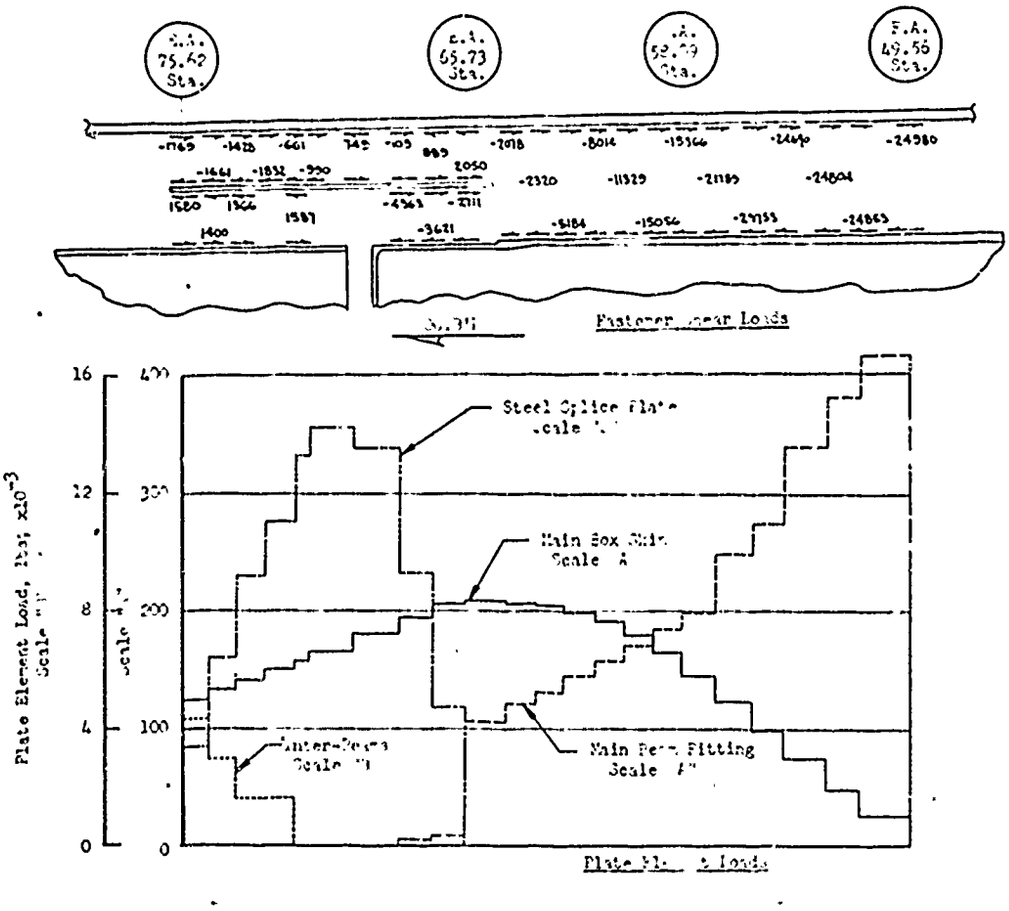

Figure 4.26 Fastener Shear Loads and Plate Element Loads at Failure, Inboard Splice Joint, Part 2, 425°F, Unsymm, (Test No. 12) Restrained-in-Bending for Thermal Moment

4.7 Thermal Moment Restraint Study, Part 2

Chordwise plots of experimental thermal strain data are shown in Figure 4.28 for two separate stations along the span of the main beam fitting. From Figure 4.20 these stations are approximately Elastic Axis Stations 67.6, and 55.6, Page 64. The data plotted was obtained from ASL magnetic tapes for tests 11 and 12, the unsymmetrical environment tests and is for the tension (cooler) side at the beginning of load application. This data, then, represents essentially the thermal strains for the stabilized temperature environment.

The experimental data tends to indicate a relatively large positive strain in the main box skin at the outboard end of the main beam fitting showing that some degree of moment fixity does exist since the unrestrained-in-bending case should produce a negative strain in the main box skin for the temperature distribution present according to the thermal strain calculations. Further evidence which tends to support the assumption of moment restraint is the plotted value of calculated thermal strain for the restrained-in-bending case which is positive (tension) and of the same order of magnitude as the peak skin strain. These facts plus the shape of the chordwise strain distribution curve indicate a general internal self-balancing moment condition in the stabilizer root area similar to that shown in the sketch in Figure 4.27.

The generalized condition shown in Figure 4.27 can logically be presumed to exist for several reasons. First, steep chordwise temperature gradients are present in the extreme root area and are produced primarily by locally heating the main box area bounded by the front and rear beams and the inboard and outboard root ribs. The front and rear box beam areas were essentially protected from direct heating lamp radiation by curtains and became heated only by conduction, thus maintaining a generally lower temperature level in these areas.

The presence of these relatively steep temperature gradients, not only through the depth (thickness) of the stabilizer, but chordwise as well, would severely affect restraint conditions when coupled with the relative torsion and bending stiffnesses of the front and rear box beam sections, the inboard and outboard root ribs, and the heavy main box structure outboard of the outboard root rib. A contributing factor to the degree of restraint present could also be the two closely spaced loading formers and their attendant clamping action on the structure just outboard of the outboard root rib.

Actually the moment restraint effects do not remain constant along the span as noted by the comparison between the chordwise plots for

two different stations along the main beam fitting (Stations 67.6, and 55.6). Generally, the experimental strain data indicates a gradually diminishing moment restraint from the outboard end of the fitting to the extreme root end. This is indicated by the reduction in positive (+), or tension, strain values at the most inboard station (Station 55.6).

The initial splice joint analysis considered only those equivalent thermal strains for the axially-loaded splice which were defined by a thermal strain analysis of the full cross-section assuming the cross-section to be unrestrained-in-bending. In view of the experimental evidence which indicated the presence of some degree of thermal moment restraint the 250°F. unsymmetrical and 425°F. unsymmetrical temperature environments (ASL tests 11 and 12) were also considered analytically assuming full thermal moment restraint along the length of the main beam fitting. The additional thermal moment is applied as a couple load and produces additional tension in the lower surface cover and main beam flange. The values of these thermal moments and couple loads are shown in Table 4.3 and the net corrected statically determinate load distributions are also shown in Table 4.3 for the two unsymmetrical temperature environments.

As a consequence of this investigation the summary tables for Part 2 (Table 5.4) show two values for analytically predicted ultimate load and ultimate applied load ratios, as well as location of failure and mode of failure. The values shown, then, represent the two extremes for thermal moment restraint (unrestrained and fully restrained elastically). The good agreement between test and analysis results for room temperature and the symmetrically heated temperature environments indicates the specific criteria and parameters related to joint description, material properties, and local joint deformation are reasonably well defined for problem description. Therefore, it is expected that the unsymmetrically heated cases should produce similar test-analysis comparison results since identical means of defining deformation criteria and material parameters are employed. A significant trend is noted in the test-analysis comparison for the unrestrained-in-bending cases where the difference in the test and analysis failing loads appears to be a function of the temperature gradient with the largest difference occurring in the 425°F. unsymmetrical case.

The final results of Table 5.4, the indication of some degree of thermal moment restraint and the diminishing restraint along the main beam fitting indicate that a rational assumption might be made for thermal moment restraint conditions in lieu of "exact" analytical results. For the type of structure typified by the horizontal stabilizer inboard splice joint, the localized heating, and significant temperature gradients, the thermal moment restraint could be presumed

to be approximately one-half without producing significant errors in the applied load ratios for room temperature simulation.

In Table 5.4 the "Failing Load Percent Deviation" column would then show about +9.2% for 250°F. Unsymmetrical and +5.1% for 425°F. Unsymmetrical and the "Calculated Failing Load" column would show 17,260 lbs. and 15,365 lbs., respectively.

Section 4.72 defines briefly the procedure used to compute the thermal moment and shows the additional couple loads used as applied load input to approximate the full bending moment restraint condition.

The chordwise temperature distribution produced is peculiar to this series of elevated temperature tests, and was produced because the leading and trailing edge sections were shielded against direct radiation from the lamps while the main box area in the splice joint was heated.

* K_T is the thermal moment rotational restraint strain and represents an elastic thermal moment of M_T in the case shown.

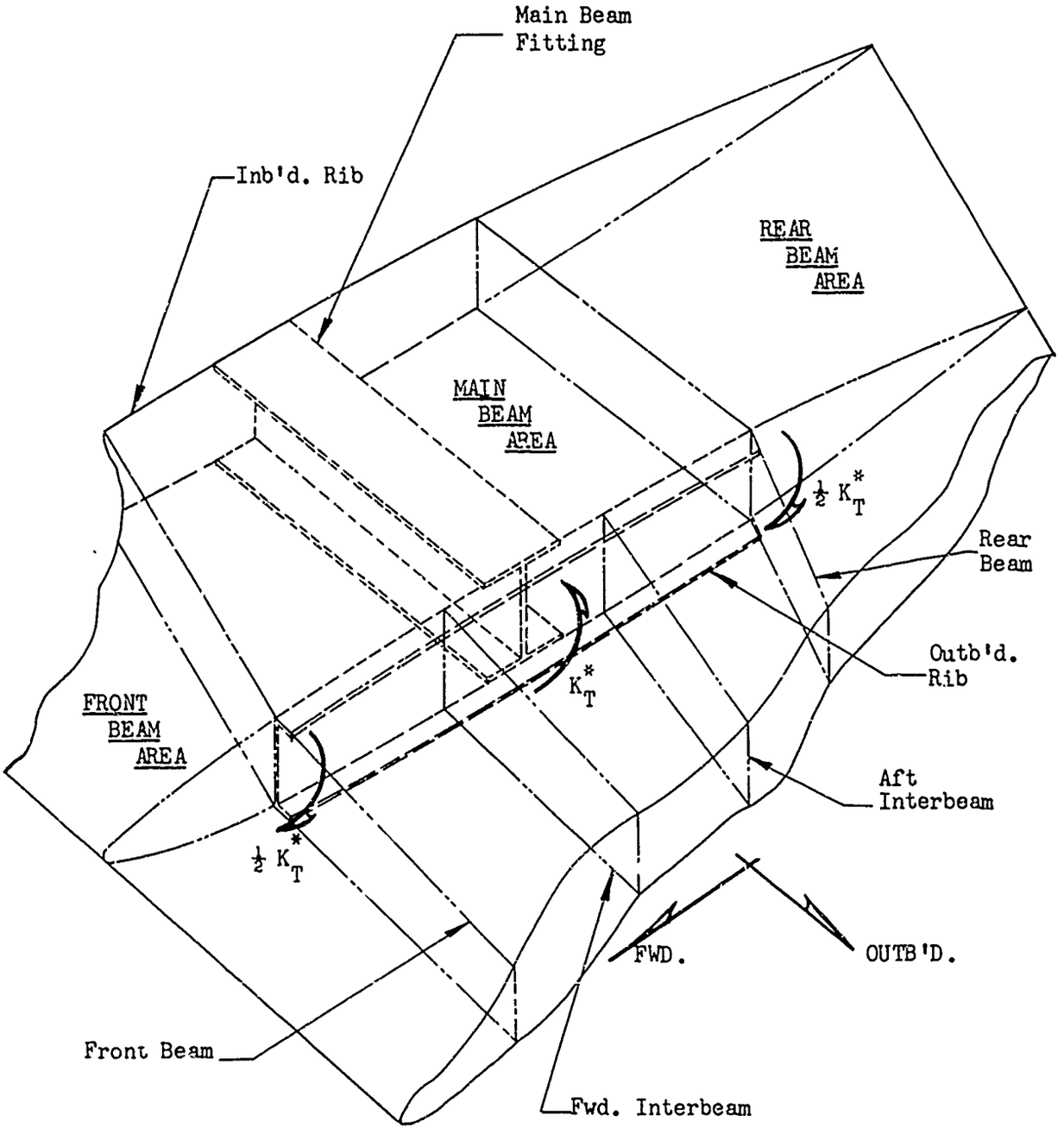

Figure 4.27. Sketch of Thermal Moment Restraint Condition (Refer to Figure 426 for Static Test Strain Gage Results)

4.7.1 Experimental Evaluation of Thermal Moment Restraint

The sketch in Figure 4.27 is a generalization of the thermal moment effects which can be presumed to be present at the outboard end of the steel main beam fitting. Since the main beam area only was heated and the front and rear beam areas were essentially protected from direct lamp radiation the maximum temperatures and temperature gradients through the depth of the cross-section tend to be higher in the main beam area. The steeper gradients in the main beam area produce a greater tendency to bow or bend but this tendency is resisted by the front and rear beam areas which tend to remain straight and unbowed since severe temperatures and temperature gradients are not present in these areas. This tendency plus inherent torsional stiffness in the rib-skin combination at the outboard end of the main beam fitting could produce, essentially, a self-equilibrating restrained thermal moment condition similar to that shown in Figure 4.27. The coefficients of "$\frac{1}{2}$" shown in Figure 4.27 on K_T for the front and rear beam areas are merely shown to represent the fact that the moment at any station is self-equilibrating and are not intended to indicate that exactly half of the thermal moment is restrained by either the front beam or rear beam area. If K_T represents an elastically applied moment, M_T, produced by the temperature distribution the general equilibrium equation is

$$C_f M_T + C_r M_T = M_T = (C_f + C_r) M_T \qquad (4.7.1.1)$$

where C_f and C_r are merely unknown moment distribution factors for the front beam and rear beam, respectively, and M_T is the elastically applied thermal moment in inch-lbs. The factors C_f and C_r cannot be determined directly except by more rigorous indeterminate analysis techniques and more extensive temperature distribution data over the leading edge box and trailing edge box areas. Furthermore, any inherent torsional stiffness or axial load components in the inboard rib area could produce similar boundary conditions at the extreme root end. The extreme condition at both ends of the main beam fitting would define complete thermal bending moment restraint for the main beam area where a constant moment would exist along the length of the main beam fitting. The maximum value of this bending moment in the elastic region would be equivalent to the full value of K_T (as elastic applied strain), or M_T (as an elastically applied bending moment), as defined by the cross-section thermal stress calculations. The values of the thermal moment, M_T, are shown in Section 4. along with the associated couple loads in the covers produced by considering M_T as an additional elastic applied moment. For calculation purposes for the restrained-in-bending case the couple loads, P_c, associated with the thermal

moments, M_T, are added, as appropriate, to the values in Tables 2.2 and 2.3 as applied loads in the statically determinate structure.

The thermal moment restraint system shown in Figure 4.27 is generally demonstrated by the chordwise strain distribution near the outboard end of the main beam fitting. The chordwise strain distribution at the stabilized temperature distribution just prior to the start of loading is shown in Figure 4.28 for a cross-section near the outboard end of the main beam fitting for 250°F. Unsymmetrical (Test No. 11) and 450°F. Unsymmetrical (Test No. 12) and for the most inboard cross-section (Elastic Axis Station 55.6) for Test No. 12. The strain gages used for plotting purposes for the tension side at the outboard station (Elastic Axis Station 67.6) were those identified in Volume III as 23b, 24b, 25b, 26b, 27b, 28b, and 29b. The strain gages plotted for the inboard station (Elastic Axis Station 55.6) are 6b, 7b, 8b, 9b, 10b, and 11b.

For 425°F. Unsymmetrical (Test No. 12), calculations show the unrestrained-in-bending thermal strain on the center main box skin element to be about -420 micro-inches and the restrained-in-bending thermal strain to be approximately +1260 micro-inches. The temperature moment strain, K_T, alone is approximately +1680 micro-inches. For direct comparison of experimental and analytical strains the calculated maximum restrained value of +1260 micro-inches compares favorably with strain gage 26b which showed a tension strain of +1790 micro-inches. This gage is located on the elastic axis near the outboard end of the main beam fitting where the outboard rib stiffness and the front and rear beam moment restraint is the largest. The change in sign of the strain coupled with the cross-section analysis comparison for the restrained and unrestrained cases and a favorable comparison with experimental strain values appears to indicate that some degree of thermal moment restraint does exist. Therefore, the effects of this restraint must be allowed for in the equivalence of the full cross-section to the axially-loaded splice joint analysis.

Figure 4.28. Chordwise Strain Plots of Experimental Data For Thermal Moment Restraint Investigation, Inboard Splice Joint Study, Part 2

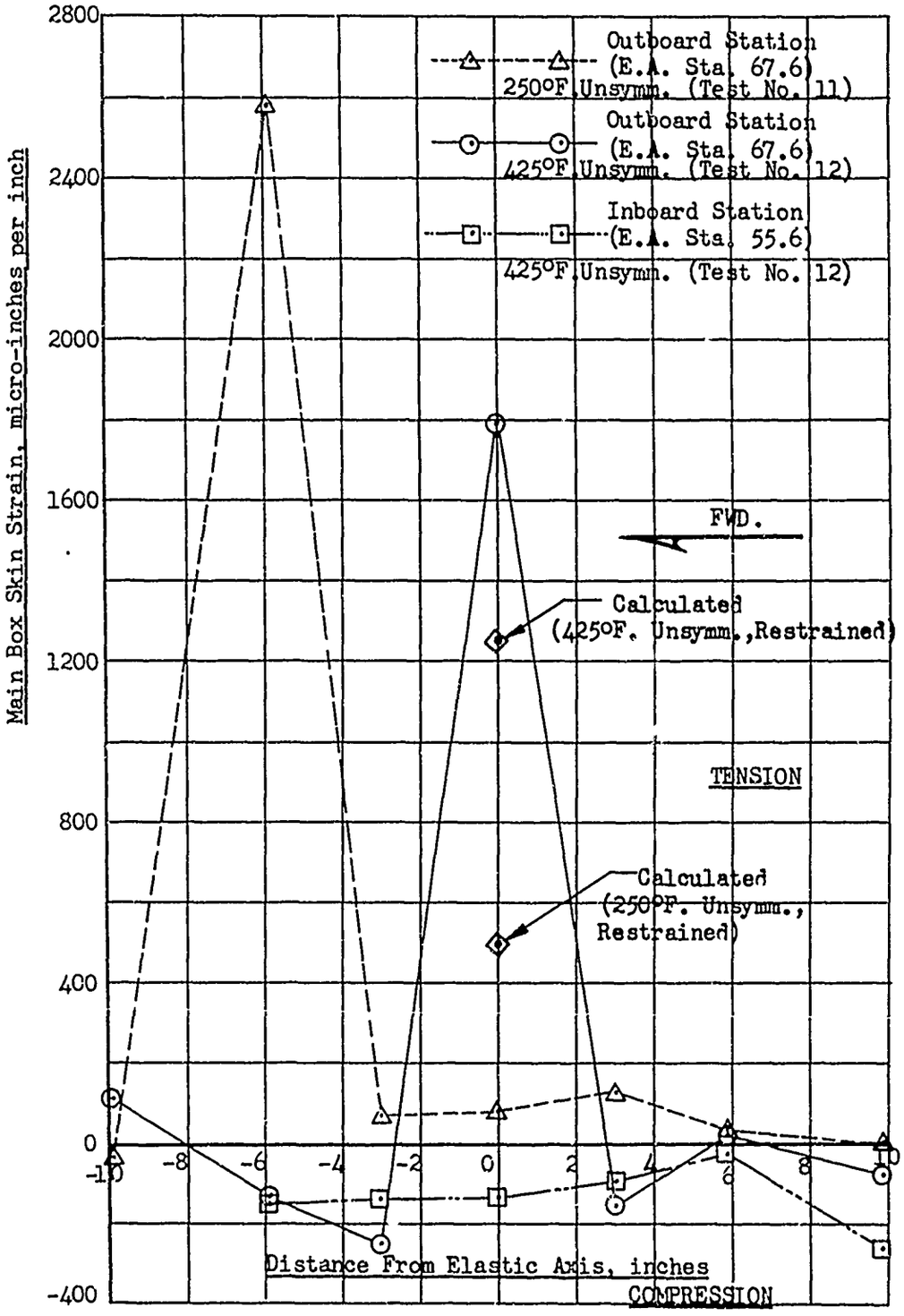

4.7.2 Thermal Moment Evaluation and Analysis Input

In order to define equivalent axial plate element thermal strains (and input temperatures for splice plate analysis) and the thermal moments for evaluation of the restrained vs. unrestrained moment condition of the unsymmetrically heated splice joints, the cross-section analysis was performed on a simplified typical cross-section as shown in the following diagram.

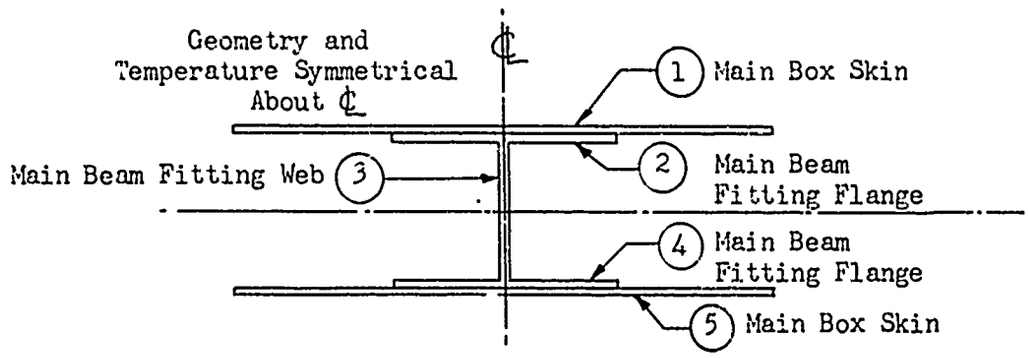

Figure 4.29 Simplified Splice Joint Cross-Section

The actual temperatures obtained from the 250°F. Unsymmetrical and the 450°F. Unsymmetrical tests were used as data input to the cross-section analysis for a +T (temperature applied) step only to obtain the thermal strains, thermal stresses, and the thermal moment as output data. From this analysis the thermal moments for the two unsymmetrically heated conditions were found to be as follows.

250°F. Unsymmetrical (Test No. 11)

Thermal moment rotation, $K_T = .000705$

From IBM data,

$EI = c^2 \Sigma E_n A_n \frac{y_n}{c} = (1.5)^2 (96.829 \times 10^6) = 218 \times 10^6$

The thermal moment is then,

$$M_T = \frac{K_T EI}{c} = \frac{.000705(218 \times 10^6)}{1.5} = 102,500 \text{ in.-lbs.}$$

450°F. Unsymmetrical (Test No. 12)

Thermal moment rotation, $K_T = .00164$

From IBM data, $EI = 218 \times 10^6$, $c = 1.5$ inches

The thermal moment is then,

$$M_T = \frac{K_T EI}{c} = \frac{.00164(218 \times 10^6)}{1.5} = 238,300 \text{ in.-lbs.}$$

For an evaluation of the effects on the predicted ultimate strength produced by the presence of thermal bending moment restraints, the extreme restraint case can be considered in the analysis where the thermal moment is considered as an elastically applied constant moment essentially over the length of the steel main beam fitting between fastener-plate intersections (56) and (69) . With the average couple height taken as 2.5 inches, additional couple loads produce an increase in tension stresses in the already-critical tension side of the horizontal stabilizer splice. These values are shown below for the two temperature environments under consideration.

Couple Loads

$$P_c = \frac{102,500}{2.5} = 41000 \text{ lbs. (250°F. Unsymmetrical, Test No. 11)}$$

$$P_c = \frac{238,300}{2.5} = 95300 \text{ lbs. (450°F. Unsymmetrical, Test No. 12)}$$

The above couple loads were added to the applied load input for ultimate load prediction for the splice joint, and the comparative results for the restrained versus unrestrained case are shown in Table 5.4 . The actual degree of restraint present in each temperature case cannot be readily ascertained, but some qualitative results and observations from strain gage data are described in Section 4.7.1. The couple loads shown above actually represent an approximate average couple load for the length of the splice joint. The actual values used in the analysis are tabulated on the following page.

1	2	3	4	5	6	7	8
		Test No. 11 250°F. Unsymmetrical			Test No. 12 425°F Unsymmetrical		
Element No.	Couple Height, inches	Thermal Moment M_T, in.-lbs. Ref. Page 78	Couple Load, P_c, lbs. (3)/(2)	Average Couple Load in Element, P_c, lbs.	Thermal Moment, M_T, in.-lbs. (Page 79)	Couple Load, P_c, lbs. (6)/(2)	Average Couple Load in Element, P_c, lbs.
56	2.38	102,500	43000		238,300	100,200	
				42500			98950
57	2.44		42000			97,700	
				41900			97500
58	2.45		41800			97,300	
				41650			96900
59	2.47		41500			96,500	
				41400			96350
60	2.48		41300			96,200	
				41250			96000
61	2.49		41200			95,800	
				41100			95600
62	2.50		41000			95,400	
				40850			95000
63	2.52		40700			94,600	
				40350			93900
64	2.56		40000			93,200	
				39700			92450
65	2.60		39400			91,700	
				39200			91200
66	2.63		39000			90,700	
				38700			90000
67	2.67		38400			89,300	
				38050			88500
68	2.72	102,500	37700		238,300	87,700	

Table 4.3. Plate Element Axial Loads in Static Main Beam Fitting Structure Due to Restrained-in Bending Thermal Moment Effects.

5.0 APPLIED LOAD RATIO SUMMARY AND COMPARISON

5.1 Part 1-Cross-Section Summary

Table 5.1 summarizes the experimental and analytical results for the six horizontal stabilizer components and the five temperature environments. The data presented in the table provides a comparison between the experimental and analytical results for the outboard former load at failure, the station at which the failure occurred, the primary mode of failure, and the ultimate applied load ratio for each test. In this table the failure load only is considered for comparison purposes without regard for any difference in failure station. The load shown in the table is the outboard former load since the bending moment at the critical cross-section is a function of that particular applied load. A comparison of the failure locations shows generally good agreement between the experimental and analytical results. The single exception was Horizontal Stabilizer No. 1 which failed at Elastic Axis Station 122 which is a significant departure from the normal failure area between Elastic Axis Stations 102 and 105. However, the failing load and the mode of failure show favorable agreement. The analytical procedures predict the room temperature failure to be compression instability at Elastic Axis Station 107.5 but the tangent bending moment line in Figure 4.7 passes through the test failure data point at Station 122. This indicates that apparently the two stations could have been very nearly equally critical and that a failure at Elastic Axis Station 107.5 was probably imminent. The proximity of the actual failure station to the outboard former indicates the possible presence of severe shear lag effects which violates the plane-strain cross-section assumptions in the analysis and may have contributed to the outboard station failure.

The room temperature outboard former loads, both experimental and analytical, are the reference values for the applied load ratio computations. The experimental reference value used was the average failing load of Horizontal Stabilizer tests 1 and Pilot Study a (14,900 lbs.). For each test the applied load ratios are defined for ultimate load by

$$R_{ap} = \frac{V_{E.T.}}{(V_{R.T.})_{Ref.}} \qquad (5.1.1)$$

where R_{ap} = applied load ratio

$V_{E.T.}$ = outboard former elevated temperature ultimate load (analytical or experimental)

$(V_{R.T.})_{Ref.}$ = outboard former room temperature reference ultimate load (analytical or experimental)

The comparison of the applied load ratios for each test is shown in Table 5.1 and, in general, shows good agreement between the predicted ratio and those obtained experimentally.

For the 425°F. (Symmetrical) test (Test No. 4) two values are given in the table for analytical results. The purpose of the two sets of values is to illustrate the importance of temperature-time dependent material property recovery data on the overall analytical results. During this particular test the heating lamps were turned off prior to the failure as a safety precaution. The element temperatures measured on the surface of the stabilizer indicated that a drop of approximately 70°F. occurred on the skin between the time of lamp shut-down and failure. The two failure loads listed in the table represent the predicted strength based on the skin element temperatures measured at failure and also on the temperatures just prior to heating lamp shut-down. It is interesting to note that the overall test results tend to indicate that the material properties appear to reflect the temperature at the time of lamp shut-down rather than the lower temperature at failure. Subsequent tests of coupons taken from each of the test stabilizers did indicate the incomplete recovery of properties to the new lower temperature. This may be due to the fact that the stabilization of certain material properties, such as the yield stress, simply did not have time to take place prior to the failure of the stabilizer. The results of the tensile coupon-stabilizer analysis data input are summarized in Table 4.2.

Table 5.2 is essentially a continuation of Table 5.1 and shows the per cent deviation of the predicted failing load from the test failing load for each horizontal stabilizer. As in Table 5.1 the outboard former load is used for comparison without considering predicted-failure-station, test-failure-station comparison.

To ensure a fair comparison of test and analytical results the summary in Table 5.3 is presented to compare test and analytical bending moments at the test failure station. The per cent deviation results from Table 5.2 combined with those from Table 5.3 provide a more complete basis for comparison of analytical and experimental results. The test ultimate bending moments shown are those present at the actual failure station, and the predicted ultimate bending moments shown are those obtained from Figures 4.7 through 4.11 in Section 4.2 on the allowable bending moment curve at the test failure station. As in the previous tables, two values are shown for Test No. 4 to account for the two temperature conditions as previously discussed.

From the summary tables it is noteworthy that the two room temperature test failures produced in two supposedly identical horizontal stabilizer assemblies differed from each other by 17 inches in location and 16 percent in bending moment. This deviation in actual test results under identical environmental conditions exceeds the test-analysis deviation for every test temperature environment. Therefore, it can be presumed that the analytical-experimental deviations are probably within acceptable tolerance limits for all of the tests including the two room temperature tests.

Horiz. Stab. No.	Test No.	Test Temp. Environ.	Outb'd Former Load At Failure, Lbs.		Failure Station (E.A. Ref. Sta.)		Primary Mode of Failure		Ultimate Applied Load Ratio	
			Test (ASL Tape)	Analytical	Test (ASL Letters)	Analytical	Test (ASL Letters)	Analytical	Test	Analytical
1	1	R.T.	14717	15230	122	107.5	Comp. Instab.	Comp. Instab.	1.000	1.000
2	2	TEMPERATURE SURVEY SPECIMEN								
3	3	250°F. Sym.	13256	13430	103	107	Comp. Instab.	Comp. Instab.	0.888	0.883
4	4	425°F. Sym.	7716	8920* 8380†	104	105.5* 104 †	Comp. Instab.	Comp. Instab.	0.517	0.585* 0.550†
5	5	250°F. Unsymm.	13553	13880	102	106	Comp. Instab.	Comp. Instab.	0.909	0.907
6	6	425°F. Unsymm.	7791	8045	103	103	Comp. Instab.	Comp. Instab.	0.522	0.528
7	Pilot Study a	R.T.	15100 (ASL Letter)	15230	105	107.5	Tension (Lower Surf.)	Comp. Instab.	1.000	1.000

* Data For Lamps Off at Failure.
† Data For Lamps On at Failure.

Table 5.1
Part 1 - Cross-Section Failure and Applied Load Ratio Comparison

①	②	③	④	⑤	⑥ $\frac{⑤ - ④}{⑤} \times 100$
Horiz. Stab. No.	Test No.	Test Temp. Environ.	Outboard Former Load at Failure, lbs. Test	Analysis	Per Cent Deviation From Test
1	1	R.T.	14717	15230	+ 3.40
2	2	← Temperature Survey Specimen →			
3	3	250°F. Symm.	13256	13430	+ 1.40
4	4	425°F. Symm.	7716	8920 * / 8360 **	+13.50 * / + 8.00 **
5	5	250°F. Unsymm.	13553	13800	+ 1.80
6	6	425°F. Unsymm.	7791	8045	+ 3.20
7	Pilot Study a	R.T.	15100	15230	+ 0.90

Table 5.2. Per Cent Deviation of Analysis Results from Test Ultimate Load, Part 1

* This value denotes the analytical results obtained when the material properties are considered to recover to the higher values appropriate to the lower temperatures due to lamp shut off.

** This value denotes the results when the material properties were considered to be those present at the higher temperature just prior to lamp shut-off.

①	②	③	④	⑤	⑥ $\frac{⑤ - ④}{⑤} \times 100$
Horiz. Stab. No.	Test Temp. Environ.	Test (E.A. Sta.)	Test Ultimate Bending Moment, inch-lbs.	Calculated Ultimate Bending Moment, inch-lbs.	Per Cent Deviation
1	R.T.	122	192,000	230,000	+16.5
2	◁——— Temperature Survey Specimen ———▷				
3	250°F. Symm.	103	427,000	436,000	+ 2.1
4	425°F. Symm.	104	238,000	258,000 * 278,000 **	+ 7.7 * +14.3 **
5	250°F. Unsym.	102	447,000	460,000	+ 2.8
6	425°F. Unsym.	103	248,000	258,000	+ 3.8
Pilot Study a	R.T.	105	455,000	457,000	+ 0.5

Table 5.3. Bending Moment Comparison at Test Failure Station, Part 1

* This value denotes the analytical results obtained when the material properties are considered to recover to the higher values appropriate to the lower temperatures due to lamp shut-off.

** This value denotes the results when the material properties were considered to be those present at the higher temperature just prior to lamp shut-off.

5.2 Part 2 - Inboard Splice Joint Summary

Table 5.4 presents a complete summary of the experimental and analytical results of the inboard splice joint portion of the study. Ultimate test loads are shown for each loading former, since, in theory, they should be equal. In addition a brief description of the test failure is shown for comparison with the failure mode predicted by the analysis procedures. Using the room temperature results as a reference, the applied load ratios for ultimate load are calculated and shown for each temperature environment for both analytical and experimental ultimate loads. The per cent deviation of the predicted ultimate load from the test ultimate load is also shown for each temperature environment and shows generally acceptable agreement considering the large number of variables present in a mechanically-fastened splice joint at elevated temperature.

Note that two calculated ultimate load values are shown for each of the unsymmetrically heated splice joints (Test No's. 11 and 12). The initial calculated results indicated by a double asterisk (**) were obtained by assuming no bending moment restraint for thermal strains. The study performed in Section 4.7 indicates that some degree of thermal moment restraint probably exists in the root region due to temperature distribution and mixed materials. Therefore, a second set of calculations was performed assuming that full bending moment restraint was present throughout the entire length of the joint. These results are noted by a triple asterisk (***) and show generally better agreement with the test values. From the study of Section 4.7 and the Test No. 12 results, it is apparent that the degree of thermal moment restraint lies somewhere between no restraint and full restraint. For example, the strain gage results from Test No. 12 tend to indicate approximately full bending moment restraint at the outboard end of the splice and diminishing inboard to no restraint at the inboard end of the main box skin. In addition the test failing load of approximately 14,300 lbs. (average) lies between the calculated values of 13,030 lbs. and 17,700 lbs. indicating that either extreme assumption was actually incorrect. Since the joint analysis procedures used were for axially-loaded splices only, the thermal moment for the restrained case was taken as the elastic thermal moment and added to the applied loads as an additional applied bending moment for purposes of this investigation. This applied bending moment was added to the applied loads as a couple load for axial load analysis where the value of this couple load is shown in Section 4.7.2.

Temperature Environment Test Condition	ASL Test No.	Test Former Loads at Failure	Description of Test Failure	Calculated Failing Load	Calculated Primary Mode of Failure and Impending Secondary Failure	Failing Load Percent Deviation	Test Applied Load Ratio	Analysis Applied Load Ratio
Room Temperature	Pilot Study and 7	17400 17200 16741 * 15425	(1) Six inboard, aft fasteners sheared (2) Same six holes in main box skin elongated inboard (3) Tension failure, main beam flange, elastic axis station 59. (No failure during Test No. 7)	18,000	(1) Fastener shear at elastic axis sta. 58 (2) high tension stress in main beam flange at elastic axis sta. 58 (Secondary	+3.9	1.00	1.0(
250°F. Symmetrical	9	15985 (outb'd) 15795 (inb'd)	(1) Ten inboard fasteners sheared (2) Same holes in main box skin elongated (3) Tension failure in main beam flange at approx. elastic axis sta. 54 to 55	17,250	(1) Fastener shear at elastic axis sta. 58 (2) Imminent shear failure and bearing failure of inb'd. six fasteners (Secondary) (3) High tension stress in main beam flange at elastic axis sta. 58 (Secondary)	+7.9	0.918	0.958
250°F. Unsymmetrical	11	15827 (outb'd) 15471 (inb'd)	(1) Nine inboard fasteners sheared (2) Same holes in main box skin elongated (3) Tension failure in main beam flange at approx.elastic axis sta. 54	16,770*** 17,750**	⊕ (See Note Below) (1) Fastener shear at elastic axis sta. 58 (2) High tension stress in main beam flange at elastic axis sta.(Secondary)	+6.7*** +11.8	0.905	0.932*** 0.986**
425°F. Symmetrical	10	12440 (outb'd) 12347 (inb'd)	(1) Tension failure, main beam flange, elastic axis sta. 57.25 (2) Holes elongated in main box skin in area of beam tension failure (3) Inboard fasteners sheared	12,420	(1) Fastener shear at elastic axis sta. 64.2 (2) High tension stress in main beam flange at elastic axis sta. 58 (Secondary)	+0.3	0.716	0.690
425°F. Unsymmetrical	12	14416 (outb'd) 14211 (inb'd)	(1) Four inb'd aft fasteners sheared (2) Holes elongated in main box skin in area of beam tension failure (3) Main beam tension failure at approx. elastic axis sta. 54 to 55	13,030*** 17,700**	† (See Note Below) (1) Fastener shear at elastic axis sta. 58 (2) High tension stress in main beam flange at elastic axis sta. 58 (Secondary)	-8.9*** +19.2	0.828	0.723*** 0.983**

* Maximum total load reached prior to failure of horn and housing assembly. No fastener, main beam, or main box skin failure.

** No bending moment restraint for thermal strains.

*** Results for full restrained-in-bending case for thermal strains. See Section

⊕ (1) Fastener shear at elastic axis sta. 58.
(2) High tension stress in main beam flange at elastic axis sta. 58 (Secondary) } 16,770 lbs.

† (1) Main beam fitting tension failure at elastic axis sta. 58.
(2) Critical fastener shear and bearing; most inboard five rows of 7/16-inch diameter Blind Bolts (Secondary) } 13,030 lbs.

Table 5.4 Summary of Results, Horizontal Stabilizer Inboard Splice Joint Study
Part 2

5.3 Approximate Applied Load Ratios Using Simplified Procedures

A simplified procedure previously demonstrated in Reference (d) was employed in order to establish the applicability of such techniques in failure load prediction. The failure of a structure under test loading at elevated temperature is largely a function of the yield strength. The success at failure prediction in this program has come as a result of careful determination of the yield stress of the elements of the stabilizer cross-section. The simplified procedure employed here involves use of a psuedo yield moment obtained by considering each element in the cross-section at yield stress. The contribution of a single element in the cross-section to the value of the yield moment is equal to the element yield stress times the element area times the distance from the centroid of the element to the centroid of the cross-section at temperature. This moment, equal to $\Sigma F_{y_n} A_n y_n$, is computed at room and elevated temperature. Then, by dividing the room temperature "yield moment" value into any of the elevated temperature "yield moment" values, an approximate applied load ratio is obtained.

Test Condition	Applied Load Ratios				Test Ratios (Table 5.1)
	Sta. 91	Sta. 102	Sta. 113	Sta. 124	
Room Temperature	1.000	1.000	1.000	1.000	1.000
250°F. Un-Symmetrical	0.932	0.918	0.919	0.938	0.909
250°F. Symmetrical	0.905	0.887	0.884	0.917	0.888
425°F. Un-Symmetrical	0.694	0.629	0.631	0.727	0.522
425°F. Symmetrical (lamps off)	0.740	0.569	0.574	0.694	0.517
425°F. Symmetrical (lamps on)	0.700	0.525	0.516	0.638	

Table 5.5 Applied Load Ratios by Simplified Method, Part 1

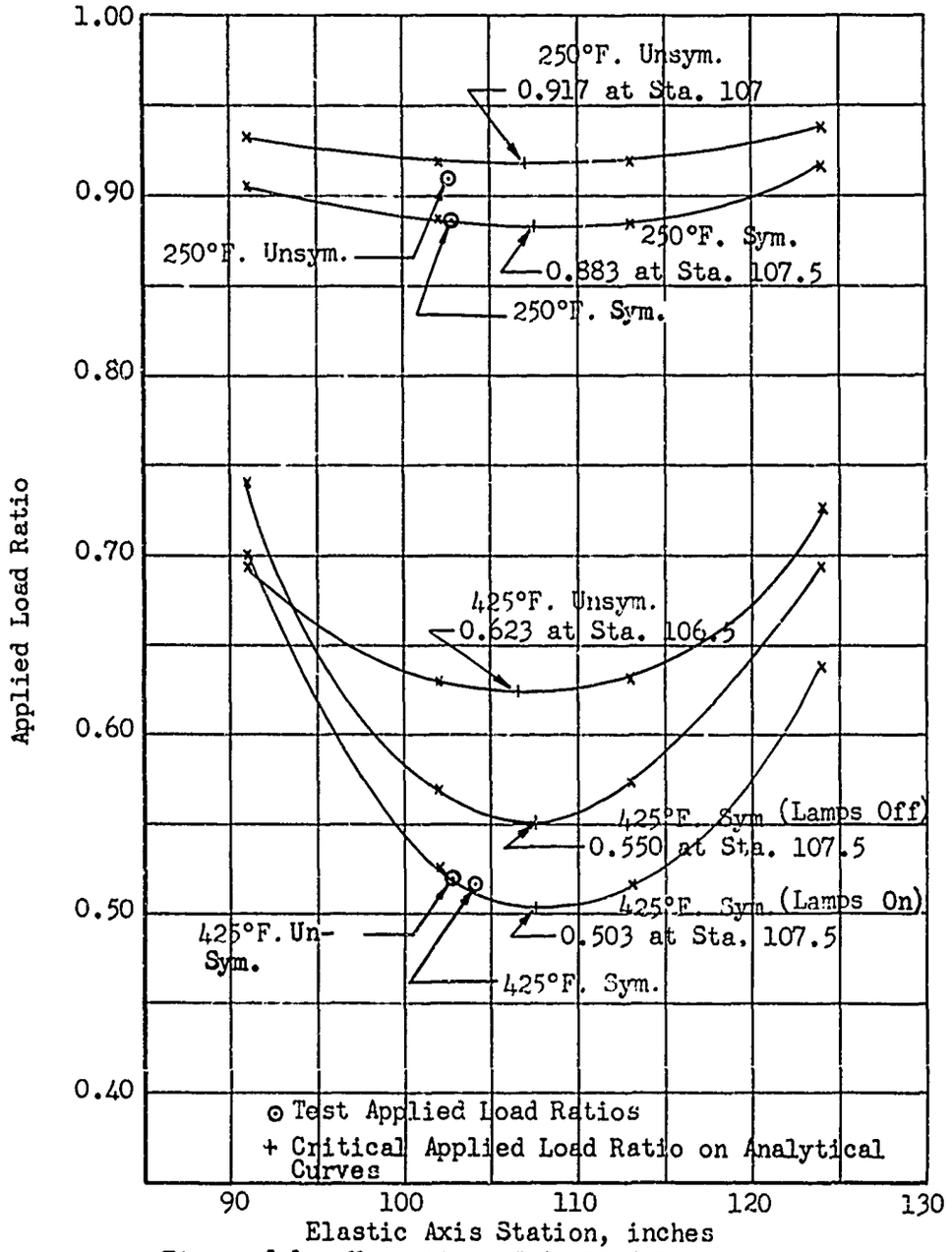

Figure 5.1 Variation of Applied Load Ratio With Station For Simplified Method

Table 5.5 shows the approximate applied load ratios computed at each station for the five tests. In the case of the 425°F. symmetrical test, the values were computed for both lamps off at failure and for lamps on at failure. The difference in the values here is caused directly by the difference in element yield stress for the two conditions.

Figure 5.1 shows plots of the approximate applied load ratios versus elastic axis station for each test. This plot provided not only a minimum applied load ratio for each test but also a failure station. Comparison with Table 5.1 , Section 5.1 , shows that the failure station prediction by the approximate applied load ratio method is in very close agreement with the failure station prediction by the load-deformation procedures of Section 2.1.1. The applied load ratios, in turn, agree very well with the test applied load ratios. The only test which does not have good agreement is the 425°F. unsymmetrical test. The difference here is due to the fact that the approximate method does not consider thermal stresses. Thus, the method will tend to over estimate the failure load for a test in the presence of high thermal gradients, and thus is unconservative. In the case of the 250°F. unsymmetrical test, the thermal stresses are not high enough for the thermal gradient to have any effect. It would appear from the results of this study that the simplified method is quite satisfactory for failure prediction under symmetrical heating. For the ratios given in Table 5.5, only six elements out of the thirty elements in the cross-section were used to compute the applied load ratios. These were the main box skin elements whose collapse caused failure of the cross-section. It is not necessary in this approximate method to include all of the elements in the cross-section so long as the principal elements are considered.

6.0 EXAMPLE PROCEDURES FOR ELEVATED TEMPERATURE STRENGTH VERIFICATION

6.1 Example Procedure To Illustrate Cross-Section Failure Prediction at Elevated Temperature From Room Temperature Test Results

The following procedure illustrates the method whereby the combined use of analysis and room temperature test results could be used to predict elevated temperature strength for horizontal stabilizer bending investigated during Part 1 of this study.

1. Room temperature static test is performed and failure occurred at a reference load of 14,908 lbs. (average of Horizontal Stabilizer No. 1 and No. 7).

2. Applied load ratios are obtained analytically using the calculated room temperature failing load as the reference value for defining the theoretical applied load ratios outlined below. (See Table 5.1).
   (a) Temperature environment; 250°F. Symmetrical, Applied Load Ratio, R_{ap} = 0.883

   (b) Temperature environment; 250°F. Unsymmetrical, Applied Load Ratio, R_{ap} = 0.907

   (c) Temperature environment; 425°F. Symmetrical
   Applied Load Ratio, R_{ap} = 0.585 (Lamps off at failure)
   Applied Load Ratio, R_{ap} = 0.550 (Lamps on at failure)

   (d) Temperature environment; 425°F. Unsymmetrical, Applied Load Ratio, R_{ap} = 0.528

3. The predicted failing loads for bending are shown in Table 6.1 by applying the theoretical ratios of Item 2 to the test failing load of Item 1. The table below also shows the actual test failing loads for the elevated temperature conditions as well as the per cent deviation of the predicted failing load from the actual test load.

1	2	3	4	5 / (3 - 4) / 3 x 100
ASL Test No.	Test Temperature Condition	Predicted Failing Load From R.T. Test, lbs.	Actual Test Failing Load, lbs.	Per Cent Deviation from Actual Test
3	250°F.Symm.	13180	13256	- 0.6
5	250°F.Unsymm.	13530	13553	- 0.2
4	425°F.Symm.	8740 8205	7716	+11.7* + 6.0**
6	425°F.Unsymm.	7880	7791	+ 1.2

* Lamps off at failure
** Lamps assumed on at failure

} Different Material Properties Used.

Table 6.1. Test-Analysis Summary For Example Procedure, Part 1

The results shown in the above table show that the elevated temperature strength test results can be accurately predicted based upon calculated applied load ratios applied to room temperature test results. An actual simulation procedure would use MIL-HDBK-5 properties which would produce, generally, slightly conservative results. This fact seems to indicate that the procedure could be accepted as a simulation procedure with some degree of confidence.

6.2 Example Procedure To Illustrate Splice Joint Failure Prediction at Elevated Temperature From Room Temperature Test Results

The following procedure illustrates the method whereby the combined use of analysis and room temperature test results could be used to predict elevated temperature strength for the horizontal stabilizer splice joint investigated during this study.

1. Room temperature static test is performed and failure occurred at a reference load of 17,300 lbs.

2. Applied load ratios are obtained analytically using the calculated room temperature failing load as the reference value for defining the theoretical applied load ratios outlined below.

   (a) Temperature environment; 250°F. Symmetrical, Applied load ratio, R = 0.958
   (b) Temperature environment; 250°F. Unsymmetrical, Applied load ratio, R = 0.986 (R = 0.932 for thermal moment restraint)*
   (c) Temperature environment; 425°F. Symmetrical, Applied load ratio, R = 0.690
   (d) Temperature environment; 425°F. Unsymmetrical, Applied load ratio, R = 0.983 (R = 0.723 for thermal moment restraint)*

3. The predicted failing loads for the splice joint are calculated below by applying the theoretical ratios of Item 2 to the test failing load of Item 1. The table below also shows the test failing loads for the elevated temperature conditions as well as the per cent deviation of the predicted failing load from the actual test load.

(1)	(2)	(3)	(4)	(5) *See Page 95
ASL Test No.	Test Temperature Condition	Predicted Failing Load From R. T. Test, lbs.	Actual Test Failing Load, lbs.	Per Cent Deviation From Actual Test
9	250°F.Symm.	16575	15890	+ 4.2
11	250°F.Unsymm.	17070 16120 *	15649	+ 8.3 + 3.0 *
10	425°F.Symm.	11940	12393	- 3.5
12	425°F.Unsymm.	12520* 17020	14513	-12.6* +15.8

Table 6.2. Test-Analysis Summary For Example Procedure, Part 2

The results of the Table 6.2 indicate that the predicted elevated temperature strength based upon calculated applied load ratios and room temperature test results may result in slightly unconservative predictions except for Test No. 10 which was fairly realistic and slightly conservative. Possibly the use of MIL-HDBK-5 material properties and minimum fastener properties from a greater number of tests would ensure slightly conservative results in most cases.

*See Table 6.2 on Page 94.

$$(5) = \frac{(3) - (4)}{(4)}$$

7.0 CONCLUSIONS

7.1 Conclusions on Part 1

In general, the results of this program indicate that the applied load ratio-room temperature static test simulation of elevated temperature design conditions can be applied to components or particular areas of components where contimuous structure plane-strain cross-sections exist. The specific loading conditions satisfactorily verified by this study are axial load, bending, and combined axial load and bending, in uniform and nomuniform elevated temperature environments. The further investigation of an approximate simplified approach to the determination of applied load ratios has indicated that a relatively good estimate of elevated temperature strength can be obtained simply by using the elevated temperature material properties and computing a "psuedo-yield bending moment" for the cross-section (bending critical).

The deflections of structures subjected to bending in elevated temperature environments can be predicted analytically once the room temperature deflections are known, particularly maximum, or tip, deflections at failure. Some evidence supporting this conclusion was obtained through the use of a simplified formula equating the ratio of the elevated temperature test deflection and the room temperature test deflection to the ratio of test failure loads multiplied by the ratio of the yield stress values of the major structural elements at the test temperatures. The analytical load-deformation procedures of Section 3.2, Volume I, coupled with the deflection analysis procedures of Section 3.4, Volume I, can be used to predict the deflected shape of a structure at failure. The prediction is limited to plane-strain type structures such as are typically found in aircraft. The deflection rate method of failure station prediction is also shown to be of considerable value for elevated temperature tests as well as room temperature tests.

Predictions are accurate to within $\pm 10\%$ of the experimental values.

7.2 Conclusions on Part 2

Part 2 of this study demonstrated the application of applied load ratio-room temperature test simulation to multi-plate, multi-fastener, axially-loaded splice joints in uniform and nomuniform temperature environments. Using redundant force-type analytical methods which allow for temperature and inelastic effects, the ultimate applied load ratios were defined within realistic material property limits and temperature ranges. Therefore, the elevated temperature splice joint strengths were verified by analytically defined applied load ratios and a room temperature static test to failure.

In order for the applied load ratios to be calculated with sufficient accuracy (and/or conservatism), MIL-HDBK-5 material properties should be selected for the design elevated temperature environment to supplement those obtained experimentally by tests of fastener-plate combinations at room and elevated temperatures. The predictions are accurate to within ±16% of the experimental values.

8.0 RECOMMENDATIONS

Based upon the results of the work reported herein, there are limitations involved with the use of the applied-load-ratio method. It is now applicable to aircraft structures which fail in bending and/or axial load, under steady-state elevated temperature environments. It is therefore recommended that further investigations be performed so that all restrictions could be removed.

The present investigation should be extended to the applicability of the applied load-ratio method to:

(1) Full-scale structures, under steady-state temperature environments, where failures are caused by torsion, combined torsion and bending, and by cut-outs in the structure. The methods should be verified by performing structural tests on suitable components, such as stabilizers (for torsion, combined torsion and bending) and a typical fuselage (for structures with cut-outs).

(2) Laboratory-type structures, in other temperature environments, which are subjected to simple loadings. The "lamps-off" condition could be one of several additional temperature environments.

The applicability of the applied-load-ratio method to mechanically-fastened splice joints was established in Part 2 of the present investigation. It is recommended that other types of fasteners be used under steady-state elevated temperatures and the same loading conditions as reported herein; the splice joints could be welded or bonded.

APPENDIX I

PHOTOGRAPHS OF HORIZONTAL STABILIZER FAILURES

The photographs provided in this section illustrate the modes of failure which were encountered during the experimental program. Representative photographs of each failed stabilizer were selected to clarify the failure descriptions in the summary tables of Sections 5.1 and 5.2. Figures AI.1 through AI.6 show the compression sides of the outboard span plane-strain cross-sections after failure. Particularly noteworthy in this series of photographs is the similar mode of failure for the temperature range from room temperature to approximately 425°F. for this aluminum alloy multi-spar configuration. Generally the failures in the outboard span regions were a compression instability failure of the aluminum alloy main box skin and spar flanges and in the same general area. The single exception to this was the primary tension failure of the pilot study stabilizer (Pilot study a) although Figure AI.1 shows only the compression surface of this stabilizer.

Figures AI.7 through AI.14 were selected to illustrate both the main beam fitting tension failures and the hole elongations in the aluminum alloy main box skins which occurred during the inboard splice joint test program. As in the outboard regions of the stabilizer the failures are seen to be quite similar in mode and location for the temperature range from room temperature to approximately 425°F. All major fractures and hole elongations shown in the photographs are on the tension surface.

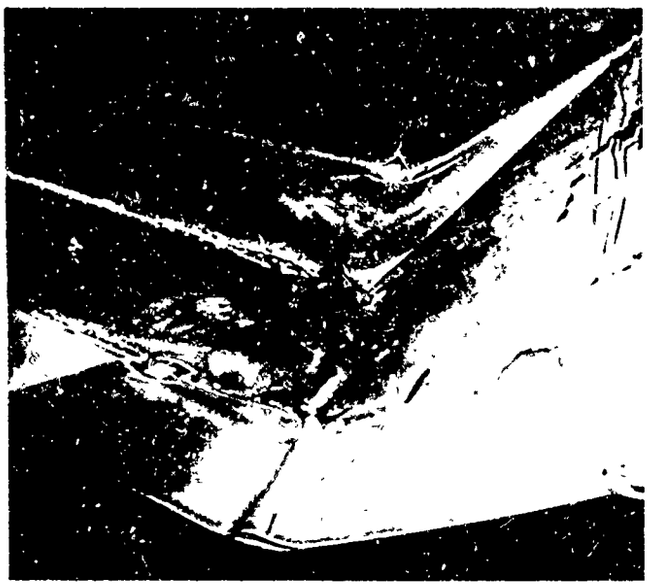

Figure AI.1. Horizontal Stabilizer Pilot Study a (Pilot Study); Room Temperature; Closeup of Compression Side After Failure

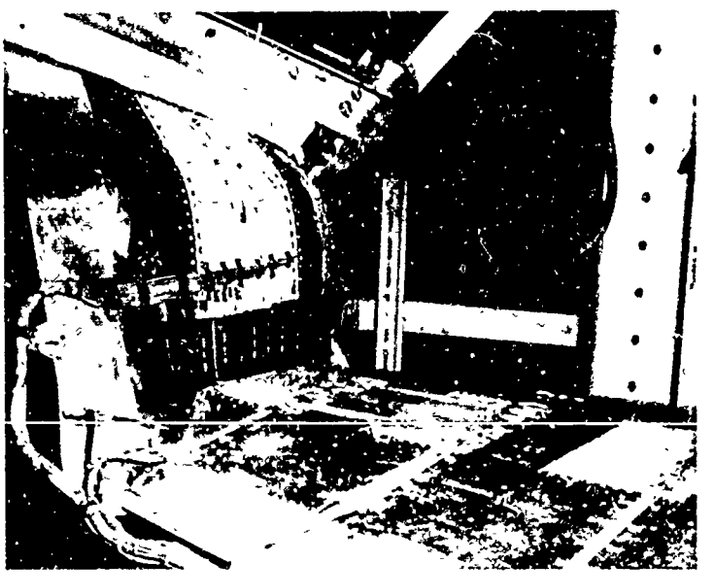

Figure AI.2. Horizontal Stabilizer Test 1; Room Temperature; Closeup of Compression Side After Failure

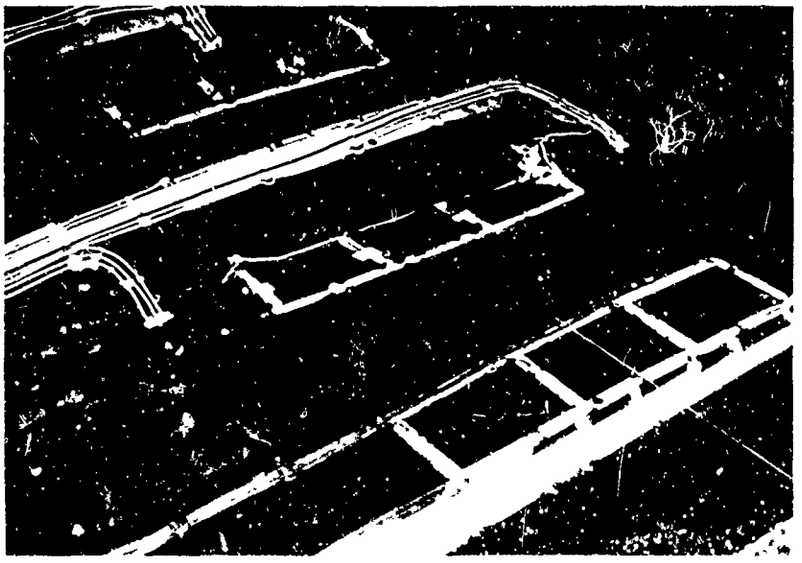

Figure AI.3. Horizontal Stabilizer Test 3; 250°F. Symmetrical; Closeup of Compression Surface After Failure

Figure AI. 4. Horizontal Stabilizer Test 4; 425°F. Symmetrical; Closeup of Compression Surface After Failure

Figure AI.5. Horizontal Stabilizer Test 5; 250°F. Unsymmetrical; Closeup of Compression Surface After Failure

Figure AI.6. Horizontal Stabilizer Test 6; 425°F. Unsymmetrical; Closeup of Compression Surface After Failure

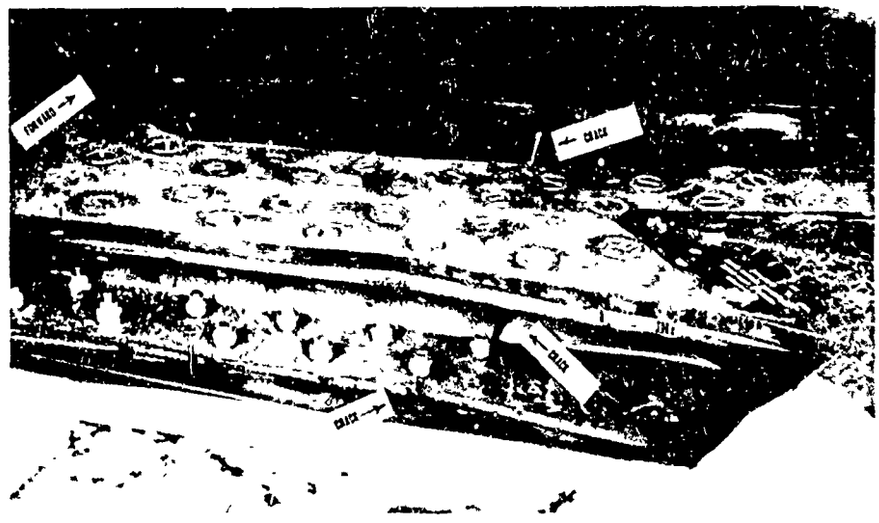

Figure AI.7. Horizontal Stabilizer Pilot Study b
Pilot Study Room Temperature; Closeup
Showing Cracks in Main Beam and
Forward Spar

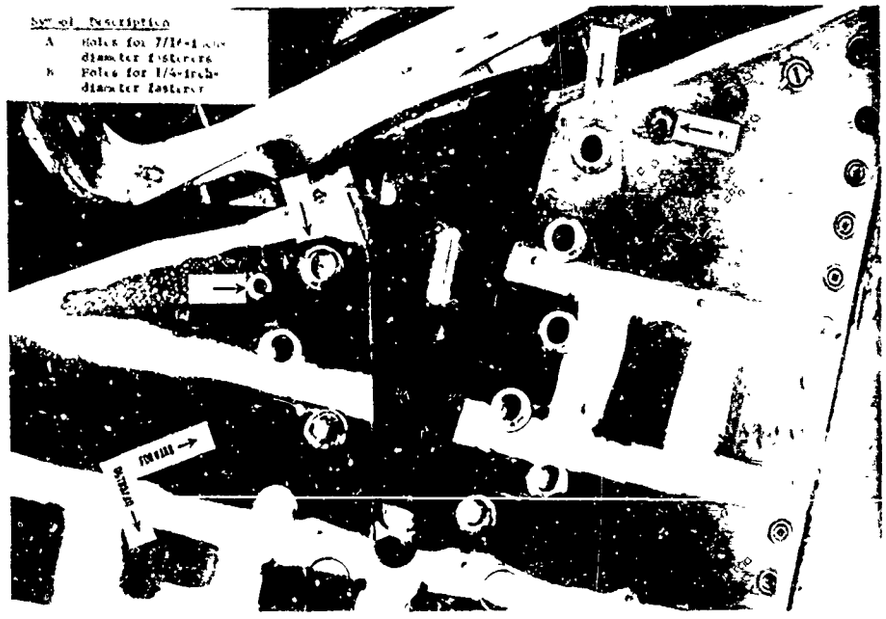

Figure AI.8. Horizontal Stabilizer Test 9;
250°F. Symmetrical; Closeup of Tension
Surface After Fastener Failures

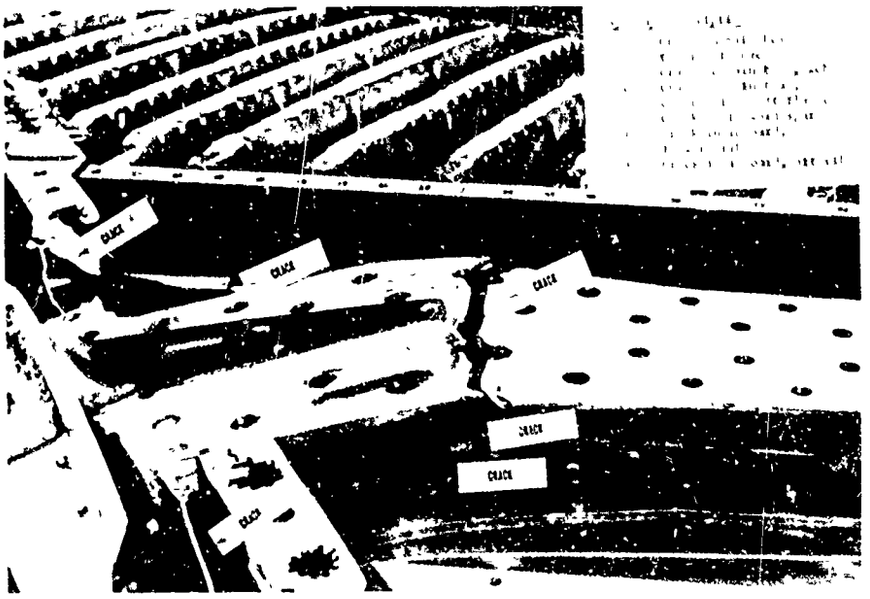

Figure AI.9. Horizontal Stabilizer Test 9; 250°F. Symmetrical; Closeup of Failure of Internal Structure

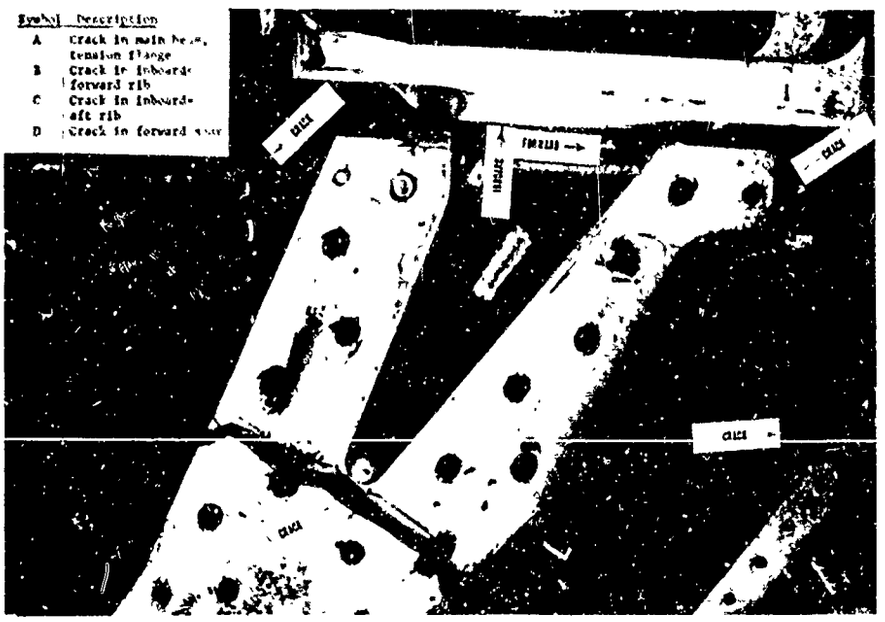

Figure AI.10 Horizontal Stabilizer Test 9; 250°F. Symmetrical; Closeup of Tension Failure of Main Beam Flanges

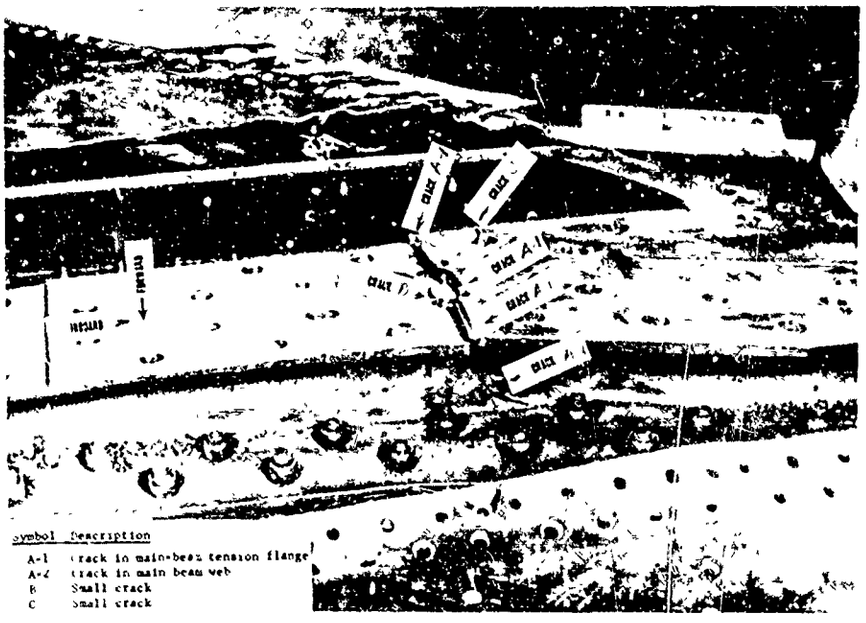

Figure AI.11. Horizontal Stabilizer Test 10; 425°F. Symmetrical; Closeup of Failure of Internal Structure

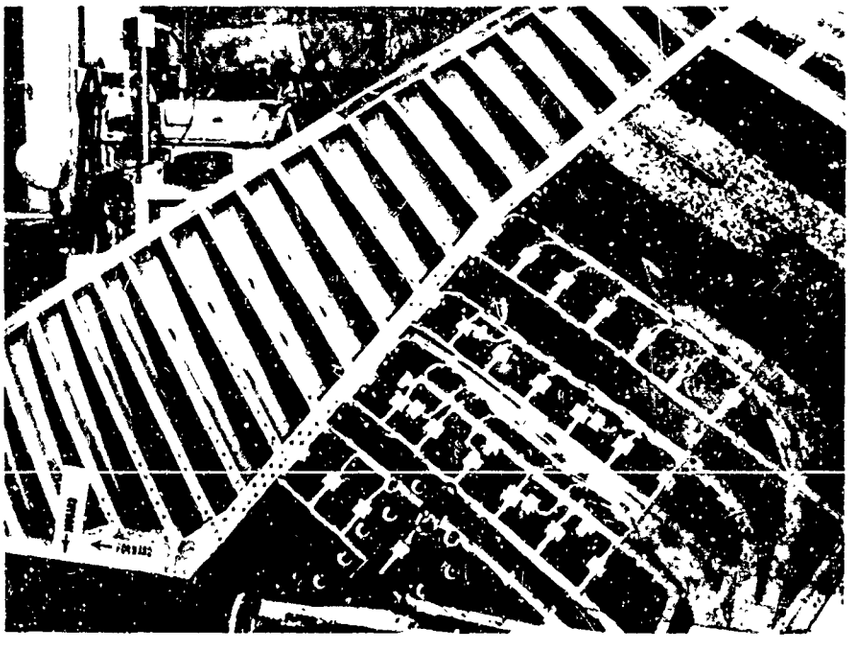

Figure AI.12. Horizontal Stabilizer Test 11; 250°F. Unsymmetrical; Inboard Portion of Tension Surface After Failure

Figure AI.13. Horizontal Stabilizer Test 11
250°F. Unsymmetrical; Closeup of Failure
of Main Beam Tension Flanges

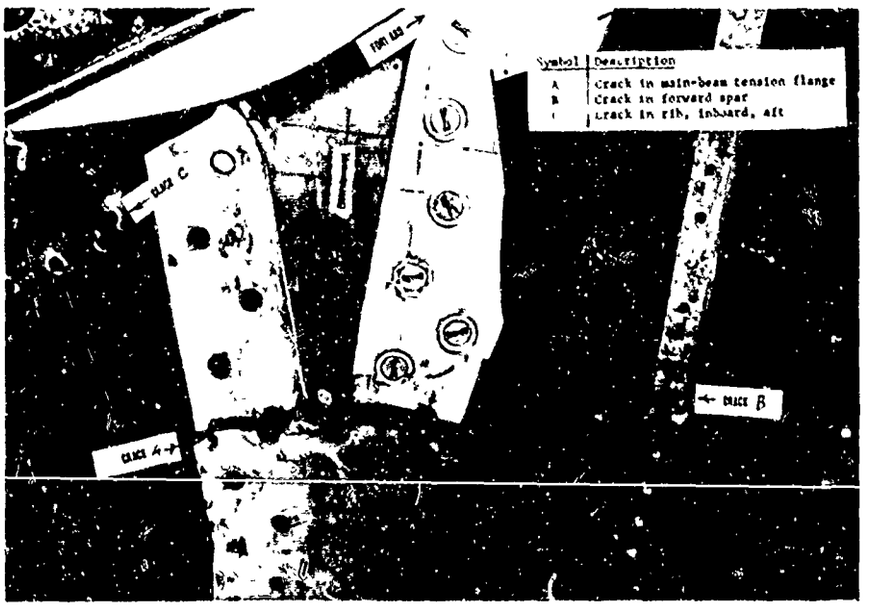

Figure AI.14 Horizontal Stabilizer Test 12;
425°F. Unsymmetrical; Closeup of Failure
of Main Beam Tension Flanges

UNCLASSIFIED

Security Classification

DOCUMENT CONTROL DATA - R&D

(Security classification of title, body of abstract and indexing annotation must be entered when the overall report is classified)

1 ORIGINATING ACTIVITY *(Corporate author)* North American Aviation, Inc., Columbus Division 4300 East Fifth Avenue Columbus, Ohio 43216	2a. REPORT SECURITY CLASSIFICATION Unclassified 2b GROUP None

3. REPORT TITLE

APPLICATION OF APPLIED LOAD RATIO STATIC TEST SIMULATION TECHNIQUES TO FULL-SCALE STRUCTURES; VOLUME IV, SUMMARY OF RESULTS, CONCLUSIONS AND RECOMMENDATIONS

4. DESCRIPTIVE NOTES *(Type of report and inclusive dates)*

Engineering Report - Volume IV

5. AUTHOR(S) *(Last name, first name, initial)*

Gehring, R. W. and Maines, C. H.

6. REPORT DATE	7a. TOTAL NO. OF PAGES	7b. NO. OF REFS
August 1966	106	7

8a. CONTRACT OR GRANT NO.	9a. ORIGINATOR'S REPORT NUMBER(S)
N156-45330 b. PROJECT NO. P. A. 1-23-83 c. d.	NAEC-ASL-1094 Volume IV 9b. OTHER REPORT NO(S) *(Any other numbers that may be assigned this report)* None

10. AVAILABILITY/LIMITATION NOTICES

Distribution of this document is unlimited.

11. SUPPLEMENTARY NOTES	12. SPONSORING MILITARY ACTIVITY
None	Naval Air Engineering Center Aeronautical Structures Laboratory Philadelphia, Pennsylvania 19112

13. ABSTRACT

The overall objective of the study is to investigate the applicability of the applied load ratio method to full scale aircraft structural components. Volume IV is a report on the correlation of theoretical and experimental results. The conclusion is that the applied load ratio method gives accurate predictions for structures loaded in elevated temperature environments to fail in bending and shear. Failure predictions apply either to a mechanically fastened splice joint or to areas where plane-strain cross-sections exist.

DD FORM 1 JAN 64 1473

UNCLASSIFIED

Security Classification

14. KEY WORDS	LINK A		LINK B		LINK C	
	ROLE	WT	ROLE	WT	ROLE	WT
Block diagrams, structural analysis Deflection of structures Deformation of structures Digital computers Elevated temperature effects Joint, splice-joints Nonuniform temperature environment effects Simulation studies Static tests Strength analysis Stress analysis Stabilizers/Control surfaces/ Structural analysis Uniform temperature environment effects						

INSTRUCTIONS

1. ORIGINATING ACTIVITY: Enter the name and address of the contractor, subcontractor, grantee, Department of Defense activity or other organization *(corporate author)* issuing the report.

2a. REPORT SECURITY CLASSIFICATION: Enter the overall security classification of the report. Indicate whether "Restricted Data" is included. Marking is to be in accordance with appropriate security regulations.

2b. GROUP: Automatic downgrading is specified in DoD Directive 5200.10 and Armed Forces Industrial Manual. Enter the group number. Also, when applicable, show that optional markings have been used for Group 3 and Group 4 as authorized.

3. REPORT TITLE: Enter the complete report title in all capital letters. Titles in all cases should be unclassified. If a meaningful title cannot be selected without classification, show title classification in all capitals in parenthesis immediately following the title.

4. DESCRIPTIVE NOTES: If appropriate, enter the type of report, e.g., interim, progress, summary, annual, or final. Give the inclusive dates when a specific reporting period is covered.

5. AUTHOR(S): Enter the name(s) of author(s) as shown on or in the report. Enter last name, first name, middle initial. If military, show rank and branch of service. The name of the principal author is an absolute minimum requirement.

6. REPORT DATE: Enter the date of the report as day, month, year; or month, year. If more than one date appears on the report, use date of publication.

7a. TOTAL NUMBER OF PAGES: The total page count should follow normal pagination procedures, i.e., enter the number of pages containing information.

7b. NUMBER OF REFERENCES: Enter the total number of references cited in the report.

8a. CONTRACT OR GRANT NUMBER. If appropriate, enter the applicable number of the contract or grant under which the report was written.

8b, 8c, & 8d. PROJECT NUMBER: Enter the appropriate military department identification, such as project number, subproject number, system numbers, task number, etc.

9a. ORIGINATOR'S REPORT NUMBER(S): Enter the official report number by which the document will be identified and controlled by the originating activity. This number must be unique to this report.

9b. OTHER REPORT NUMBER(S): If the report has been assigned any other report numbers *(either by the originator or by the sponsor)*, also enter this number(s).

10. AVAILABILITY/LIMITATION NOTICES: Enter any limitations on further dissemination of the report, other than those imposed by security classification, using standard statements such as:

(1) "Qualified requesters may obtain copies of this report from DDC."

(2) "Foreign announcement and dissemination of this report by DDC is not authorized."

(3) "U. S. Government agencies may obtain copies of this report directly from DDC. Other qualified DDC users shall request through

_____."

(4) "U. S. military agencies may obtain copies of this report directly from DDC. Other qualified users shall request through

_____."

(5) "All distribution of this report is controlled. Qualified DDC users shall request through

_____."

If the report has been furnished to the Office of Technical Services, Department of Commerce, for sale to the public, indicate this fact and enter the price, if known.

11. SUPPLEMENTARY NOTES: Use for additional explanatory notes.

12. SPONSORING MILITARY ACTIVITY: Enter the name of the departmental project office or laboratory sponsoring *(paying for)* the research and development. Include address.

13. ABSTRACT: Enter an abstract giving a brief and factual summary of the document indicative of the report, even though it may also appear elsewhere in the body of the technical report. If additional space is required, a continuation sheet shall be attached.

It is highly desirable that the abstract of classified reports be unclassified. Each paragraph of the abstract shall end with an indication of the military security classification of the information in the paragraph, represented as *(TS), (S), (C), or (U)*.

There is no limitation on the length of the abstract. However, the suggested length is from 150 to 225 words.

14. KEY WORDS: Key words are technically meaningful terms or short phrases that characterize a report and may be used as index entries for cataloging the report. Key words must be selected so that no security classification is required. Identifiers, such as equipment model designation, trade name, military project code name, geographic location, may be used as key words but will be followed by an indication of technical context. The assignment of links, roles, and weights is optional.